Miniature Distributed Occulter Telescope: mDOT

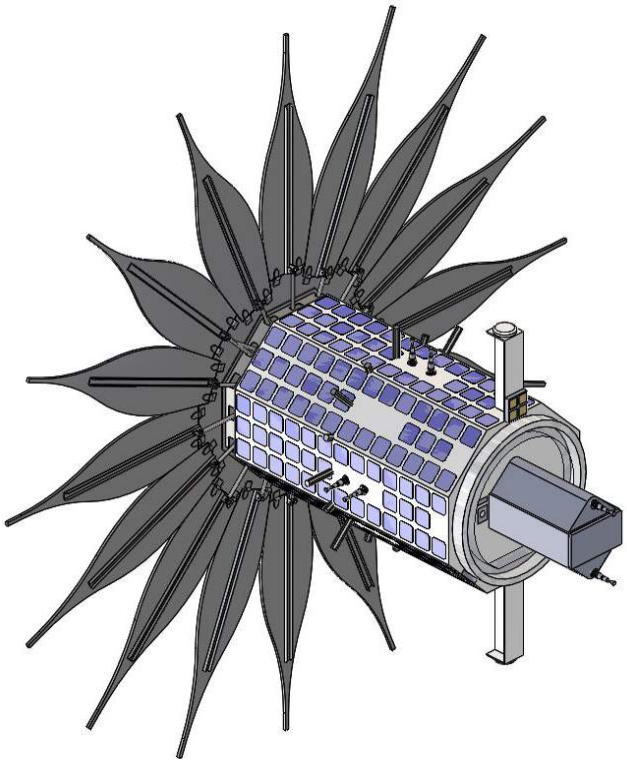

[6]

Export Controlled Material Statement

The document does not contain any export controlled information.

Restricted Use Statement

The information (data) contained in this study report listed in the table below constitutes a trade secret and/or information that is commercial or financial and confidential or privileged. It is furnished to the Government in confidence with the understanding that it will not, without permission of the offer or, be used or disclosed for other than evaluation purposes; provided, however, that in the event a contract is awarded on the basis of this study report or quotation, the Government shall have the right to use and disclose this information (data) to the extent provided in the contract. This restriction does not limit the Government's right to use or disclose this information (data), if obtained from another source without restriction.

Restricted Use Information

Section Number	Type of Information	Page Numbers

Contents

mDOT

Miniaturized Distributed Occulter/Telescope for Direct Imaging of Extrasolar Dust Disks

PI: Bruce Macintosh, Stanford University, bmacintosh@stanford.edu

Starshades enable exoplanet imaging using a large free-flying occulter spacecraft to block the light of a star. mDOT uses novel orbit architectures and precision navigation and maneuvering to enable a small-scale starshade mission in Low Earth Orbit. Circumstellar dust disks trace the formation and evolution of planetary system, but could represent a potential obstacle to future exoplanet imaging missions. With the light of the target star suppressed mDOT will observe zodiacal-equivalent disks at unprecedented sensitivity

Objective	Targets and observations	Key Requirements
Constrain size and composition of dust particles near young stars	Measure short-wavelength brightness of known young-star debris disks	Inner working angle 2” 450 nm imaging 1” resolution Surface brightness 20-22 mag/square arcsecond
Determine ratio of scattered light to thermal emission for disks seen only in IR	Measure scattered-light surface brightness of mature nearby stars with IR excess	Inner working angle 1” 1” resolution Surface brightness 18-22 mag/square arcsecond
Measure presence of dust around nearby stars	Measure scattered-light surface brightness of mature nearby stars at 1-5 AU scales	Inner working angle 0.6” 1” resolution Surface brightness 21-23 mag/square arcsecond

- Microsatellite starshade (3-m starshade, 246kg, 192W, ~1x1x1m)
- Cubesat telescope (9 cm telescope, 12kg, 100W, ~10x20x30cm)
- Cubesat is hosted and ejected by microsatellite
- Orbit: Sun-synchronous (>500km, 98deg)
- 3-5 minute science observations during node crossings
- 1 to 9 observation passes per target
- Orbit precesses in RA to successive targets
- 11 5N green propellant thrusters (81 kg fuel)
- High level of GNC autonomy

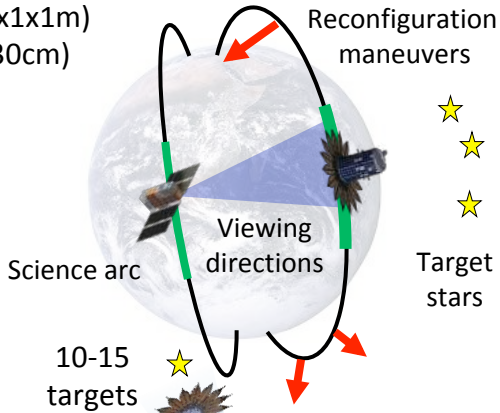

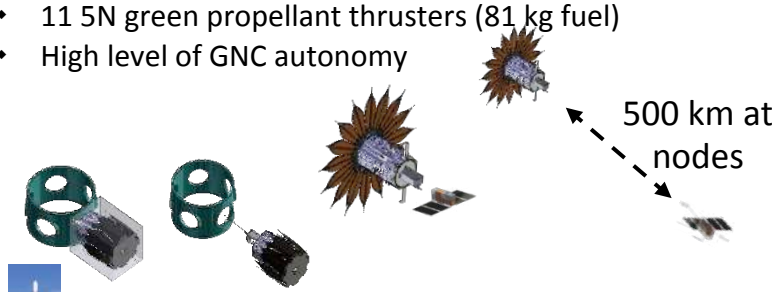

<1 day	3 weeks	4 weeks	11 months	1 week
Launch	Deployment/ Commissioning	Formation acquisition	Science: 1-9 obs per target, New target every 1-4 wks	Decomm

mDOT

Starshade (Stanford, JPL, Tendeg)	
Diameter	3m (16 petals)
Suppression	10^{-7} (10 Fresnel)
Shape Tolerance	0.1 mm
Deployment	Single-stage motorized
Structure	Carbon-fiber with precision-etched amorphous metal foil

Telescope (Stanford, Ames, Planet)	
Aperture (f)	9.2cm (15.5)
Wavelength range	400-490 nm (B band)
Pixel Size (Nyquist)	3.45µm (0.5 arcseconds)
Resolution (Stability)	1'' (0.2'')
Image stabilization	Mirrorcle tip/tilt mirror
Detectors	2xIMPERX CMOS (1.2MP) (guiding and science)

Microsat starshade (Ames)		
Rel nav	2 cm, 0.1 mm/s	DIGITAL
Att know/ctrl	0.2 deg/1 deg	Bus/ADCS
S/C DV	940 m/s	Green Prop

Nanosat Telescope (Blue Canyon)		
Rel nav	2 cm, 0.1 mm/s	DIGITAL
Att know/ctrl	0.1 deg/0.45 deg	Bus/ADCS

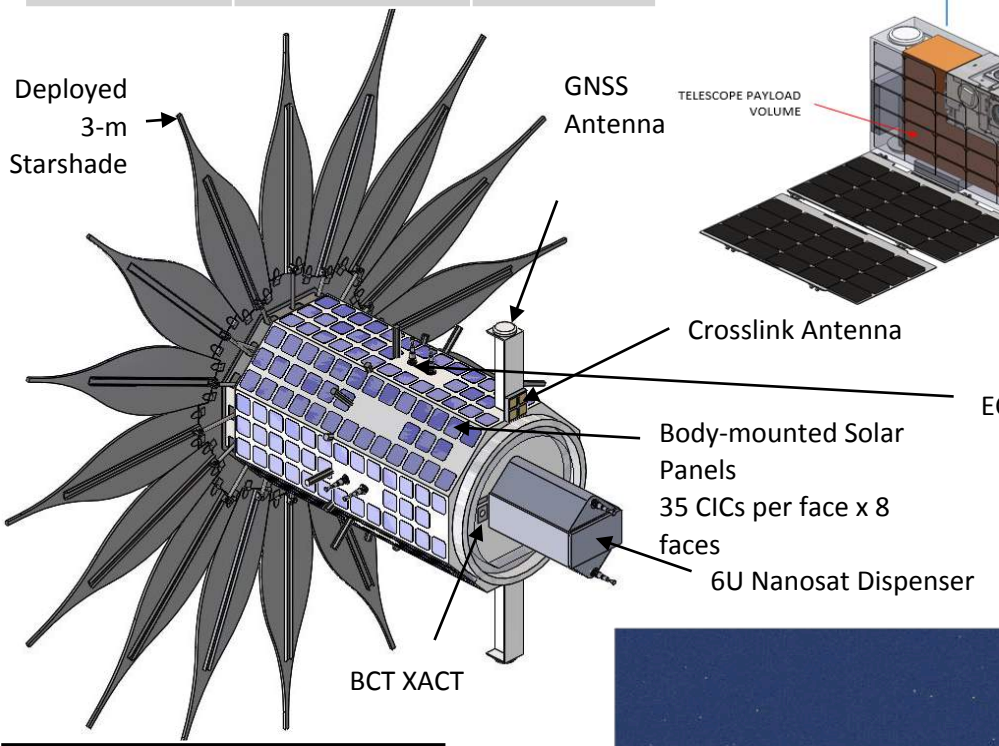

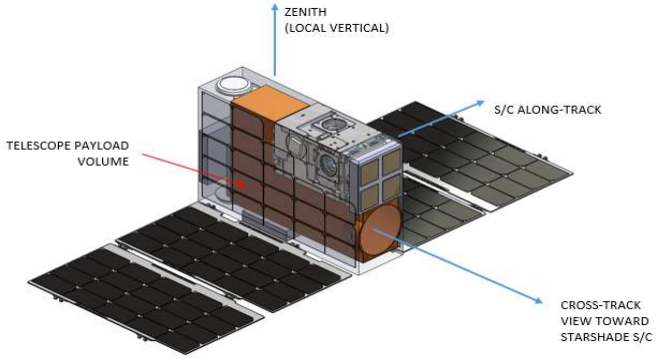

Science Targets for baseline DRM	
Known young disks	3
Dusty nearby stars	1
Other nearby stars	3
Reference stars	6

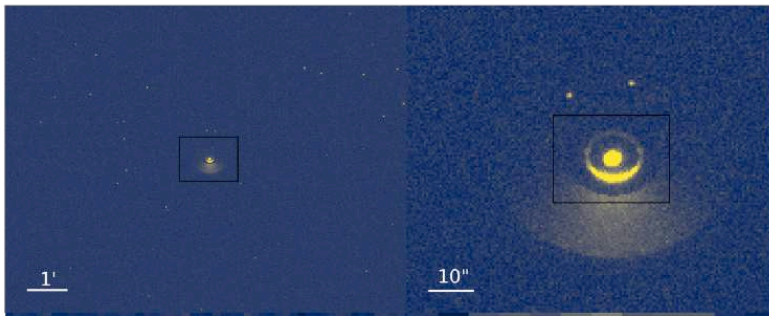

Simulated 8x5 min exposure of Epsilon Eridani showing inner, outer, and intermediate disk and background stars

Study Team: Bruce Macintosh (PI, Stanford), Simone D'Amico (co-PI, Stanford), Adam Koenig (Stanford), Ames Research Center (ARC) Mission Design Team, Eduardo Bendek (Ames/JPL), Keith Grogran, Stuart Shaklan (JPL), Tendeg LLC, Tyvak LLC
Science Team: B. Macintosh, A. Madurowicz, R. de Rosa (Stanford), T. Greene (Ames), J. Debes (STScI), E. Douglas (Arizona), R. Jensen-Clem, G. Duchene, T. Esposito (Berkeley)

6

1 Executive Summary

The miniaturized Distributed Occulter Telescope (mDOT) will provide unprecedented direct measurements of brightness of extrasolar dust disks in the near-ultraviolet spectrum. This addresses key science questions in the 2010 Astrophysics Decadal Survey and the 2019 Exoplanet Science Strategy through three objectives: constraining the properties of dust particles that make up these disks; measuring the intensity and geometry of faint disks detected only in thermal radiation; and searching for new disks around nearby stars. A secondary demonstration objective of mDOT is to increase the technology readiness level (TRL) of starshades and satellite formation control to TRL 6 paving the way for Probe-class or epochal flagship-scale missions such as HabEx.

These objectives are met by deploying a formation consisting of a microsatellite ($1m^3$, 246kg, 192W) and a nanosatellite (6U, 12kg, 100W) into a sun-synchronous low Earth orbit (LEO, ~98deg, LTAN of 9AM-3PM or 9PM-3AM). The satellites are launched combined as a secondary payload compatible with the ESPA Grande ring for a total mission lifetime of 1.1 years. The microsatellite is equipped with a 3m diameter starshade with 16 petals that is designed to suppress the light from the host star by more than seven orders of magnitude in the B-band (360-520nm) in a shadow 500 km from the starshade. The inner working angle for this design is 0.6 arcsec, which is much better than achievable through a single microsatellite with a conventional coronagraph. The petals are deployed simultaneously by a single hub with a set of radial linkages. The petals are precisely manufactured (0.1mm tolerance in critical error modes) using precision-etched amorphous metal foil so that the light diffracting around the starshade destructively interferes to create a shadow suppressing the starlate by more than 10^7. The nanosatellite is equipped with a 9.2cm aperture telescope that is used to image the dust disks from within the shadow produced by the starshade. The telescope is a modified version of the payload on Planet's Dove constellation that includes a secondary detector and a tip/tilt mirror used to stabilize the images to 0.2arcsec. This telescope can detect the science targets with cumulative integration times on the order of several minutes.

The nominal baseline of 500km required for scientific observations is established in the cross-track direction through a 4o difference in RAAN. This baseline is acquired over four weeks after deployment of the nanosatellite from the microsatellite using a sequence of maneuvers that exploit earth oblateness to reduce delta-v cost. Scientific observations are conducted during passes over the node in eclipse and last 2-5 minutes each, depending on the declination of the target (within 10 o of ±8o, specified before formation acquisition). Longer integration times are achieved by repeated observations over consecutive orbits. To minimize the delta-v cost required to image many science targets, the operations concept exploits the complete volume of the shadow produced by the starshade (30cm diameter, 10 km length). During observations, the starshade spacecraft only performs maneuvers to control the relative position perpendicular to the line of sight, allowing the inter-spacecraft separation to passively drift. The delta-v cost is further reduced by using earth oblateness effects to passively align the formation with targets of different right ascension

6

2 Science

2.1 Science Background

The study of extrasolar planets as a field has advanced extremely rapidly over the past three decades. This has focused primarily on detection of planets themselves through transit and Doppler techniques, and high-contrast imaging of the most massive young planets in the near-infrared.

In addition to planets, planetary systems contain many smaller bodies – asteroids and comets and leftover planetesimal debris from the planet-forming process. Solid bodies with sizes between 1 m and roughly the size of Earth are almost undetectable with current techniques, but their presence can be inferred from the circumstellar dust produced by their collisions and evolution. In our solar system, this is seen as the "zodiacal light", a diffuse glow in the ecliptic plane that is traced to the erosion of comets and collisions of asteroids. Integrated over our whole system and seen from outside, this zodiacal light would be the second-brightest component of our solar system after the sun – a hundred times brighter than Jupiter. The outer-solar-system Kuiper belt produces a similar disk of material. Younger stars will have larger numbers of planetesimals on more chaotic orbits; the system of small bodies surrounding them are often referred to as "debris disks".

Such dust can be detected in two ways. First, because the particles absorb starlight, they will warm up and radiate mid to far-infrared radiation with their equilibrium temperature depending on the distance from the star. This produces excess infrared radiation making the star seem much brighter at long (10-1000 μm) wavelengths and can be detected easily when the disk is massive; the first clear evidence of circumstellar dust was the excess IR radiation seen around stars like Vega. Second, the dust particles will scatter the visible starlight and can be seen directly in polarized or unpolarized visible and near-IR images such as Figure 2-1.

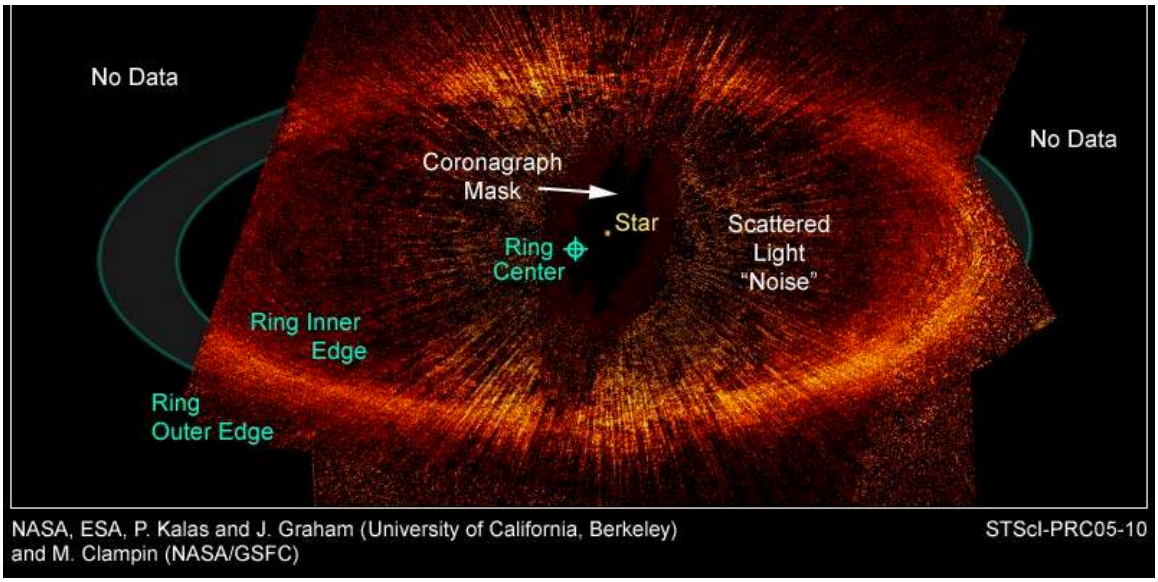

Figure 2-1: Hubble Space Telescope Image of a large (>100 AU) massive debris disk surrounding the star Fomalhaut.

because this brightness is diffuse and hidden in the glare of the sun it is almost undetectable in extrasolar systems; current detection limits for thermal emission from inner-solar-system dust (1σ) are typically 10-100 times the solar system level for nearby stars. Even with the most advanced

[6]

coronagraphs such as the Gemini Planet Imager the debris disks that have been imaged in scattered light are thousands of times brighter than our solar system and present on scales of 100 AU or more.

Since the emission is diffuse, the low resolution of a small telescope does not limit sensitivity the way it would for imaging a point source such as a planet. Instead, the small telescope merely limits spatial resolution. Although fine structures in the disk are not visible at low resolutions, the total brightness and bulk properties of the disk can still be measured, if the star does not mask the disk. By blocking the light from the star, a space telescope equipped with a starshade occulter has the potential for unprecedented sensitivity to these disks.

2.2 Science Objectives and Required Observations

In its mission to characterize the circumstellar dust disks that trace the presence and evolution of planetary systems, mDOT has three primary objectives

Objective 1. Constrain the properties of dust particles – primarily particle size – for known young, bright dusty debris disks previously seen in scattered light at longer wavelengths

Objective 2. Measure the intensity and basic geometry of scattered-light emission of fainter dust disks so far only detected through their thermal emission, to constrain the ratio of scattered light to thermal emission

Objective 3. Search for new dust disks around nearby stars, including potential targets of future direct-imaging exoplanet missions such as the WFIRST starshade or HABEX/LUVOIR, to determine if their target sample includes stars with sufficiently

Each objective in turn requires observations of a different class of targets, but in all cases, the basic observation is the same. A target star will be observed by the telescope spacecraft, using the starshade spacecraft to occult the star. The mission can maintain alignment for approximately 5 minutes per orbit. A series of ten 5-minute observations allows the mission to reach a sensitivity to diffuse emission of ~22 magnitudes/square arcsceond, depending on the exact brightness of the target star. In addition, the mission observes a separate star, expected to have no circumstellar material, as a point spread function (PSF) reference, to calibrate the residual diffracted light from the target star. Appendix 9 discusses the targets in more detail.

The observations are defined by two key figures of merit: the inner working angle (IWA) and the surface brightness sensitivity. The IWA is the smallest angle at which an object or structure near the target can be well detected. The required IWA is simply set by the physical scale r that we wish to probe in target systems, and the distance d to the target star

$$IWA_{req} = \frac{r}{d}$$

If r and d have the same units, this will give IWA_{req} in radians; if r is in astronomical units and d in parsecs, this gives in IWA_{req} arcseconds.

[6]

For our typical targets, IWA_{req} is on the order of one arcsecond with a goal of ~0.6 arcseconds for Objective 3.

The surface brightness sensitivity depends on the properties of the disk, primarily the dust density and the spatial scale (in AU) of the disk. Since most of our targets have not previously been observed at mDOT wavelengths, we estimate these from longer wavelength observations or models of our own zodiacal dust; see Appendix 9 for discussion and ***Figure 3-4*** for estimates for our targets.

2.3 Impact on Mission and Instrument Design

For a starshade, IWA is set by the geometric diameter of the starshade D and its distance *z*.

$$IWA = \frac{D}{z}$$

These two parameters are also constrained by the desired contrast level of the starshade (roughly set by the Fresnel number *F*).

$$F = \frac{r^2}{z\lambda}$$

The combination of an upper limit on the required IWA and a lower limit on the Fresnel number gives a joint constraint

$$r = \frac{F\lambda}{IWA}$$

$$z = \frac{F\lambda}{IWA^2}$$

(There is also a weak dependence on the diameter of the required shadow, which is set by the telescope diameter and navigational precision.) Full-scale starshades such was the WFIRST Rendezvous proposal operate at IWA~0.1 arcseconds, F~14, λ~1 mm and hence end up with R~15m and D~60,000 km and hence require operation at locations such as the Earth-Sun L2 point. However, with a relaxed IWA, small telescope, and short wavelengths, mDOT operates in a very different regime, with a 1.5m radius starshade at ~500 km, making operation in Earth orbit practical.

The second key high-level performance requirement for the starshade is the degree of starlight suppression – the amount of light that diffracts past the starshade into the telescope shadow. We define this as the ratio of the total spectral flux arriving from a star at the starshade to the flux in the telescope plane. Detailed simulations (Appendix 9) show that a suppression of 10^{-7} allows us to achieve our primary science goals – at that suppression, the mission will be detector-noise-limited for stars fainter than ~3rd magnitude. Surface brightness sensitivity will also be set by traditional noise terms such as detector noise and local zodiacal light, driving telescope diameter/collecting area and detector properties. For the bright, diffuse circumstellar dust, a ~10 cm telescope will be able to achieve the

needed sensitivity levels. Detection of extrasolar planets would require a 20-30 cm telescope, and is not within the bounds of this study.

A final science driver is the need to observe a broad sample of targets. For mDOT, this is ultimately limited by mission delta-V capabilities as fuel is expended to align the formation on new targets and maintain position during science observations, and the interaction between the scientific drive to observe arbitrary positions in the sky and the orbital architecture which limits us to regions near the celestial equator. The mDOT architecture described here has sufficient capability to observe ~10 targets and reference stars.

2.4 Relevance to NASA

The science objectives discussed above address two key areas of potential discovery identified in the 2010 Astrophysics Science Decadal Survey: “How do circumstellar disks evolve and form planetary systems?” and “Do habitable worlds exist around other stars?”. The dust particles in young disks trace the formation process of their planetary systems, and physical properties such as size are related to the evolutionary and collisional history of the disk itself. The lower-density disks around mature nearby stars also provide clues as to their planetary systems but also represent a potential obstacle to future direct exoplanet imaging missions, where the light they scatter will increase required exposure times. The ground-based HOSTS survey with the Large Binoncular Telescope Interferometer was funded to address this mission risk by measuring thermal emission from such disks. mDOT will complement HOSTS by directly measuring the scattered visible light that is the actual noise source for exoplanet imaging, allowing LBTI observations to be converted into visible light surface brightness more precisely. A secondary demonstration objective of mDOT is to increase the technology readiness level (TRL) of starshades and satellite formation control to TRL 6 paving the way for Probe-class or epochal flagship-scale missions flying in the future such as HabEx.

6

2.5 Science Traceability Matrix

Table 2-1: Science traceability matrix.

Science Objectives	Measurement Objectives	Measurement Requirements	Instruments	Instrument Requirements	Data Products
Constrain the particle sizes of dust in young bright debris disks	B-band surface brightness of known disks	B-band surface brightness 21 magnitudes per square arcsecond Target stars B>5 mag	Starshade occulter Telescope and camera	Suppression 10^{-6} Inner working angle 1” Wavelength 400-500 nm Field of view 10” Integration times up to 50 minutes 10 cm telescope	PSF-subtracted and flux-calibrated disk images
Measure the scattered light brightness distribution of disks detected only in thermal emission	B-band surface brightness of disks to constrain IR to visible ratios Inclination and asymmetries	B-band surface brightness of 22 magnitudes per square arcsecond Target stars B>2 mag	Starshade occulter Telescope and camera	Suppression 10^{-6} Inner working angle 1” Field of view 20” Integration times up to 50 10 cm telescope minutes	PSF-subtracted and flux-calibrated disk images
Search for new dust disks in inner systems of nearby stars	Integrated B-band brightness of scattered light from dust	B-band surface brightness of 21 magnitudes per square arcsecond Target stars B>0 mag	Starshade occulter Telescope and camera	Suppression 10^{-7} Inner working angle 0.6” Field of view 4” Integration times up to 50 minutes 10 cm telescope	PSF-subtracted and flux-calibrated images Disk brightness measurements or limits

6

3 Science Implementation

3.1 Payload

The mDOT mission includes two payloads: a telescope hosted on the nanosatellite and a starshade hosted on the microsatellite. During the science phase, these are used in concert: the starshade and telescope align along the line of sight to the target star, blocking its light and allowing faint structures near the star to be visible. **Figure 3-1** shows a sample observatiobn.

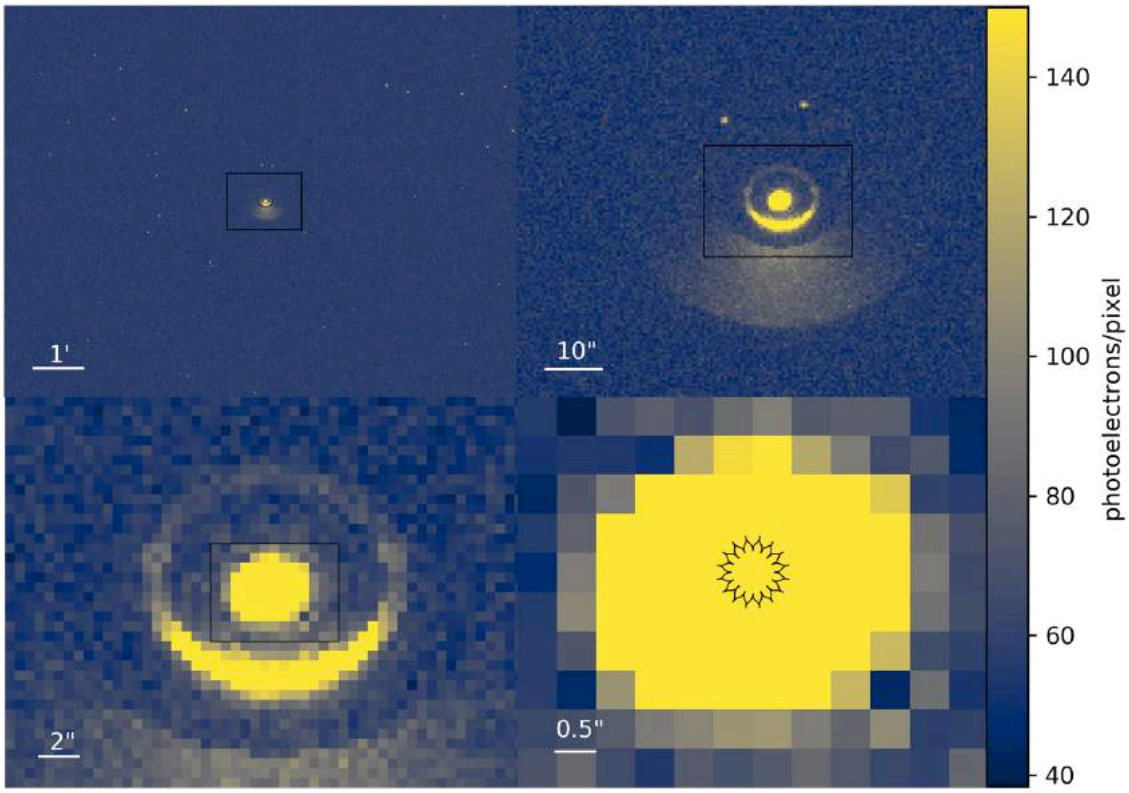

Figure 3-1: Simulated mDOT images of three circumstellar dust rings surrounding the star Epsilon Eridani (See Appendix 9.)

3.1.1 Telescope

The telescope instrument has been designed to meet the functional requirements specified on the STM (Table 2-1) which requires a resolution of 1.1 arcsec or better at 400nm wavelength.

To reduce costs, a search was conducted for off-the-shelf space telescopes with flight heritage that can be repurposed for this mission and can fit in a 4U volume including the cameras and guiding. After discussing the requirements with multiple vendors, Planet Labs offered to make available the design of their PS2 telescope for the mDOT mission. The actual design of the PS2 cannot be disclosed, but we can describe the system basic parameters. It has an aperture of 9.2cm resulting in a resolution of 1.09arcsec,

6

and field of view larger than 1 degree. For visualization purposes, Figure **3-2** shows a simplified version of the telescope with an output that matches the real design.

The telescope uses two identical Imperx Cheetah C4120 cameras with 3.45um pixels. The first one, or guiding camera, will sample the FoV and serve as a high-precision star tracker. The second camera will observe the target and will have a negative lens to reach nyquist sampling. The light will be separated using a dichroic. In this way the guider camera observes Lambda>500nm and the science camera Lambda <500nm. Both cameras will observe the entire field but with different plate scale, band, and exposure time. The guider camera images will have lower sensitivity due to shorter exposures and greater diffracted light but still could be analyzed to provide color information on bright disks. The camera can read out the entire sensor in 12bit at 14Hz, and it has a global shutter with internal and external control that allows reading out without smearing the image. As a result, no mechanical shutter is needed. The guide camera will be read out at a faster rate over a subarray portion of the image.

To stabilize the image in the focal plane and avoid smearing due to pointing error tip/tilt control we will use the Mirrorcle S6180 mirror and piezo actuated mount for the dichroic. The guiding camera will image background stars within 1 deg FoV resulting in an average of 2.1 stars mv=8 and 8.1 stars mv=9.

The pointing information from the background stars will be used to drive the Mirrorcle mirror (active fold) in front of the science camera to stabilize down to 0.2arcsec (Beierle, Norton, Macintosh, & D'Amico, 2018). In addition, the BCT XB1 bus is capable of receiving pointing information from the payload in order to improve the native S/C pointing reducing the stroke and speed of corrections in the active fold; as a design trade in future phases we will explore whether precision information from the guide camera would sufficiently stabilitize the spacecraft without the tip/tilt mirror. .

In regular operation each camera consumes 2.6W. A heat pipe connected to the S/C radiator is necessary to maintain the camera and its detector at ambient temperature.

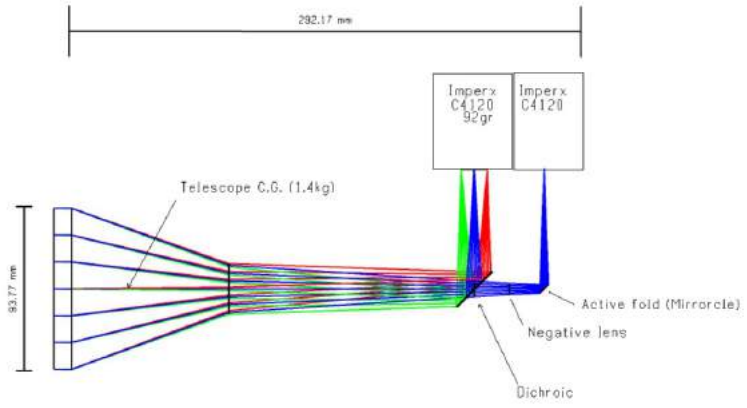

Telescope		
Aperture	9.2	[cm]
Effective f/#	9	[]
Focal length	70	[cm]
Weight	1400	[gr]
HFoV	1.484	[deg]

[6]

Camera		
Px size	3.45	[um]
Px count	4112	[px]
Mass	91.8	[gr]
FoV	1.2	[deg]
Payload mass		
Telescope	1400	[gr]
Cameras	184	[gr]
Optics	70	[gr]
Mounts	140	[gr]
Harnesses	179	[gr]
Total mass	**1973**	**[gr]**

Figure 3-2: mDOT telescope instrument diagram and key properties.

3.1.2 Starshade

The starshade payload is designed to meet the functional requirements specified in the STM (Table 2-1), which include optical contrast of 10^{-7} or better between 360 and 520 nm and an inner working angle of 0.6arcsec. The starshade design is also subject to constraints to ensure that it is realizable and compatible with the ESPA Grande ring and the mission operation concept (see Section 4.2).

Using conventional starshade scaling relations (Glassman, Lo, Arenberg, Cash, & Noecker, 2009) with a desired Fresnel number of 10 at 440nm, the designed starshade is 3m in diameter and requires a separation of 500±5km from the telescope to achieve the required contrast. The starshade includes a 1m diameter central deck mounted to the spacecraft bus and 16 petals each 1m in length. The petal shapes are computed by solving a variant of Vanderbei's optimization problem that maximizes the depth of the shadow produced by the starshade in a specified volume and bandpass (Koenig A. , 2019; Koenig, D'Amico, Macintosh, & Titus, 2015). There is a gap of 0.5mm between adjacent petals and the petal tips are 1mm wide ensure that the design can be manufactured using conventional techniques.

6

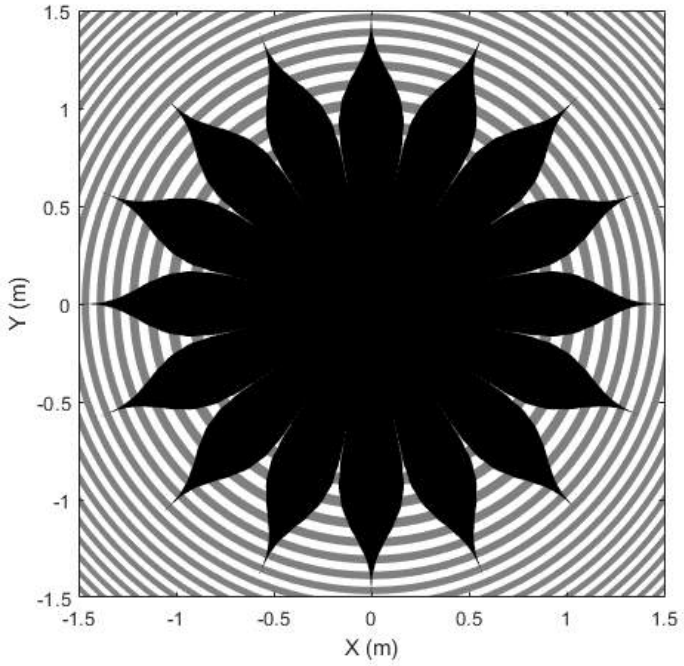

Starshade Key Properties		
Diameter	3	[m]
Deck diameter	1	[m]
Petal length	1	[m]
Petal gap width	0.5	[mm]
Petal tip width	1	[mm]
Mass	23.2	[kg]

Figure 3-3: Starshade shape including Fresnel half-zones (gray and white) and key properties.

Because the combined starshade and telescope must produce an optical contrast of 10^{-7} or better, it is necessary to ensure that the starshade is accurately manufactured and deployed. Collaborators at JPL developed a manufacturing and deployment error budget (Table 3-1) using the same model used for Exo-S (Shaklan, et al., 2010) and other full-scale starshades. Due to the relaxed contrast requirement as compared to full-scale starshades for exoplanet imaging (which require contrast of 10^{-10} or better), the mDOT starshade has more relaxed manufacturing and deployment tolerances. Specifically, the critical error mode (oscillations in the petal shape) has a tolerance of 0.1 mm, which is an order of magnitude larger than the tolerance for full-scale starshades (which call for a 10 micron tolerance (Shaklan, et al., 2010)). Due to its small size, the mDOT starshade can be constructed with fewer components, making it easier to satisfy these tolerances.

Table 3-1: Starshade manufacturing and deployment error budget.

[6]

	Name	Distribution	Tolerance (3-sigma)	Units	Contrast	Description
In-plane	**Edge Segment Shape**	random	0.2	mm	1.17E-08	Equal energy distribution in cyclical distortions of 0.5, 1, 2,…, 10 cycles per petal edge
		bias	0.1	mm	6.83-08	All petals the same
	Petal 1-cycle width preserving	random	2	mm	1.19E-10	S-shape petal deformation
	Petal quadratic bend	random	2	mm	2.70E-13	Width-preserving cantilever beam bending
	Petal radial position	random	1	mm	6.37E-09	Petal radial position relative to nominal design
		bias	0.25	mm	5.69E-09	All petals displaced the same amount
	Petal tangential position	random	2	mm	2.60E-09	Petal tangential position relative to nominal design (motion along petal base)
	Petal interface clocking angle	random	0.02	rad	1.17E-09	Petal in-plane angular orientation relative to nominal design
Out-of-plane	**Petal quadratic bend**	random	2	mm	2.34E-14	Out-of-plane tip displacement
		Bias	2	mm	2.39E-13	All petals have same displacement
	Petal rotation about base	random	0.02	rad	1.04E-14	Rigid body rotation about base (tip moves out-of-plane)
	Petal rotation about spine	random	0.02	rad	7.02E-11	Rigid body rotation about spine (petal edges move out-of-plane, one up the other down)
		bias	0.01	rad	2.28E-09	All petals rotate equally
TOTAL CONTRAST					**9.82e-08**	

To satisfy the volume constraints of the ESPA Grande ring, each petal is attached to a hinge that is folded along the body of the spacecraft bus at launch. More details on the ESPA Grande envelope and design elements that ensure compatibility are described in Section 4.2.3 Detailed description of the mechanical design information for the starshade and its deployment system can be found in Section 4.2.4.1.3.

[6]

3.2 Sensitivity

In order to accurately model the sensitivity of the mDOT instrument to extrasolar debris disks, a fiducial instrument model must be assumed, sources of noise contributions must be estimated, and brightness of the target debris disks must be estimated. The instrument properties and noise sources used for this purpose are summarized in ***Table 3-2***.

Table 3-2: Instrument properties and noise sources.

Instrument Properties		Background light and noise sources	
Starshade Suppression	10^{-7}	Light Leak	Target Magnitude - 17.5
Telescope Diameter	10 cm	Starshade backlight[1] (from Earth during daylight)	22.2 magnitudes
Optical Transmissivity	0.95	Starshade backlight (from Full Moon)	30 magnitudes
CCD Quantum Efficiency	0.65	Local Solar Zodi Foreground	22.7 magnitudes / arcsec^2
CCD Size (angular FOV)	1280 x 960 pixels (10.65' x 7.98')	CCD read noise	5 electrons RMS
Filter Wavelengths	400-500 nm	CCD dark current	0.01 electrons / pixel / second

The detailed modeling of the instrument sensitivity and of the estimated brightness of the science targets is discussed in Appendix 9.

[1] Earthshine reflecting off the starshade assuming an albedo of 0.1; this can be controlled by observing during Earth shadow passage.

[6]

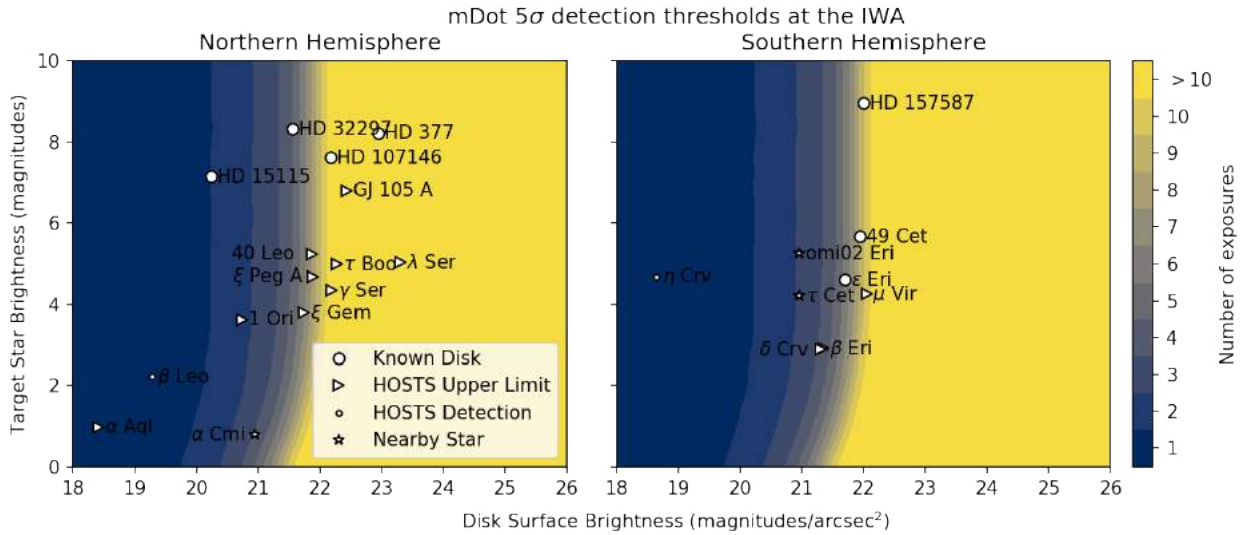

Figure 3-4: Number of 5-minute science exposures required to detect a given B-band surface brightness at IWA as a function target star brightness. Targets from the northern and southern DRMs are plotted.

Figure 3-4 shows the sensitivity of the instrument, plotting the number of 5-minute science exposures (orbital passes) required to reach a given sensitivity level expressed as a 5-sigma limit per square arcsecond. For B>4 mag, observations are limited by detector noise (and hence are independent of star brightness); for B<4 mag, at the inner working angle sensitivity is limited by the light diffracting past the starshade. A broad range of targets are accessible. These exposure times were used to construct the design reference mission target lists.

3.3 Science mission profile

Section 4 discusses the operation phases of the mission. During the science phase the mission executes science observations of a series of targets. Before observations of a target, the formation is configured so that the starshade and telescope spaceraft are aligned with the target as the formation crosses the equator and the telescope is oriented to point at the science target. During each pass, the occulter spacecraft maneuvers by firing its thrusters to maintain the alignment so that the telescope spacecraft is located in the dark shadow region. These observations will typically also be carried out in earth shadow to minimize earthshine reflected by the starshade and sunlight diffracted from its edge. A typical science exposure lasts five minutes, before the relative acceleration becomes too great to maintain the formation. After the pass, thrusters are used to offset the spacecraft and prepare for the next pass. During a single pass, the science detector on the telescope spacecraft carries out a long exposure on the target. To avoid light from thruster firings contaminating the image, the camera will be (briefly) shuttered during each maneuver.

The sun-synchronous orbit precesses by approximately 1 degree per day. After two to ten passes, the orbit has precessed sufficiently that the target is no longer observable and the science phase for that target ends. The individual images from the science passes are downloaded for ground processing. The spacecraft then configure themselves for the next target and observe it after the field of regard has precessed sufficiently. Over the course of the mission the field of regard shifts eastward, allowing a series of targets to be observed. However, targets must have a declination relatively close to +9 or -9 degrees – the inclination of the sun-synchronous orbit; targets too far north or south will produce large

relative accelerations between the spacecraft and require prohibitive amounts of fuel. Which declination range is accessible (north or south of the equator) depends on the time of launch and LTAN; we have evaluated both northern and southern DRMs with the northern set used as a baseline.

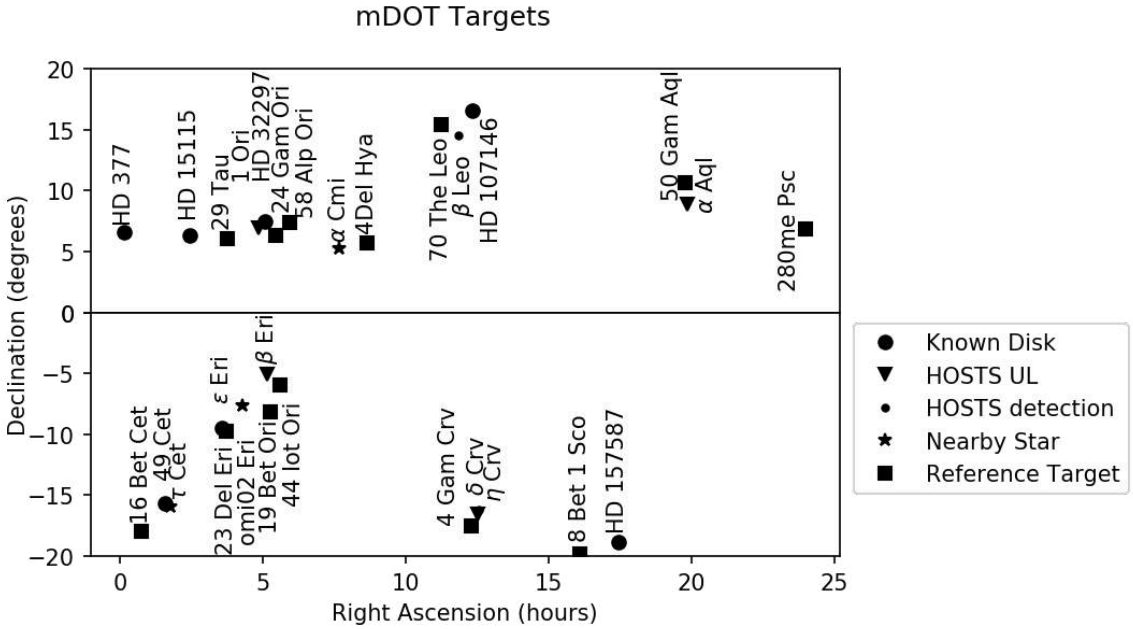

Figure 3-5: Location of potential targets for a northern or southern mission profile. .

3.4 Calibration

Before or after each science target we will also observe in starshade mode a point spread function (PSF) reference target at a similar location in the sky to measure the light diffracting past the starshade. Typically these will be brighter than the science target to minimize necessary integration time.

To calibrate the optical properties of the telescope, the mission will obtain out non-occulted images (i.e. using only the telescope spacecraft) of star fields containing stars of known brightness to measure the instrumental throughput, telescope point spread function, and plate scale. Since these observations do not use the starshade they do not consume fuel, and are not listed in the DRM target lists – scheduling will be set based on the phasing of the mission orbit.

Detector properties such as flat-field will be calibrated during ground testing. Instrumental dark current will be measured on-orbit during the period between science passes.

3.5 Data Analysis Approach and Ground Data System

The Ground Data System (GDS) provides the software, hardware, facilities, and networks necessary for designing operations, as well as implementing and conducting the mission. The nature of mDOT does not require special GDS due to its LEO orbit and data throughput. The most demanding part of the mission lies in its autonomous navigation and control functionalities. While it is common that GDS supports this, mDOT navigation and control requirements demand for a transfer of these tasks from GDS to the onboard software. Because of this, GDS only needs to support the onboard processing and verify calculations including calibration, therefore nominal configuration is adequate for this design but should be revisited through design phases. Beyond this, there is no need for additional support. Therefore, a

standard mission operations center is acceptable. Since the majority of the design is custom, and build and test operations will be performed on the NASA Ames campus, it is logical to co-locate hardware expertise during operations. The NASA Ames Multi-Mission Operations Center (MMOC) has a history of flying SmallSat missions, such as LCROSS, Kepler, LADEE, and IRIS, and the upcoming Starling1 mission (Sanchez, et al., 2018) in collaboration with Stanford. Data files, products, archive, and analysis among others will be handled in a similar manner as the aforementioned missions and/or will be transferred to Stanford for data analysis which is nominal for the MMOC. For more information on the MMOC see Section 4.2.2.2.

Science data will be archived at Stanford using the data architecture developed for the Gemini Planet imager (GPI), and processed with an adapted version of the GPI data reduction pipeline, simplified to support the direct imager of mDOT rather than GPI's integral field spectrograph.

4 Mission Implementation

The miniaturized Distributed Occulter/Telescope (mDOT) will provide direct measurements of brightness of extrasolar dust disks in the near-ultraviolet spectrum. This is done through a controlled formation of two spacecraft, a Starshade Spacecraft (SS) and a Telescope Spacecraft (TS), in sun-synchronous low Earth orbit (>500 km altitude, ~98deg, Noon/Midnight LTAN - Local Time of the Ascending Node). The spacecraft are launched together as a single secondary payload compatible with the ESPA Grande ring for a total mission lifetime of 1.1 years. The TS is later deployed from the SS as is discussed in Section 4.2.1.1. It is noted that the mission concept is compatible with LTANs other than noon/midnight as long as one of the nodes of the SS and TS orbits is in eclipse. This corresponds to LTANs of 9AM/9PM-3PM/3AM.

4.1 General Requirements and Mission Traceability

The Mission Traceability Matrix (MTM), Table 4-1, provides, as a basic systems engineering tool, a logical flow from mission functional objectives through mission design requirements, spacecraft and platform requirements to operational requirements. For the MTM below, the mission functional requirements were derived from the mDOT Study Proposal document. Spacecraft and operational requirements were then developed to drive the overall system design and concept of operation. The driving requirement for mDOT is the ability for the SS to maintain its relative position with respect to the TS to within ± 15 cm during each Observation.

6

Table 4-1: mDOT Mission Traceability Matrix.

Mission Functional Requirements	Mission Design Requirements	Spacecraft/Platform Requirements	Operations Requirements
Optical contrast of 10^{-7}	A starshade casting a starlight shadow on an observer telescope orbiting in controlled formation and aligned with target star	• Starshade Spacecraft (SS) with 3 m starshade capable of maintaining its cross-track distance from the Telescope Spacecraft (TS) within 500±5 km during observation period. • SS capable of autonomously determining its relative position with respect to the TS to 2 cm (3D, RMS). • SS capable of autonomously maintaining its relative position with respect to the TS to within +/-15 cm, max. • SS capable of obtaining real time position knowledge of TS • SS and TS to conduct observation in eclipse	• Monitoring of TT&C, health monitoring • Post-processed relative navigation accuracy of 2 cm (3D, RMS) for performance verification during observation phase • Post-processed relative position control accuracy of ± 15cm max during observation phase • Nominal planning cadence to preplan two weeks' activities
Inner working angle <1''	Baseline separation between spacecraft is 500 km in cross-track direction with science spectrum of interest of ~400 nm	• SS to deploy a 3 m starshade and be observed by the TS • SS capable of adjusting orbit relative to telescope by 500 km (4^{o} shift in orbit plane) during initial formation acquisition	• Processing of TS payload telemetry • Processing of TS and SS navigation data to confirm formation relative positions • SS and TS conduct observations during equatorial crossing
Signal-to-noise-ratio>10	The telescope shall be able to image dust disks with a surface brightness of 21 mag/arcsec^2.	The TS carries a 10 cm RC telescope design capable of achieving a Nyquist sampling of 400 nm and a resolution of 1 arcsec.	• SOC verifies science data quality after each Observation and adjusts observation parameters for the next target

6

Cumulative Exposure time 5-25 min	The formation relative motion must be controlled during target star observation to within ±15 cm lateral (perpendicular to line-of-sight) and to within ±5 km longitudinal (along line-of-sight)	• SS to determine RAAN difference to achieve a cross-track separation of 500 +/- 5 km during observation period. SS to be able to quickly compute its next position and maneuver to maintain the 30 cm diameter shadow perpendicular to the LOS. • TS to maintain its pointing attitude throughout each Observation. • TS memory to store all image data taken	• Science Planning to accommodate Multiple Observations per target, where Observations are conducted during consecutive orbits • Science Data Volume of 10-600 MB per Observation
Stability of image 0.2”	Telescope camera to avoid point spread function smearing due to pointing errors and jitter	• TS pointing accuracy better than 0.45 deg ensures the placement of the target star within the telescope FOV (0.90 deg). Orbit altitude of >500 km minimizes atmospheric induce jitter. • Telescope pointing jitter of less than ~10”	• SOC verifies science data quality
Multiple targets +/- 10 deg from nominal declination	The absolute and relative orbits must be selected to ensure that the SS propulsion system can support the observation of at least 10 science targets, this implies Reconfigurations to align the formation with different targets (declination changes are active while right ascension changes are passively acquired)	• 800 m/s Delta-V required. • Resultant thrust vector acts as closely as possible through SS CM	• Mission replanning to address off-nominal target Observations (within ±10deg declination off nominal declination) to minimize propellant expenditure for orbit reconfiguration • Different Target Configuration maneuver planning • SOC verifies science data quality

[6]

Repeated observations of same target (1-10)	Reconfigurations to align the formation with the same target one orbit later (i.e., for repeated observations)	• SS has knowledge of TS current position and the target star • SS can maneuver to the occulting position along the line-of-sight between TS and target star • TS transmits its GNSS raw measurements and navigation data to the SS so that the SS can plan and execute thruster firings accordingly	• MMOC and SOC/Mission planning for Same Target Formation acquisition • Same Target Configuration commands uplinked prior to start of target Observation (sequence must cover all successive same target Observations)

[6]

4.2 Mission Concept

4.2.1 Mission Design

4.2.1.1 Mission Operations Phases

Mission operations for mDOT are divided into six phases: 1) Launch, 2) SS deployment and commissioning, 3) TS deployment and commissioning 4) Formation acquisition, 5) Science, and 6) Decommissioning. Table 4-2 includes the major events that the mDOT spacecraft would experience during each of these phases of the mission life cycle. The state of the formation during each of these phases is illustrated in Figure 4-1. Advancing to the next mission phase requires that all activities associated with the current mission phase have been performed and satisfied. Phase duration is an estimation based on the number and complexity of events that need to be executed during the phase.

Table 4-2: mDOT Mission Operations Phases.

Mission Phases	Duration	Segment/Events
Launch	<1 day	-Stowed Starshade Spacecraft (SS) is carried into SSO attached to ESPA Grande -Primary payload is released
Starshade Spacecraft Deployment and Commissioning	2 weeks	-ESPA Grande releases SS into SSO - SS conducts validation and calibration process for subsystems, including ADCS sensors, actuators, and propulsion system -SS conducts communications and data exchange with MMOC
Telescope Spacecraft Deployment and Commissioning	1 week	-SS ejects TS in cross-track direction per ground command - TS conducts validation and calibration process for subsystem (including ADCS sensors). -Instrument calibration and verification -TS conducts communications and data exchange with SS and MMOC
Formation Acquisition	4 weeks	-SS maneuvers to achieve 500 km cross-track separation from TS through a difference in RAAN -SS and TS perform relative navigation to simulate their performance during target star observation

6

Science	11 months	-At least 10 target stars identified, their observations scheduled, number of revisits established, observation durations estimated -SS and TS conduct **Different Target Formation Reconfiguration** for the observation of the next target star -**Observation**: TS captures image data of the target star while shadowed by the starshade -SS and TS conduct **Same Target Formation Reconfiguration** for the next revisit of the same target star during the next consecutive orbit -Downloading of image data, health and orbit data and uploading of SS and TS updated commands are performed per schedule -During non-Observation periods, TS conducts target pointing to test and calibrate camera sensitivity, image quality, etc.
Decommissioning	1 week	-SS is commanded to fire its thrusters to reduce its velocity for gradual reentry -TS is commanded to orient its solar arrays in the velocity direction to increase drag for gradual reentry -Science data processing, archival, and publication

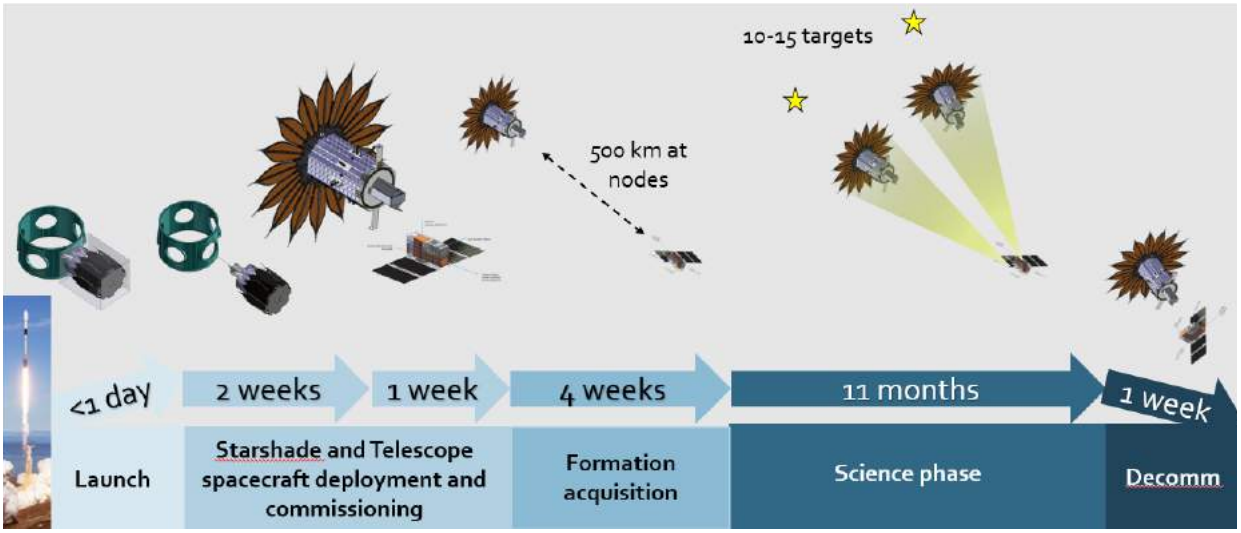

Figure 4-1: mDOT mission operations phases.

Launch Phase

At launch, the 6U NanoSat TS will be stowed inside the NanoSat deployer onboard the larger 255 kg SmallSat SS, forming the mDOT secondary payload. The mDOT payload attaches to an ESPA Grande launch adapter for ridesharing with a primary payload for launch to a sun-synchronous orbit (SSO). Both the TS and SS are stowed with both battery power and RF transmissions inhibited. For this study, mDOT

[6]

performance evaluation is based on a 600 km SSO orbit with a noon/midnight LTAN (see Section 4.3.3 for further explanation).

Starshade Spacecraft Deployment and Commissioning

Once ejected from the ESPA Grande, the SS power subsystem is activated by the release mechanism, which in turn provides stand-by power to the other subsystems. The SS remains in stowed configuration and may experience tumbling while it develops some distance from the stage. Note that the SS was fully charged prior to integration, and the partial battery charge is sufficient for this short segment of the mission. After an elapsed time of about 100 seconds (and resulting 100-meter distance from the ESPA ring), the SS deploys the starshade petals, fully exposing the star trackers, sun sensors, and the radial and tangential thrusters to space. The deployment is a one-time deployment; after confirmation of starshade deployment and alignment verification, the motor is shut down for the remainder of the mission (see Section 4.2.4.1.3). The ADCS (Attitude Determination and Control System) performs position and attitude determination. If the SS happens to be tumbling, the ADCS issues reaction wheel-based attitude control commands to detumble the spacecraft. Once the spacecraft has attained 3-axis stability, the SS then orients the body-mounted solar panels toward the sun. The spacecraft communicates with the KSAT network of Ground Stations (the baselined NASA Near Earth Network asset for this study) via S-band to downlink its orbit parameters and health status. Ground operators evaluate the data received and uplinks updated spacecraft commands. The uplinked commands are stored in the spacecraft on-board computer memory for execution at specified times or conditions. Ground communication is a scheduled event and can occur only when the spacecraft have a line-of-sight to the ground station.

The SS performs check-out tests by executing a series of commands to verify that all subsystems are performing per specification, including data transfer and communication to the ground as a part of the commissioning process. Successful demonstration of these verification tests, including its ability to (at a later time) communicate with the free-flying TS and to perform maneuvers in response to TS measurements and navigation data inputs, completes the commissioning process. The commissioning phase includes the calibration of the propulsion system on the SS.

Telescope Spacecraft Deployment and Commissioning

After the MMOC has confirmed successful commissioning of the SS, it schedules the command sequence which will deploy the TS in the cross-track direction using the 6U ISIS DuoPack CubeSat Deployer housed within the SS.

Immediately after exiting the 6U dispenser, the TS generates power from its body-mounted solar panels. The deployable solar arrays are released after a timer elapses to minimize recontact risk with the SS. After the ADCS has stabilized the spacecraft and battery top-off is complete, the TS conducts vehicle checkout to verify the functionalities of the subsystems. The telescope payload assembly, which includes its control electronics, camera, and cooling unit (Thermal Electric Cooler), will perform a series of tests to verify that its science instruments are performing as specified. In addition, the TS performs crosslink communication with the SS by sending and receiving data at 220 kbps (maximum radio capability) in S-band. Through ground command, the TS will conduct target pointing to determine its pointing control and accuracy.

6

Formation Acquisition

After successful deployment of the TS, the SS performs a sequence of cross-track maneuvers such that after four weeks the two spacecraft have built a cross-track separation distance of 500 km through a difference in RAAN. During this separation period, the SS and TS conduct crosslink communication tests to verify their S-band connectivity. The SS receives from the TS the TS raw GNSS measurements and navigation data while it transmits its computed thruster firing times and durations to the TS in parallel. Additionally, the ground segment downloads captured images from the TS and provides high-level guidance commands to the SS and TS for to verify that the formation can align with a specified target with the required 10cm accuracy. Successful demonstration of crosslink communication and formation alignment at the nominal separation certify that both spacecraft are ready to proceed to Science phase operations.

Science Phase

The majority of the mission lifetime is spent in the Science phase, where target star observation is conducted while the spacecraft are in eclipse (see Figure 4-2). Science phase operations are divided into Observation Sequences and Different Target Formation Reconfigurations. Each Observation Sequence consists of a set of Target Star Observations which are 2 to 5 minutes in duration and centered at the ascending or descending node (depending on LTAN). The number and duration of these observations is pre-computed and uploaded to the formation via telecommand. The planning process for each Observation Sequence accounts for the predicted durations of camera shutterings due to thruster firings. Between the Target Star Observations, the SS performs a sequence of maneuvers to re-align the formation with the target star.

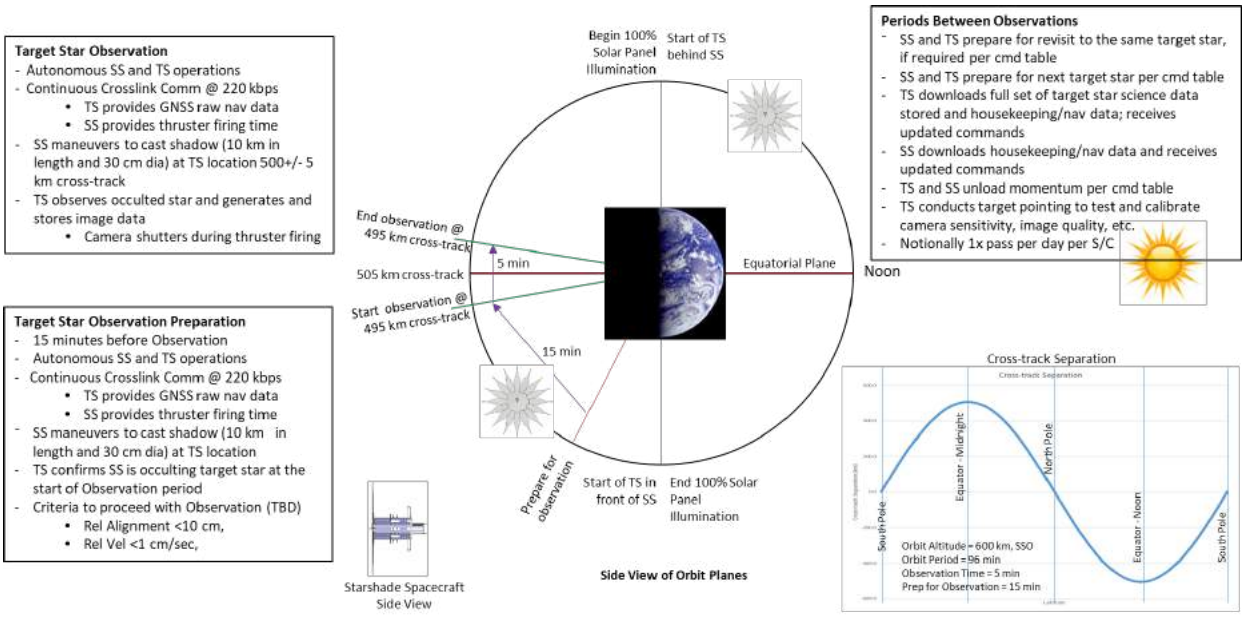

Figure 4-2: mDOT Concept of operations during Science phase.

A Target Star Observation Preparation is conducted 15 minutes before the start of each observation. During this period, the TS transmits raw GNSS measurements and navigation data to the SS at 220 kbps. This enables the Distributed multi-GNSS Timing and Localization (DiGiTaL) (Giralo & D'Amico, 2018)

navigation system to compute relative state estimates with the centimeter-level accuracy. Using these state estimates, the SS maneuvers to ensure that the TS is in the shadow produced by the starshade. The shadow is 500 km from the starshade along the line of sight (LOS) and is 30 cm in diameter (in the plane perpendicular to LOS) and 10 km in length (along the LOS). Additionally, the reaction wheels on the TS are used to align the boresight of the telescope with the target star and stabilize the attitude so that the tip/tilt mirror can stabilize the image in the science instrument. Before the start of the Target Star Observation, the SS verifies that the formation is properly aligned (relative position error of ≤10cm and relative velocity error of ≤ 1 cm/s in plane perpendicular to LOS) and the TS verifies that the starshade is occulting the target star. If both of these criteria are satisfied, the formation begins the Target Star Observation.

During a Target Star Observation, the TS continues transmitting raw GNSS measurements and navigation data to the SS to enable accurate relative navigation. The SS uses the state estimates from DiGiTaL to plan maneuvers using the radial and tangential thrusters to keep the telescope within the shadow produced by the starshade. The starshade primarily maneuvers in the radial direction to counteract the relative acceleration perpendicular to the LOS between the spacecraft, thereby keeping the telescope inside the 30 cm diameter shadow. In parallel, the SS sends its computed thruster firing times to the TS. The telescope Camera uses the thruster firing times to synchronize its shuttering action to prevent plume flashes from contaminating the occulted star image. Once either the TS leaves the boundary of the shadow or a specified time has passed, the current Observation ends.

At the conclusion of an Observation Sequence, the SS performs Different Target Reconfiguration for the next target star scheduled in the command table. During these periods, the spacecraft download science and navigation data to the ground, desaturate the reaction wheels using the magnetorquer rods, and conduct periodic camera calibrations. The process for preparing, conducting, and exiting target Observation is repeated for each target star. mDOT is expected to observe at least ten target stars during its mission life of 1.1 years. There is no driving science data latency requirement, so science data collection is opportunistically scheduled with the NEN, notionally at the conclusion of each same target star Observation set.

Figure 4-3 below illustrates the concept of operation of the mDOT system elements during the Science Phase of the mission. All activities performed by the SS and TS are planned and coordinated by the Multi-Mission Operations Center (MMOC), with inputs from the Science Operations Center (SOC), by uploading updated command tables to both spacecraft. SS and TS execute these commands autonomously until the MMOC intervenes or uploads new command tables. Both spacecraft receive GNSS signals from GPS, Glonass, and Galileo constellations to generate their GNSS measurements and navigation data. The KSAT ground station in Norway serves as a link between the spacecraft and MMOC. Ground communication to downlink data and uplink updated commands is a coordinated event and is performed one spacecraft at a time. Stored image data and spacecraft health status data are transmitted to the Ground at 3.3 Mbps in S-band.

6

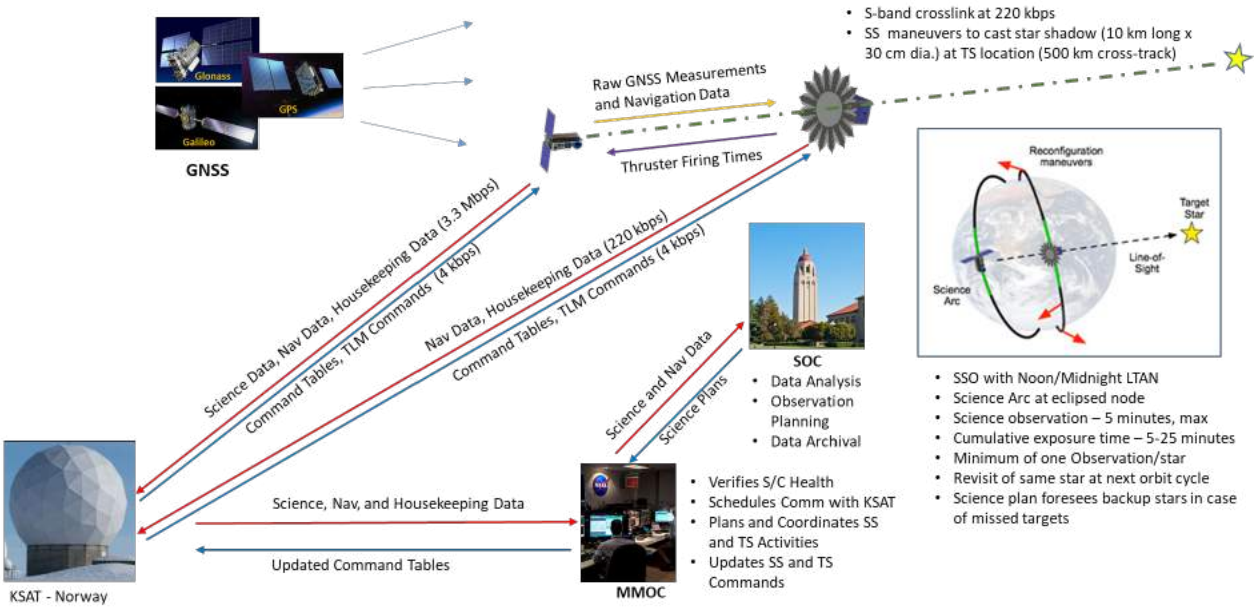

Figure 4-3: mDOT mission architecture.

Decommissioning

At the end of the mission, ground control will issue final commands to the TS and SS. The TS is commanded to orient its solar panels in the velocity direction and the SS is commanded to orient the starshade in the velocity direction to maximize the effects of atmospheric drag on the spacecraft, causing a gradual reentry. The SS is commanded to perform a sequence of maneuvers once per orbit opposite the velocity direction until the remaining propellant is depleted, accelerating reentry into the atmosphere. The SS will be commanded to execute maneuvers opposite the velocity direction once per orbit until the remaining propellant is depleted. This will decrease the perigee altitude of the spacecraft orbit, accelerating its reentry into the atmosphere. See Section 4.3.3.1 for a discussion of the preliminary lifetime analysis performed.

4.2.1.2 Orbit Design & Target Visibility

The absolute orbit of the mDOT mission is an SSO (~98deg inclination) with a local time of the ascending node (LTAN) between 9AM-3PM or 9PM-3AM. This orbit was selected to ensure that one of the nodes is always in earth's shadow. Observations are performed at this node to ensure that the starshade is not illuminated by sunlight or earth albedo during observations, thereby minimizing the noise in images collected by the camera. SSOs are also desirable orbits for a wide range of earth observation missions, providing many launch opportunities. The nominal altitude of the orbit is 600 km to minimize the effects of differential drag on the formation while still allowing passive de-orbit within 25 years if the spacecraft maximize their area in the velocity direction at decommissioning (Section 4.3.3.1). The requirements and nominal parameters for the orbit are provided in Table 4-3.

Table 4-3: Absolute orbit requirements.

Requirement	Limits	Nominal Value
Orbit altitude (km)	≥500	600
Eccentricity	Any	0.001

6

Science mission duration (yr)	≥1	1.1
LTAN	9AM-3PM or 9PM-3AM	12AM

We have previously demonstrated that the delta-v cost of observing a target star using a formation in earth orbit can be reduced by only performing maneuvers to counteract the relative acceleration perpendicular to the line of sight during observations, allowing the inter-spacecraft separation to passively drift (Koenig A. , 2019; Koenig, Macintosh, & D'Amico, Formation Design of Distributed Telescopes in Earth Orbit for Astrophysics Applications, 2019). The shadow produced by the starshade is long enough (10 km) to enable observations up to five minutes in duration in LEO. The delta-v cost can be further reduced by ensuring that the formation is aligned primarily in the positive or negative cross-track direction when observations are performed such that the starshade and telescope orbits have equal semimajor axes. To maximize the number of targets mDOT can observe, the formation alignment is allowed to deviate by up to 10^{o} in the (anti-)along-track direction during observations (see green cone in Figure 4-4). While increasing the separation in the along-track direction increases the delta-v cost of observing a target, this effect is mitigated by properly selecting the number and duration of observations (Koenig A. , 2019). Using this approach, the formation can be aligned with a science target with a specified right ascension and a declination in the range of -18^{o} to 2^{o} (Figure 4-4 left) or -2^{o} to 18^{o} (Figure 4-4 right) at any time, depending on the sign of the cross-track separation at the node in eclipse.

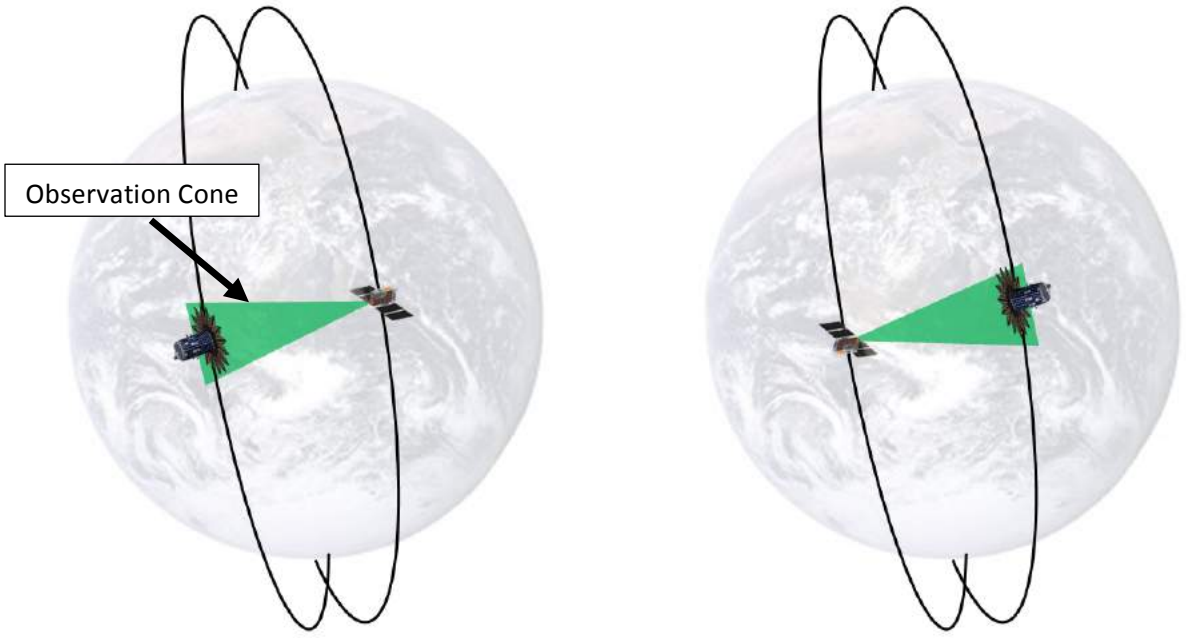

Figure 4-4: mDOT relative orbits for observing targets in the southern celestial hemisphere (left) and northern hemisphere (right).

Because the RAAN of the absolute orbit drifts over time due to earth oblateness, the formation passively aligns with science targets with different right ascension. Accordingly, the delta-v cost of aligning the formation with a different target primarily depends on the difference in declination. With this in mind,

[6]

Figure 4-5 shows the portions of the sky that can be imaged in science plans focusing on the northern hemisphere (red) and southern hemisphere (blue) including known targets of scientific interest.

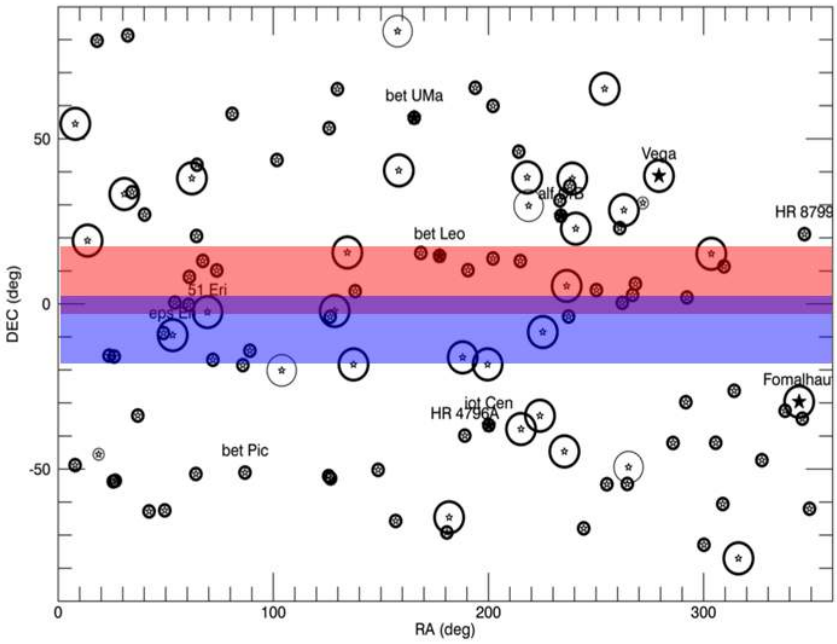

Figure 4-5: Candidate science targets for mDOT variants focusing on northern hemisphere (red) and southern hemisphere (blue).

As demonstrated in Appendix 9, there are sets of targets in both the northern and southern hemispheres that satisfy the science objectives of the mission. It is hereafter assumed that the baseline mission uses the northern hemisphere science plan for simplicity.

To minimize the delta-v cost of the mission, each target is observed then the pointing vector is as close as possible to the (anti-)cross-track direction, which also ensures that the orbits of both spacecraft have the same semimajor axis. It follows that the relative orbit of the formation includes a 4^o offset in RAAN with small differences in the mean anomaly and eccentricity vector. During each observation of a target, the inter-spacecraft separation passively drifts between 495km and 505km.

Next, it is necessary to consider the safety of the formation. Passive collision avoidance can be ensured using the well-known relative eccentricity/inclination (e/i) vector separation technique (D'Amico & Montenbruck, Proximity Operations of Formation Flying Spacecraft using an Eccentricity/Inclination Vector Separation, 2006). Using this method, a user-specified separation in the plane perpendicular to the flight direction by constraining the relative eccentricity and inclination vectors to be (anti-)parallel. Because the relative inclination vector (which includes the difference in RAAN) is so large for mDOT, it is evident that the point of closest approach is over the poles. Accordingly, it is sufficient to demonstrate that the magnitude of the relative eccentricity vector is larger than the expected difference in the semimajor axis of the orbits (≤3km including combined effects of maneuvers and precession of the absolute orbit over a 10-orbit observation sequence). To ensure a minimum separation of 1km, which is deemed sufficient to ensure passive safety in the event of an extended loss of maneuvering capability, it is necessary to ensure that the angle between the pointing vector to the target and the cross-track direction is at least 0.35^0. Figure 4-6 shows the evolution of the relative position in the radial/cross-track

[6]

plane over one orbit for formations configured to observe targets with 0.35° (blue), 0.5° (red) and 1° (yellow) offsets in the (anti-)flight direction. It is evident from this plot that the minimum separation is 3km for the target with a 0.35° offset, which is sufficient to guarantee a 1km separation with the worst-case difference in the semimajor axis of the orbits. Increasing the along-track offset monotonically increases the minimum separation between the spacecraft.

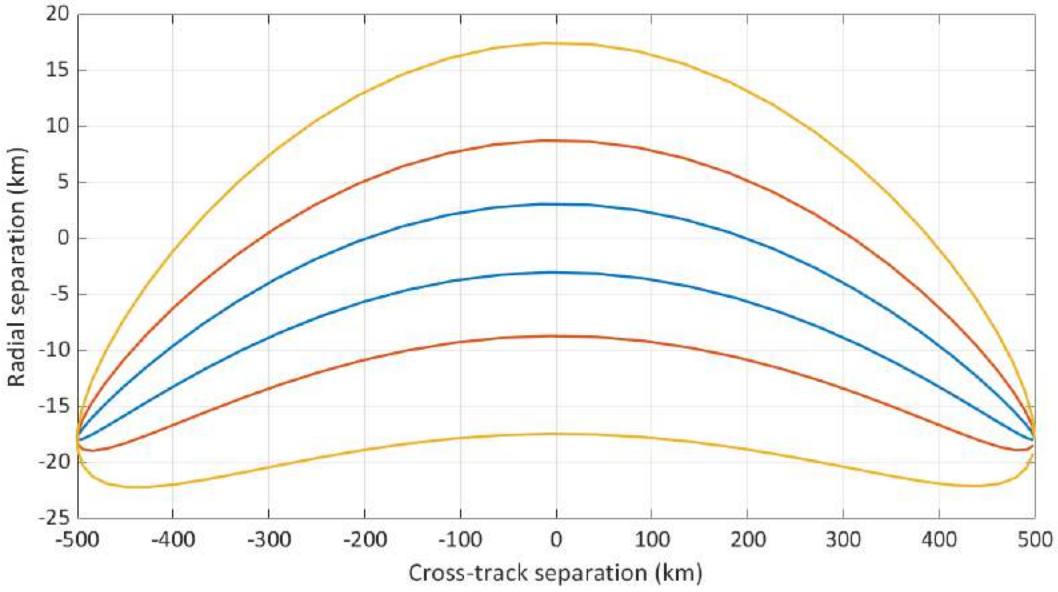

Figure 4-6: Evolution of relative position in radial/cross-track plane for one orbit following observations of targets with 0.35° (blue), 0.5° (red), and 1° (yellow) offsets in the (anti-)flight direction.

The delta-v budget for mDOT is provided in Table 4-4.

Table 4-4: Mission delta-v budget.

Allocation	ΔV (m/s)	Burn Duration (min)
Formation Acquisition	275	107
Science Phase	400	133
Safe Modes	25	8
De-Orbit	50	16
Margin (25%)	190	-
TOTAL	940	264

The delta-v budget for the science phase was validated by conducting high-fidelity simulations of the mission for the science plan described in Appendix 9. These simulations include navigation errors, dynamics modeling errors, and maneuver execution errors consistent with the performance of the DiGiTaL navigation system and ECAPS thrusters. The control logic used in these simulations described in detail in (Koenig A. , 2019) and is similar to that described in Section 4.2.4.1.8.3. The breakdown of the delta-v costs of Science Phase operations for this simulation is provided in Table 4-5.

[6]

Table 4-5: Science Phase delta-v budget.

Target Star	Observations (m/s)	Same Target Reconfiguration (m/s)	Different Target Reconfiguration (m/s)
alf CMi	11.6	3.7	13.2
16Zet Hya	24.4	22.1	33.2
70 The Leo	13.0	3.3	17.0
Beta Leo	3.2	0.0	15.4
HD 107146	34.8	21.2	28.7
50 Gam Aql	34.4	21.2	7.6
alpha Aql	4.8	1.8	14.1
HD 15115	4.0	0.6	10.5
29 Tau	4.3	0.8	8.0
1 Ori	8.7	5.7	3.2
HD 32297	8.1	6.0	4.7
24 Gam Ori	1.8	0.0	5.1
58 Alp Ori	0.9	0.0	-

4.2.2 Mission Operations Concept

mDOT has multiple phases as described in Section 4.2.1.1. All activities performed by the SS and TS are planned and coordinated by the ARC Multi Mission Operations Center (MMOC), with inputs from the Science Team, by uploading updated command tables to both spacecraft. SS and TS execute these commands autonomously until the MMOC intervenes or uploads new command tables. Both spacecraft receive GNSS signals from GPS, Glonass, and Galileo constellations to generate their GNSS measurements and navigation data. The (NEN) KSAT ground station in Norway serves as a link between the spacecraft and the MMOC. Ground communication to downlink data and uplink updated commands is a coordinated event and is performed one spacecraft at a time.

In preparation for launch and operations, the operations team will perform hardware-in-the-loop compatibility testing, perform simulations and training exercises of the mission lifecycle, and verify documentation.

4.2.2.1 Mission Operations

The mDOT MMOC personnel develop procedures to ensure that operations are conducted in a reliable, consistent, and controlled manner using lessons learned during the mission and from previous missions. To maximize efficiency and quality, Mission Operations implements proven techniques and processes from prior missions. The development process includes reviews that require presentation of relevant lessons identified from the NASA lessons learned database and their application to the subject material of the review. mDOT's operational staff has mission operations or ground system experience on previous missions. Further, most operators are selected from mDOT team members who have conducted I&T or worked on mDOT spacecraft subsystems. This approach reduces the need for staff training on spacecraft subsystems or standard operational protocols. Only the operational tools,

processes, and procedures specific to mDOT need to be learned and rehearsed, and many of those are learned incrementally through iterative GDS tests and MOS simulations. Prior to launch, the GDS is fully developed, tested, and passes operational readiness tests. MOS operator training focuses on the launch phase, deployment, orbit transfer, commissioning and science operations, with GDS personnel supporting the simulations. Six months prior to commissioning, staffing increases to support scaled operational readiness tests and increased operator training prior to deployment, commissioning, and science operations.

4.2.2.2 Mission Operations Center

mDOT Mission Operations are conducted in ARC's MMOC, which has extensive experience supporting missions using the NEN (such as KSAT) and has been used to fly many LEO missions (in addition to lunar missions). The MMOC is composed of the facilities, networks, IT equipment, software, and system administration services needed by flight projects to effectively and efficiently perform all mission functions, including planning, scheduling, command, telemetry processing, and science analysis. The MMOC can accommodate a wide range of software and hardware, including those required for LEO missions. In recent years, ARC has flown SmallSat missions, such as LCROSS, and LADEE, as well as the larger Kepler and IRIS missions. The MMOC enables and supports flight and science operations for ARC spaceflight missions. The MMOC's ready-to-use (turnkey) services reduce start-up time and shorten procurement and provisioning. The MMOC facilities and data systems are FISMA-compliant and operated in accordance with a NASA-approved security plan (CD-9999-M-ARC-3234). The ARC Mission Network pairs with NASA's restricted IONet and CSO PIP/SIP networks, enabling secure connectivity to ground stations on the Near Earth Network. The MMOC will accommodate any command and telemetry handling software required by a mission and has historically supported ASIST, ITOS, OASIS, TREK and InControl. The MMOC also supports custom-designed science data pipelines for a variety of projects ranging from the capture of image data for IRIS to the complex, multi-terabyte system that produces derived science products for Kepler. While not currently planned for mDOT, Remote Operations Centers (ROCs) and facilities at other sites can be implemented for Spacecraft subsystem support and analysis to ensure access to expertise during critical operations. The MMOC provides secure network, telemetry and voice connectivity between the MMOC and ROC. Interfaces to the ROC are provided by the MMOC and managed under the MMOC FISMA security plan. Simulators and testbeds are a joint development and implementation activity between the Spacecraft and MOS/GDS (Mission Operations Systems/Ground Data Systems) teams. Requirements are jointly established and phased schedules are implemented to ensure availability and support when required. Both the Spacecraft and MOS/GDS teams have budget allocations and schedules within the integration master schedule (IMS) for the necessary development and implementation.

4.2.2.3 Ground Software

Table 4-6 lists the key software products used in mDOT operations. Ground software is developed, tested, and maintained under the guidance of ARC's Intelligent Systems Division. The Intelligent Systems Division, with the support of the NASA Office of the Chief Engineer Capability Leadership Team for Software, maintains a Capability Maturity Model Integration (CMMI) Maturity Level 2 rating. Since mDOT is a Class D mission, the CMMI appraisal and rating is not required. However, mDOT benefits from the CMMI appraisals and processes at ARC and could easily meet such a requirement. Software classifications is determined using the 7150.2B SWE-020 Guidelines and by using the Software Engineering Handbook (SWEHB) Interactive Classification Tool. The resulting classifications then undergo

[6]

independent software classification by Software Assurance. The GDS software is expected to be Non-Safety Critical since the Spacecraft launches powered off, and there are lockouts throughout the pre-launch and launch phases of the mission. Because of the heavy reliance on COTS, GOTS, and established systems, maintenance to the software and systems is not expected to be extensive. When a change is required during the mission, changed components are rolled into a point release, tested, approved, and only then deployed to operations. All changes, as well as the current version descriptions, are configuration controlled in accordance with the GDS Software Configuration Management Plan.

Table 4-6: Software products used in mDOT mission.

Computer Software Configuration Item (CSCI)	Description
Telemetry and Commanding	Used for commanding the Spacecraft and connecting to ground stations for both commanding and receiving telemetry. Real-time control and monitoring system used to control Spacecraft and Spacecraft components during development, test, and on-orbit operations. Includes command switching and payload commanding as well as command gateways. This CSCI communicates with NEN.
Situational Awareness Tools	Used to display health and status telemetry.
Procedure Execution	Tool used for building and moving through sequences of commands/procedures. Used to step through procedures in a collaborative environment (e.g. Sim, Operations).
Data Management and Archival	Used for managing data on the ground during the mission, as well as assembling products for delivery to appropriate science archives (e.g., STSci MAST or IPAC).
Planning	Used for planning both science and non-science operations, including activity planning and command sequence generation. May include automated planning.
Engineering Analysis Tools	Used in engineering analysis to monitor trends and predict health. Simulate or model power consumption, thermal, link margin.

[6]

4.2.2.4 Ground Station Usage

mDOT uses KSAT network of ground stations (part of NASA Near Earth Network) for LEOP, TT&C and data acquisition. Both mDOT spacecraft, SS and TS, use S-Band links to KSAT network of ground stations. Passes with KSAT provide tracking data, commanding, downlink of housekeeping data (including DiGiTaL data), and Science data.

Communication events occur every week for TT&C and data acquisition is as scheduled by mission control. KSAT allows flexibility in schedule priority and change if mDOT would need so. The location in the orbit where these opportunities occur is usually at both poles where KSAT has ground stations (Svalbard and Troll). These tracks cover spacecraft maintenance passes (including commanding), tracking passes and data acquisition passes. The scheduled track length for a communication passes is a minimum of 10 minutes, after an allowance for Acquisition of Signal (AOS) and Loss of Signal (LOS). mDOT plans for 30 to 60 minutes per week for Science Data (~5 passes in total and for TS only) and one pass per week per spacecraft for maneuver planning. The study team confirmed with a KSAT representative that this is well within the capability of KSAT (see documentation in Appendix PP).

To track the Spacecraft, KSAT needs to know the spacecraft configuration parameters (e.g., data rates). The spacecraft has a fixed set of configurations and events. KSAT develops, with mDOT input, a set of Nominal Sequence of Events (NSOEs) used during the mission, and as part of the scheduling process, mDOT selects which NSOE is used for each track. mDOT does not expect to have dynamic changes during the mission.

As mentioned in Sec. 7.2.5 (Communication) the mDOT team will further assess the feasibility to use KSATLite assets vs KSAT.

4.2.2.5 Science Operations Center

Science operations will be coordinated at Stanford. A database of science targets and their properties will be maintained using the data architectures developed by the science team for the Gemini Planet Imager and the WFIRST CGI - https://plandb.sioslab.com/ - containing target stellar properties, disk properties, etc. Using this, we will develop observing sequences including exposure times and camera settings, reference star information, number of exposures and science passes needed, calibration requirements such as dark exposures, etc. This will then be transferred to the MMOC to develop the spacecraft sequences for each target.

Once observations have been executed, data products will be transferred to the science center and processed by an automated pipeline. The envisioned data products are

Level 0: Raw imager frames

Level 1: Imager frames processed with dark subtraction and bias correction

Level 2: Imager frames calibrated into astrophysical flux units

Level 3: Combined imager frames from each target, PSF-subtracted using reference stars, and associated data such as sensitivity curves or estimated uncertainties for each pixel.

4.2.3 Launch Vehicle Compatibility

mDOT requires an ESPA Grande support structure on a launch vehicle with a 5 m fairing or larger. The mDOT team will need to coordinate with the launch vehicle provider to ensure the mDOT design meets

[6]

the launch environment of the selected launch vehicle, but the team expects that the Atlas V, Delta IV, or Falcon 9 could be configured to satisfy the necessary SS launch envelope. With the exception of the TS Dispenser and rear thruster protruding through the interface ring and into the interior of the ESPA Grande, the SS conforms to the ESPA Grande secondary payload envelope of 1.0 m high x 1.1 m wide x 1.4 m long, measured from the ESPA Grande 24-inch ring interface. The 1.4 m length limit corresponds to a 5 m fairing.

The ESPA User's Guide (November 2018) states that auxiliary payloads are allowed to take advantage of the ESPA internal volume, if this volume is not occupied by a propulsion system or other mission element. Assuming an ESPA with no internal elements, mDOT would be allocated a "pie slice" of the internal volume. The allocation of the ESPA internal volume should be confirmed, once the mission integrated payload stack is defined, by the launch vehicle provider and/or the mission integrator.

As the design is refined, optimization can include recessing the 6U dispenser partially into the SS body to reduce the protrusion into the ESPA internal volume. This would shift the propellant tank location away from the ESPA interface, so management of the CG location would be the limiting factor. In the event that ESPA internal volume is not made available to auxiliary payloads, SS propellant tank size would need to be reduced to make room for the dispenser within the body, with a corresponding impact to propellant budget and science observation time.

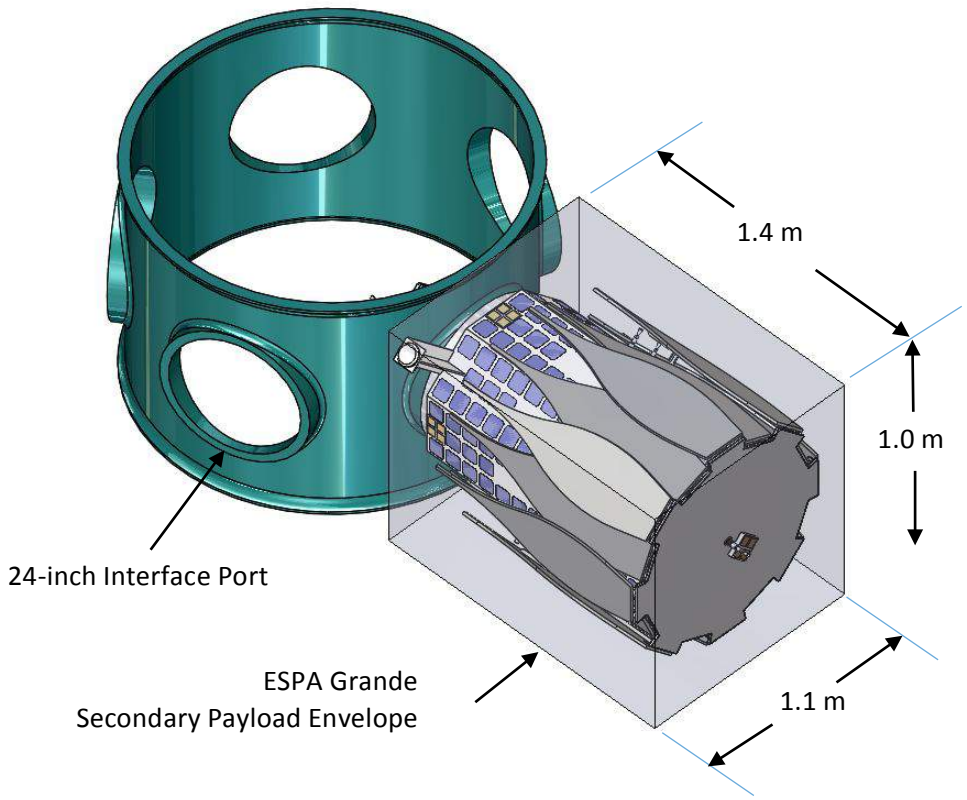

Figure 4-7: The stowed Starshade fits within the ESPA Grande volume allocation.

6

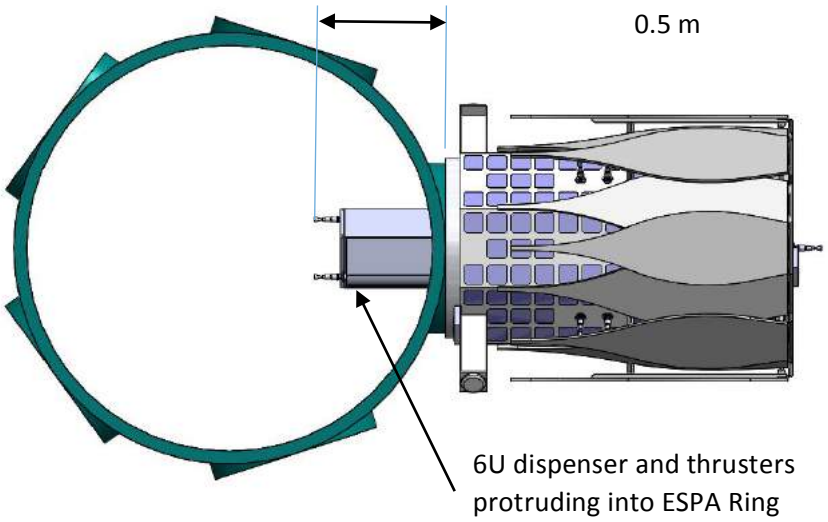

Figure 4-8: The Dispenser end of the Starshade Spacecraft protrudes into the ESPA Grande interior through the 24-inch port.

The SS will be deployed from the ESPA Grande using a 24-inch separation ring (Planetary Systems Inc. Lightband or similar). The current ESPA allocation for mDOT mass is 320 kg. The ESPA 24-inch port is rated for up to 465 kg when the center of mass is located within 50.8 cm (20 inches) from the ring interface.

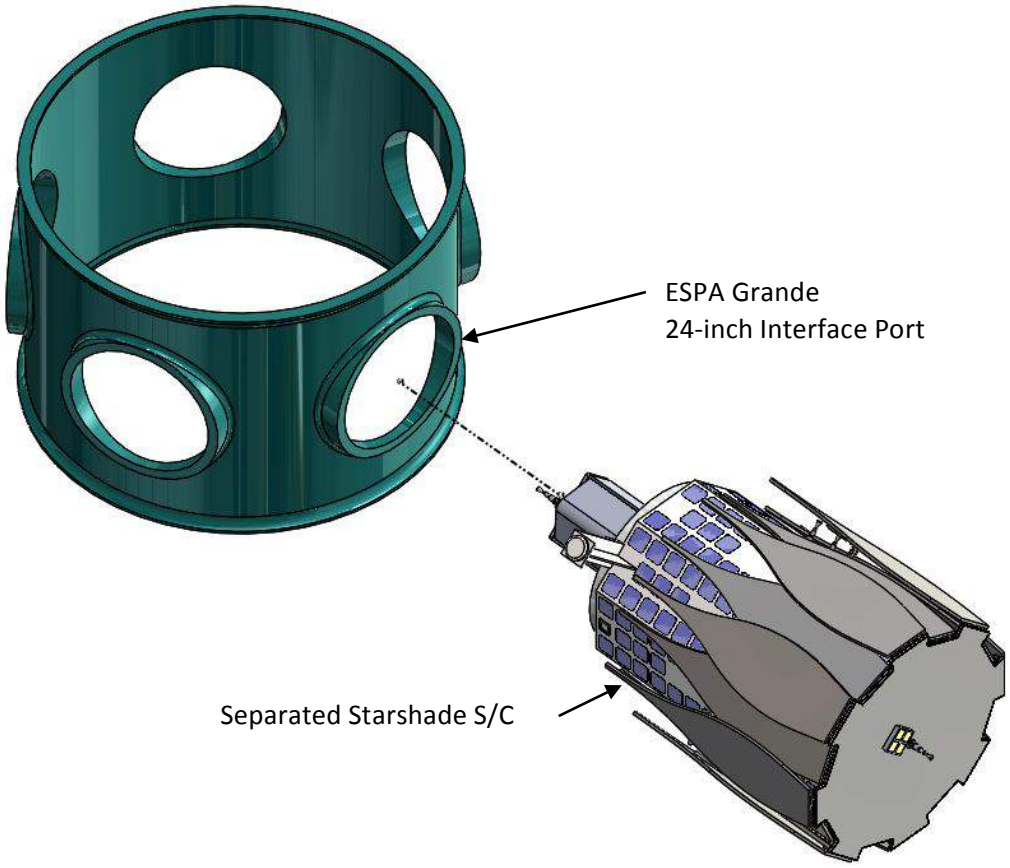

[6]

Figure 4-9: Springs in the separation ring send the Starshade Spacecraft to a safe distance from the primary Spacecraft before Starshade deployment.

4.2.4 Flight System Capabilities

4.2.4.1 Starshade Spacecraft

The SS consists of a small spacecraft with approximately 1.0 m x 1.4 m x 1.1 m octagonal structure which provides support to the 16-petal starshade. The starshade is 3m in diameter with petals manufactured to within 5 microns pattern shape tolerance (TBR). The starshade is stowed during launch and deployed like an umbrella by a motor after the SS has been ejected from the ESPA Grande. The TS is carried inside a 6U Deployer mounted at the opposite end of the SS. Eleven (11) 5N green propellant thrusters are arranged in pairs, plus one single on the starshade, to provide radial, tangential, and normal velocity control independent from spacecraft attitude. There are two pairs of thrusters used for radial velocity adjustment, two pairs for tangential, and a pair and single thrusters for normal velocity adjustments. Placement and orientation of the radial and tangential thrusters were selected to minimize plume impingement onto the petals while also minimizing rotational torques due to the shifting of spacecraft center of mass over time. Solar cells and six Cesium patch antennas populate the spacecraft body panels. One crosslink patch antenna is mounted on the starshade hub and one on the opposite panel. Two vertical structures pointing in opposite directions, designed to be out of view of the TS during Observations, provide support to the GNSS antennae. SS avionics, including propellant tanks and batteries, are located as opposite to the starshade in the spacecraft as possible; this helps to balance the spacecraft (center of mass near geometrical center) as well as to minimize plume impingement of radial and tangential thrusters on the petal edges.

Table 4-7 provides a summary of the major subsystem components of the Starshade Spacecraft.

Table 4-7: Starshade Spacecraft Subsystems.

Subsystem	Major Subsystem Components	TRL
Payload	Starshade Hub with 16 Deployable Petals, Starshade Deployment Motor, Snubbers (from TENDEG)	5*
Structure	Aluminum Primary Structure	7
	ISIS DuoPack CubeSat Deployer	9
	Planetary Systems, Standard Lightband, 24 inch diameter	9
C&DH	Tyvak SBC with Tyvak Linux BSP Operating System	9
	ARM Cortex A8+ DSP Coprocessor	
	512 MB RAM	
	NAND-Flash 8 GB SD-card	

[6]

Electrical Power System	Body-mounted UTJ Solar Cells from SPECTROLAB	9
	LG INR 18650HG2 300mAh Battery Cells (32 cells)	9
	EPS Stack, BioSentinel legacy	6
Communication	Two (2x) Cesium SDR	6
	S-band with Tx/Rx Module (TRM) – Primary and Redundant	5*
	4x S-band patch antennas (2 for crosslink, 2 for downlink/TT&C) – Primary and redundant	5*
ADCS	BCT Nano Star Trackers (2x)	9
	BCT MICD Coarse Sun Sensors (2x)	9
	BCT RW4 Reaction Wheels (4x)	9
	Microcosm MT-140 Magnetorquer Rods (3x)	9
	BCT XACT Gen3 ADCS Processor	9
GNC	Guidance, Navigation, and Control software, including DiGiTaL, developed by Stanford	5*
Thermal	Combination of active and passive control; have provided allocation for heaters, MLI, and temperature sensors	8
	Preliminary analysis completed for starshade	
Propulsion	11x 5N HPGP Thrusters from Bradford – ECAPS	5*
	LMP-103S Green Propellant	6
	77.9L (propellant load volume) Propellant Tank from ATK	9
Flight Software	cFE/cFS, Blue Canyon (XACT)	8

*Please see Section 4.4 for a discussion of Technology Development activities

6

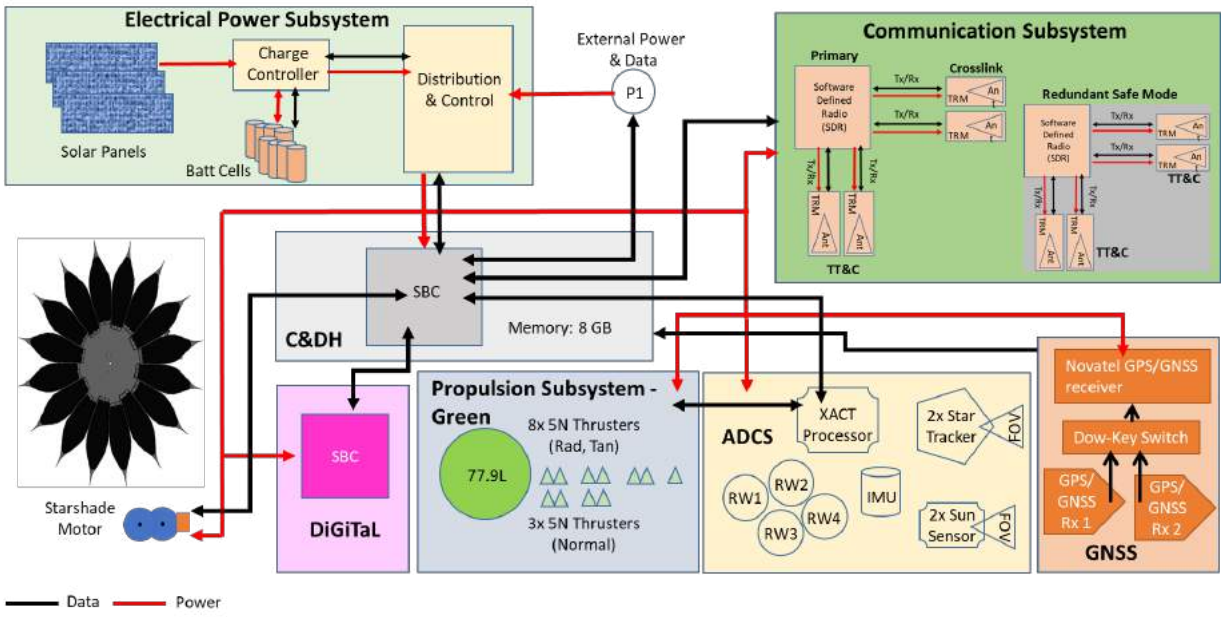

Figure 4-10: Starshade Spacecraft Functional Block Diagram.

4.2.4.1.1 Flight System Margins

Table 4-8 below shows the current estimates of Starshade Spacecraft system margins (not including the Telescope Spacecraft).

Figure 4-11: Starshade Spacecraft Margins Summary.

Resource	CBE	Allocation / Requirement	Margin
Dry Mass (kg)	138	---	---
Prop Mass (kg) (81.2 kg for delta-V)	96	---	---
Lift-off Mass (kg) (incl. 12kg TS)	246	320	23%
Solar Power (W) - EOL	177	37	>>100%
Battery Power (Whr)	345.6	187	85%
Battery DOD (%)	19.2	80	60.8
Relative Position Navigation Accuracy (RMS)	2 cm (3D)	6 cm (R, T); 1km N	
Relative Position Ctrl Accuracy (MAX)	10 cm (R,T)	15 cm (R, T)	
Pointing Control Accuracy (deg)	0.002	1.00	>>100%
Pointing Knowledge Accuracy (deg)	0.002	1.00	>>100%

[6]

Slew Rate (deg/s)	0.125	>0.063	98%
Margin = (Req or Allocation – CBE)/Req or Allocation			

4.2.4.1.2 Spacecraft Structure

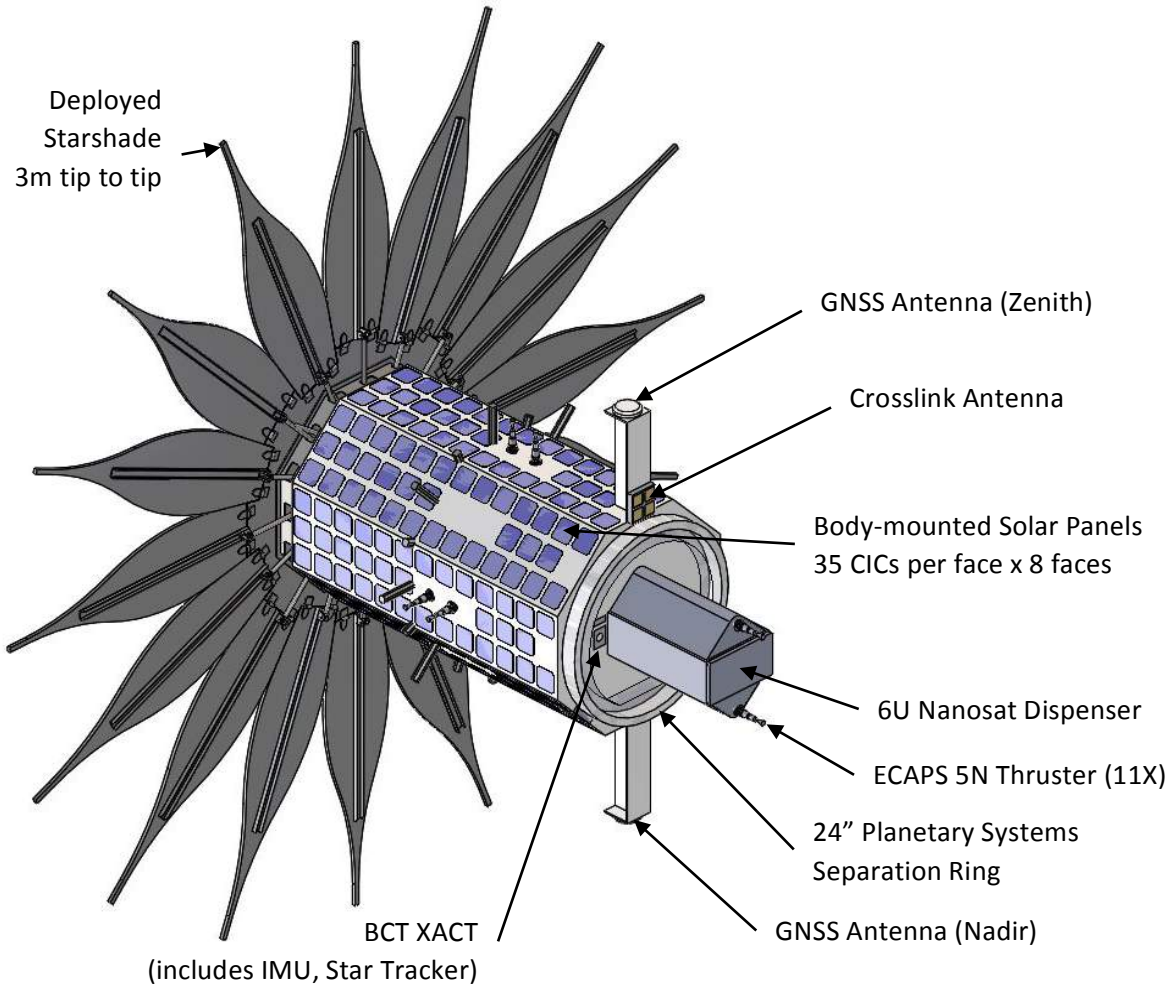

Figure 4-12: Rear view of starshade spacecraft.

The mDOT SS is sized for mounting to an ESPA Grande. The main components of the spacecraft are shown in Figures Figure 4-12, Figure 4-13, Figure 4-14, and Figure 4-15. The main body of the spacecraft is an octagonal structure, 70 cm across. This is large enough to mount on a 24-inch separation ring while small enough to allow the 3-m diameter starshade structure to fold over the octagonal body without exceeding the ESPA Grande volume constraints. The spacecraft body and internal support structure are constructed primarily of aluminum (subject to change with future thermal analysis). Each face of the octagonal body is covered with 35 solar cells. Once the starshade is deployed, the body-mounted panels are exposed to the sun and are sufficient to meet power needs.

6

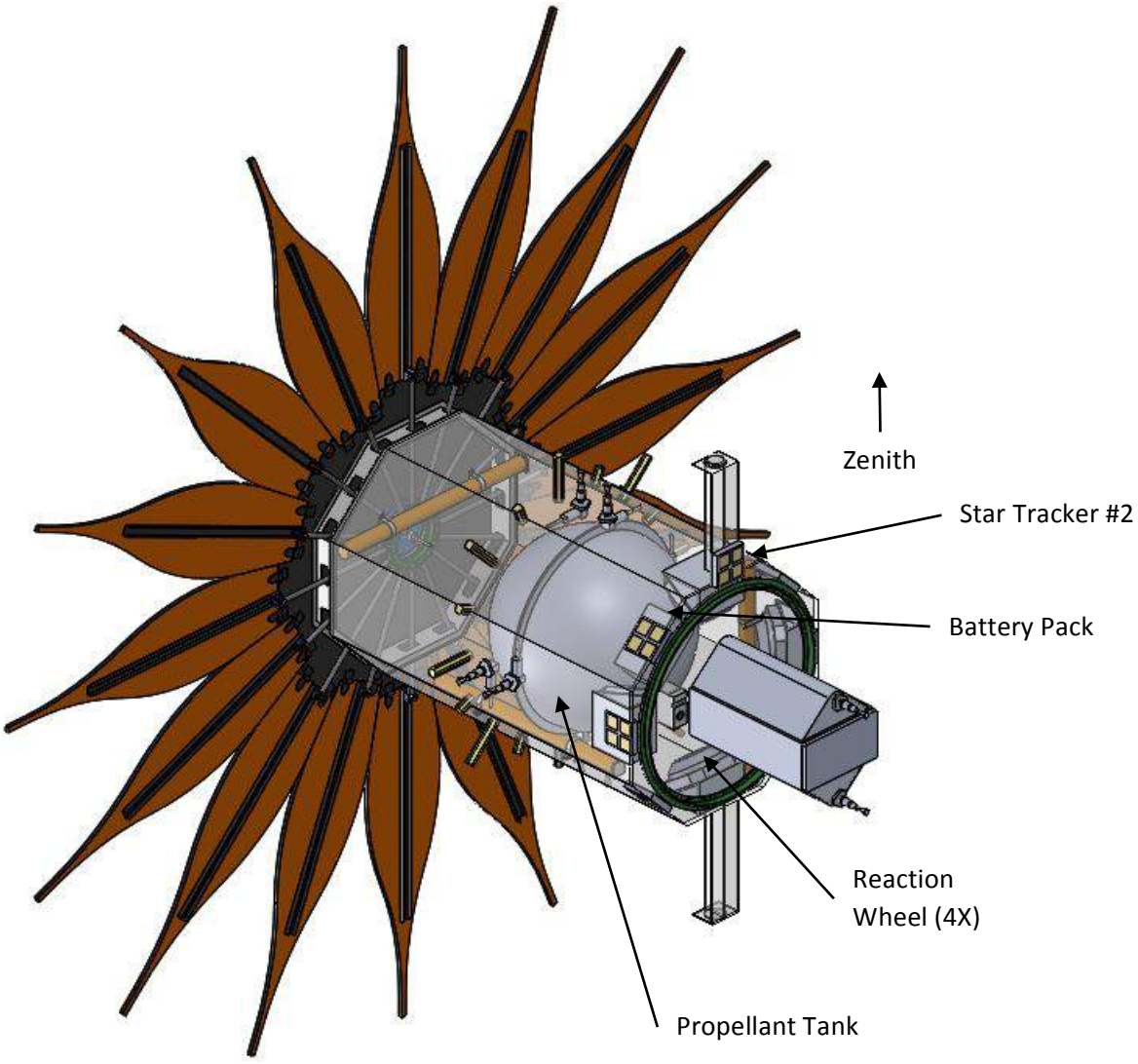

Figure 4-13: Rear view of starshade spacecraft without exterior.

6

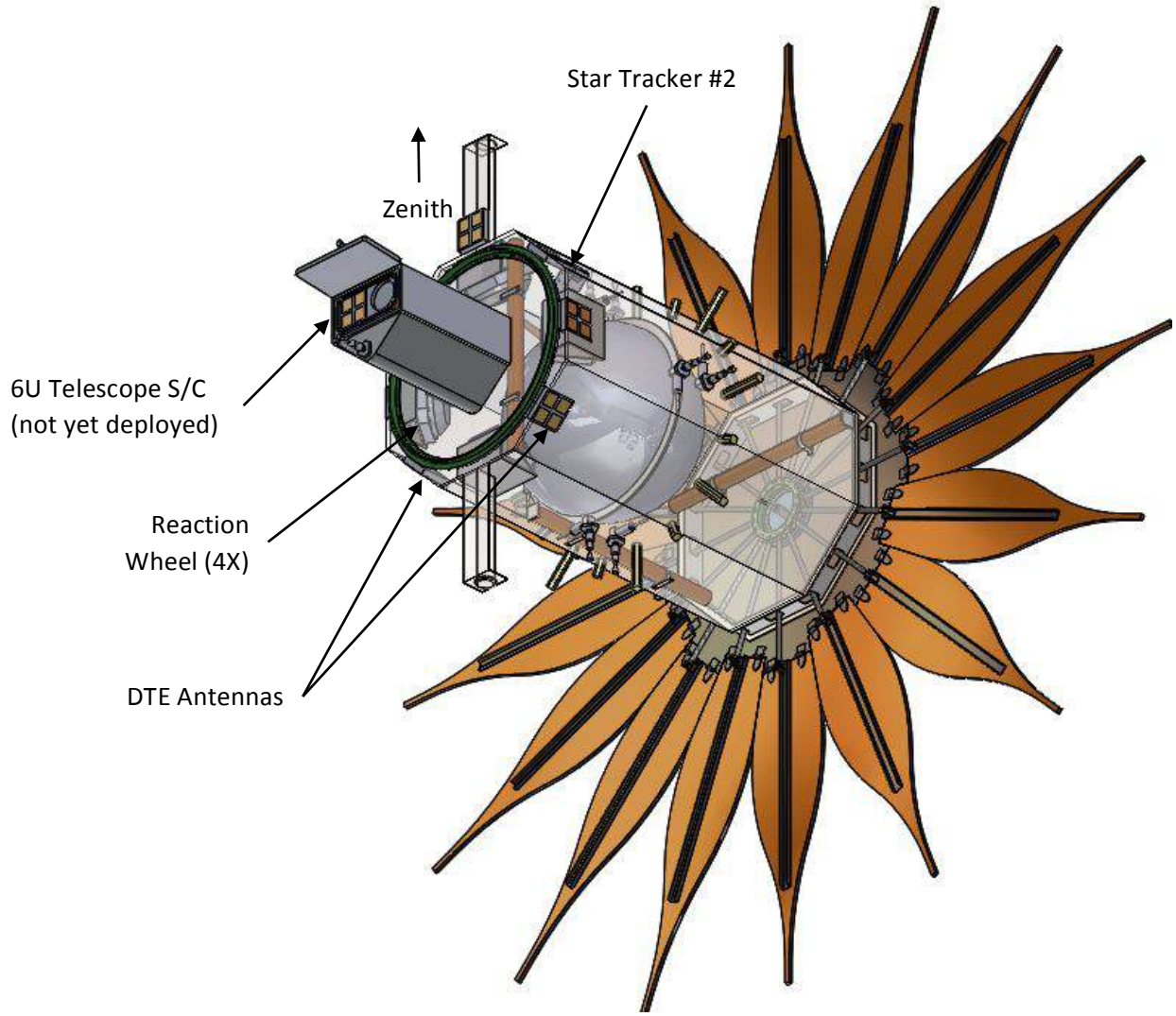

Figure 4-14: Rear view from below of starshade spacecraft without exterior.

6

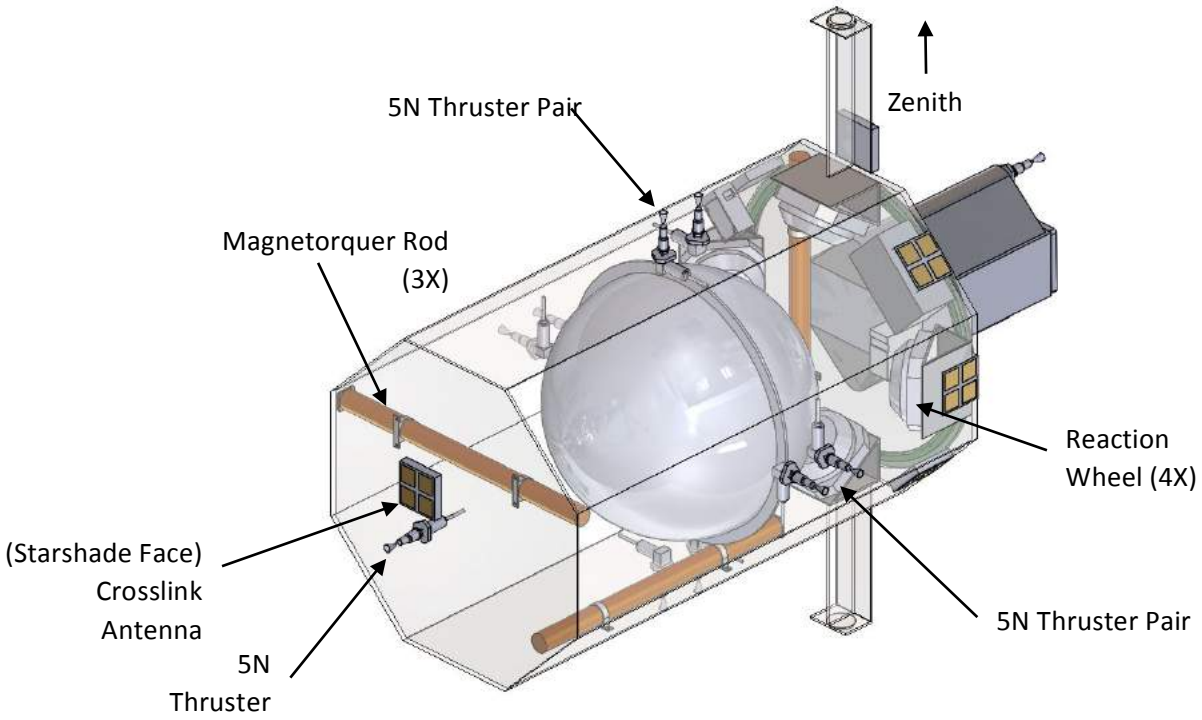

Figure 4-15: Internal view of starshade spacecraft (starshade payload not shown).

Pairs of 5N thrusters are mounted on the +/- axes to allow for 3-axis translational control. The face of the starshade is the only surface with a single 5N thruster. The thrusters are located such that a net thrust is provided through the center of mass (for the deployed configuration). The 91-liter fuel tank (77.9L fill capacity) is located along the axis of the octagonal body. The tank carries 81 kg of available ADN green propellant (LMP-103S) at launch.

The 6U NanoSat dispenser is mounted opposite of the starshade and protrudes through the 24-inch separation ring. A pair of 5N thrusters straddle the dispenser. The location of the dispenser along the main axis of the spacecraft ensures that release of the TS will have minimal impact on the center of mass of the SS and also will minimize tumble at release.

Two star trackers are positioned with orthogonal fields of view. One looks along the main spacecraft axis. It is located looking opposite the starshade, in the direction of the target star. The dispenser shades the star tracker from the thruster flare. This ST could also be located on the face of the starshade with similar performance. The other star tracker is mounted in one of the upper octagonal faces.

Four reaction wheels are located within the spacecraft against the 24-inch interface plate. They are oriented along tetrahedral axes, providing 3-axis attitude control with redundancy. Three, 68-cm long magnetorquer rods are placed orthogonally as available volume allows. The radios, power system, and computer are located close to the interface plate and positioned to keep the center of mass within 2 cm of the body axis. The center of mass is within 51 cm of the 24-inch ESPA interface in the launch configuration.

Patch antennas are located on the face of the starshade, on the dispenser end of the SS, and on the two lower octagonal faces, 45 degrees off nadir. Four additional patch antennas are mounted to four of the

[6]

unoccupied faces and connected to a separate Cesium radio for redundancy. Two GPS/GNSS antennas are located on extension arms in the zenith and nadir directions. The extensions are intended to maximize the antennae's field of view (allowing for 120 degrees FoV) unobstructed by the large starshade.

4.2.4.1.3 Starshade Payload

The design approach taken when designing the mDOT starshade was to create a stand-alone, plug and play system to the greatest degree possible. This approach allows development, fabrication and testing of the starshade independent of the bus which should reduce cost and schedule. The current best estimate for the mass of the subassembly is 23.2 kg (28 kg allocation).

Mechanical Design Overview

The starshade design consists of 16 deployable precision petals which are mounted onto a structural base deck. The deck structure is the mounting plate for the petal hinges, the petal central deployer mechanism, and the precision structural interface to the aft end of the bus. When the petals are stowed, they fold up parallel to the bus central axis. The petals are seated in cup/slotted cone devices onto 16 posts with brackets that are integrated into the bus and restrained. A resettable launch restraint/release device is mounted to the end of the post. Releasing this device disengages the petals so that they can be deployed to their final position by the deck mounted deployment mechanism rotating its linkage arms that connect this mechanism to the individual petals. The petals are rotated down and locked out in this position through tapered pin engagements at the hub.

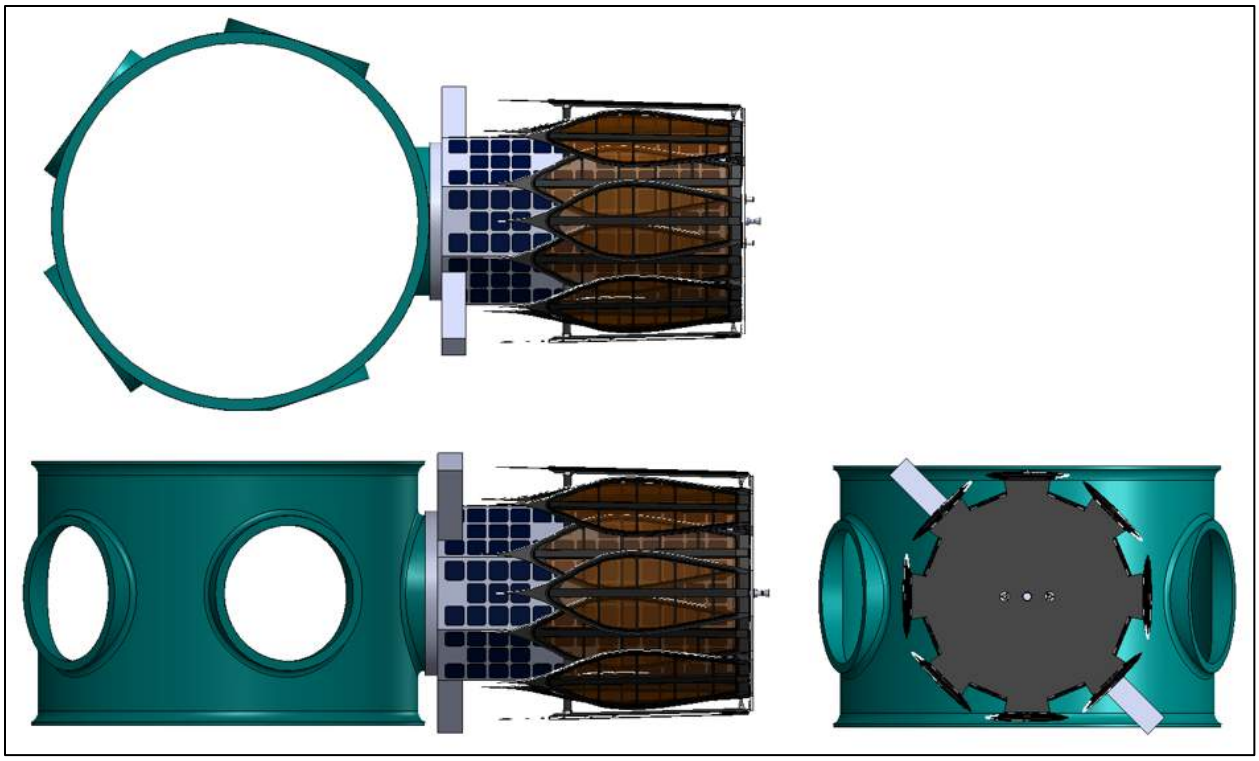

Figure 4-16: mDOT 3-view of starshade spacecraft attached to ESPA.

6

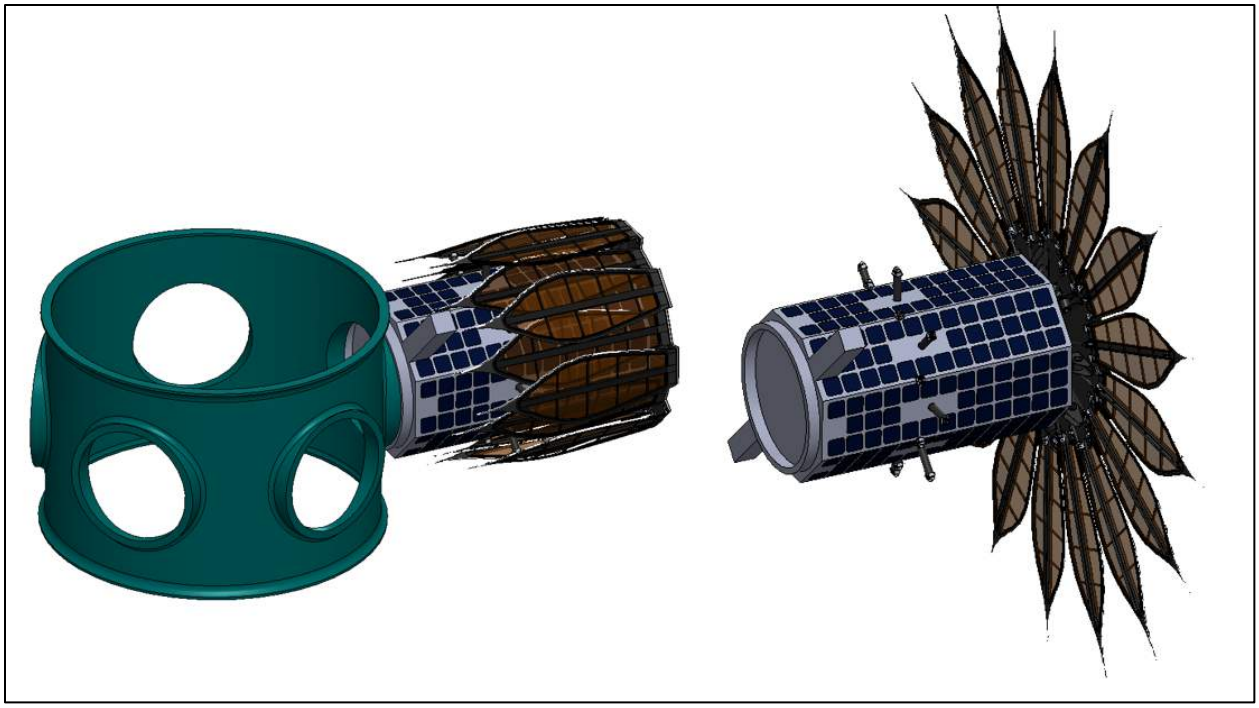

Figure 4-17: mDOT starshade spacecraft shown attached to ESPA and deployed.

Figure 4-18: mDOT starshade stowed configuration and first motion.

6

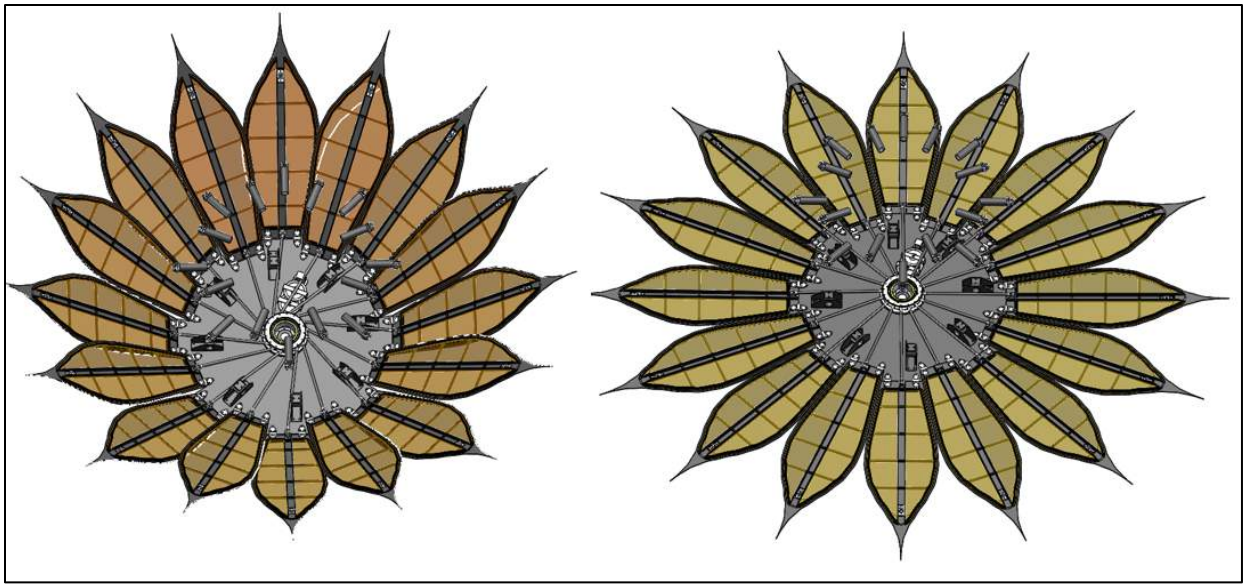

Figure 4-19: mDOT starshade deploying to final configuration.

Starshade Deck

The primary structural element of the starshade is the deck. The deck is a low CTE carbon honeycomb sandwich panel sized for launch loads. Precision bushings are bonded into its faces using jigs to ensure final alignments of all precision mount locations.

The petals are mounted around the perimeter of the deck in a staggered radial pattern. This stagger allows the widest section of the petal teardrop shape to pass each other as the petals are rotated from a horizontal deployed to vertical stowed position and back again. In the stowed position, the petals are seen at alternating radial distances to ensure that edges of adjacent petals never make contact.

The deck has a pattern of trunnion brackets that are the mounting points of the starshade assembly to the bus. Final FEA work will determine the proper kinematic mount required between the starshade attach points and the bus. Alignment features will be incorporated such that the bus star trackers can be aligned with the starshade structure.

Several pass-throughs are provided in the starshade deck so that an aft thruster mounted to the bus can pass through down the vehicle centerline. The thruster and deck will have a light seal closeout attached at final assembly. A star tracker and additional sensors/antennae can also be mounted on the aft deck which looks outboard.

6

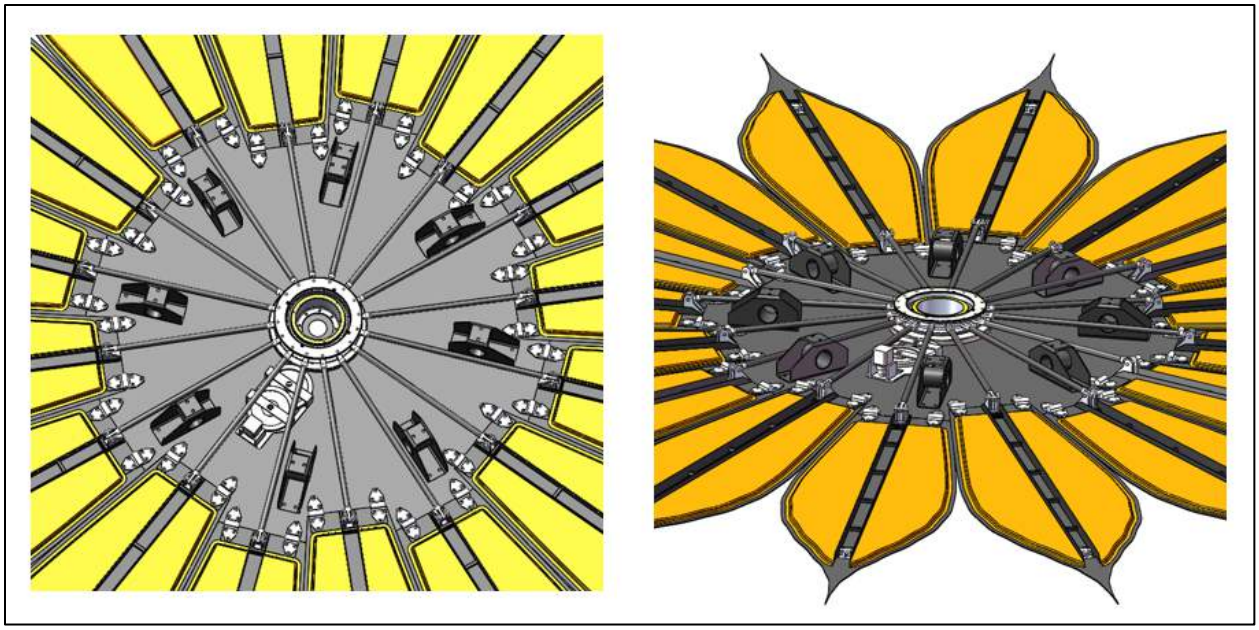

Figure A.4-20: Starshade structural deck and deployed petals.

Petal

The starshade petals are comprised of an axial spine and cross battens that are bonded to a lightweight structural petal frame. Bonded onto the sides of the structural frame are optical edge assemblies. Bonded to the optical edge is the precision etched amorphous metal foil which creates the outermost perimeter of the petal profile. All structural petal components are constructed using near zero CTE CFRP materials whose layups and final configurations are designed to minimize all thermal petal distortions on orbit.

The open lattice structure of the petal is closed out with a multi-layer Kapton shield. The telescope side outer Kapton is opaque and black. Additional Kapton sheets are layered together and spaced with low density foam or other separator materials. The separation in the individual blanket layers greatly minimizes the ability of micro-meteoroid holes to align with the telescope. The shield perimeter is connected to the structural elements of the petal in a way that local stress in the shield caused by thermal distortions cannot be transferred into the petal frame ensuring the petal shape is unaltered.

6

Figure A.4-21: Petal construction.

Hub and Linkage Arm

Dual precision hinges are mounted to the petal root ends which are in turn mounted to the starshade structural base. Mounted between the base hinges of each petal is a clevis fitting that creates the connection points of the individual linkage arms back to the hub deployer mechanism. To stow or deploy the petals, the hub is rotated by an encoded motor through a gear train or timing belt. The rotational motion of the hub pushes or pulls the linkage arms connected between its perimeter and each petal clevis. The petals are stowed or deployed with this relative motion.

Each linkage arm is constructed from a low CTE carbon tube. Both ends of the linkage arm have bonded fittings outfitted with spherical bearings that accommodate the angular mismatch of the kinematics of the linkage arm rotation with the hub's horizontal plane and the vertical swing of the clevis on the deploying petals. One end of each of the linkage arms has a precision length adjustment feature so the final deployed alignment of the petal can be set by adjusting the arm length during assembly.

The hub is outfitted with dual spring-loaded tapered pin deployment lockout latches. When the hub rotates so that the linkage arms are radial to the hub and in line with the petals, the tapered pin locks the hub rotation. The pre-adjusted arm lengths ensure the petals deploy to a planar configuration.

[6]

Another option for petal positioning is to use a hard stop or latch mechanism on each petal. Then the linkage arm will only act as a deployment actuator and will not be critical in the final petal position.

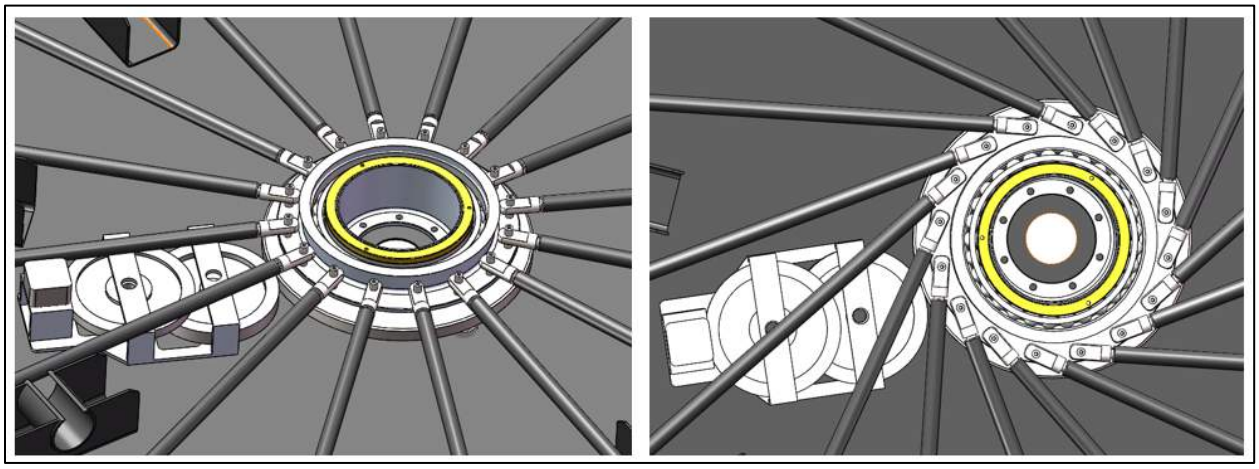

Figure A.4-22: Hub shown in deployed and stowed rotational position.

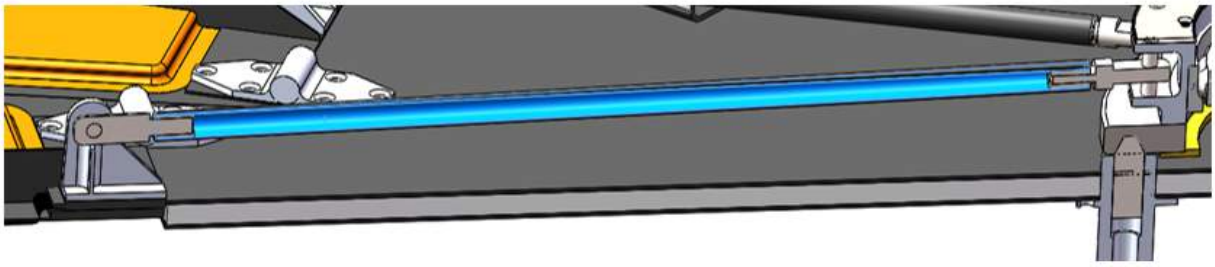

Figure A.4-23: Linkage arm cross-section.

6

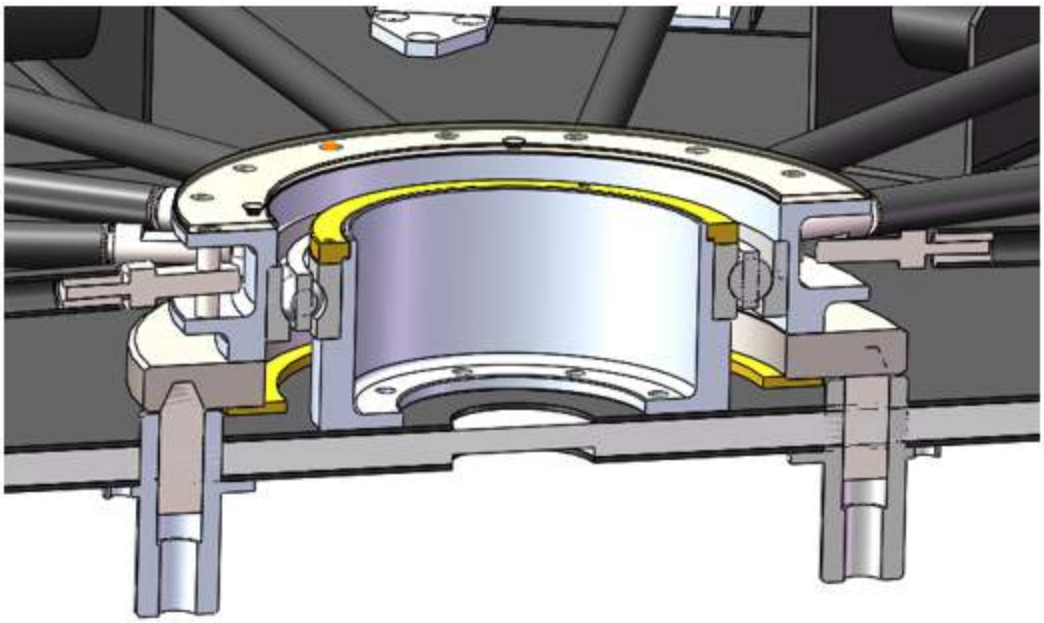

Figure A.4-24: Deployment hub cross-section showing deployed position latch pins.

Petal Launch Restraint

Each petal is secured in its vertical stowed position using a cup/cone set of fittings and a resettable restraint/release device mounted onto 16 separate bus mounted structural post brackets. The petal interface plate has a tapered slot to accept the cone fitting of the release device. This plate is mounted to the stiff U channel in the center of the petal frame. The petal linkage arms are rotated to create a small preload on the stowed petal between the petal hinges and the restraint post. The final vertical position of these bus mounted posts can be set to accommodate the bus and solar array design.

6

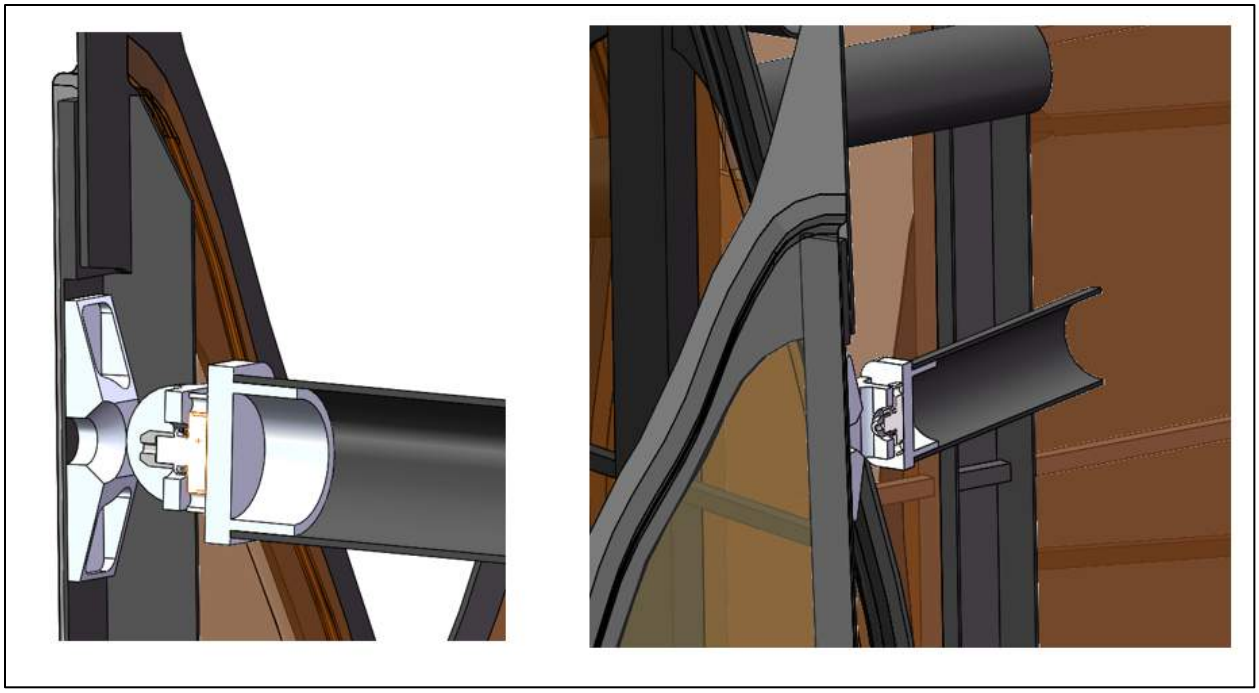

Figure A.4-25: Petal to bus restraint post and release device in section.

It may be possible to move the active release devices from the post positions described above to a position between the starshade deck and the end of the bus. A passive snubber post mounted higher on the bus structure would still be required but would not require the active release device to be located on it. The geometry of a configuration like this however requires the restraint force between the restraint device and the petal to be high due to its poor mechanical advantage. A design trade will be done to see if a preferred alternative design is possible that eliminates the need for 16 release devices.

Results of structural and thermal analysis conducted for this starshade design is included in Appendix A.7.

4.2.4.1.4 Propulsion

The propulsion system must be selected to satisfy five requirements. First, the thrust must be sufficient to keep the formation aligned with each of the target stars. Second, the duty cycle of the thrusters should be kept under 50% to ensure that the camera is not shuttered the majority of the time during observations. For the science plans considered in Appendix 9, it was found that a thrust of 10N is sufficient to control the formation with short thruster firings (<5 seconds). Third, the propulsion system should have the largest possible specific impulse to meet the delta-v requirement for the mission with reasonable propellant mass (<100kg). This results in a minimum specific impulse of 220s. Fourth, the starshade spacecraft must be able to generate thrust in any direction without performing an attitude maneuver to ensure that the formation can controlled during observations with the starshade facing the target star. Finally, the propulsion system must generate thrusts that act through the center of mass of the spacecraft to minimize the momentum accumulated in the reaction wheels during observations.

[6]

To meet these requirements, the selected propulsion system consists of a set of 11 5N high-performance green propellant thrusters from Bradford ECAPS (Figure 4-26). These thrusters have a specific impulsive of 240s, and a density 24% higher than hydrazine.

Figure 4-26: Bradford ECAPS 5N high-performance green propellant thruster.

The thrusters are positioned to provide torque-free translation maneuvers at all times during the mission accounting for the shifts in the center of mass due to propellant expenditure. This means that thrusters should not generate a rotational torque about the SS; fully satisfying this desirable condition does necessitate that thruster directionality is aligned with the axes of center of mass (CM). The SS has thrusters aligned in the positive/negative direction of each of the principal axes, as shown in Figure 4-27. Only a single 5N thruster is located in the Body X axis because of a constraint imposed by the starshade petal structure. A small value of 0.1 meter is considered as a baseline for L1 in Figure 4-27 so that the reaction wheels can compensate for undesired toque generated from misalignment of thruster nozzles and provide for control in the event of a malfunctioning nozzle pair. This thruster arrangement provides 10N thrust per axis in the plane perpendicular to the line of sight during observations, meeting the thrust requirement for the mission.

[6]

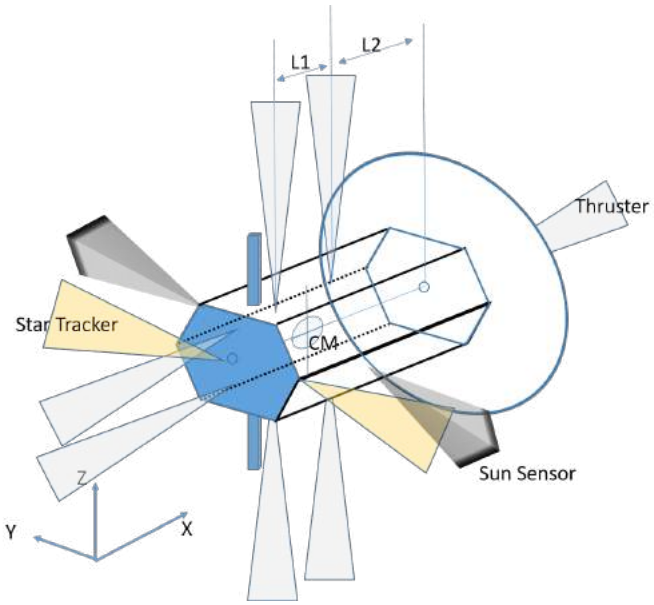

Figure 4-27: Thruster layout in body frame.

4.2.4.1.5 Command and Data Handling

The SS C&DH performs the following functions: (1) execute and verify commands to all bus components, (2) capture, store, and transmit telemetry and event logs from all Spacecraft components, (3) verify the state-of-health (SOH) of the spacecraft including watchdog and error detection and corrections, (4) store and execute onboard stored sequences, and (5) support payload data storage and compression.

For TT&C operations, the Tyvak Single Board Computer (SBC) with Endeavor 800 MHz flight microprocessor has been selected for size, weight and power characteristics. For DiGiTaL/GNC operations, the Tyvak SBC with endeavor 800 MHz flight microprocessor has also been selected. Selection at this phase is based on DiGiTaL/GNC legacy testing on the system.

The Tyvak SBC with endeavor 800 MHz flight microprocessor runs Linux BSP and can store 8 GB of data while consuming less than one (1) watt of power. This SBC is assessed to TRL 9. Note, the Tyvak SBC hardware is typically purchased within the package of a spacecraft bus and is not typically on the market. Conversations with Tyvak have commenced and can be followed up or similar hardware can be easily selected. Performance parameters for the Tyvak SBC are stated in Table 4-8 below.

Table 4-8: Starshade Spacecraft C&DH, Tyvak SBC.

Operating System	Tyvak Linux BSP
Processor Architecture	ARM Cortex A8+ DSP Coprocessor
Clock Speed	800 MHz
LINPACK Benchmark	38 MFLOP
RAM	512 MB
Nonvolatile Memory	512 MB NAND-Flash, 8 GB SD-card

6

Power Consumption	< 1.0 W

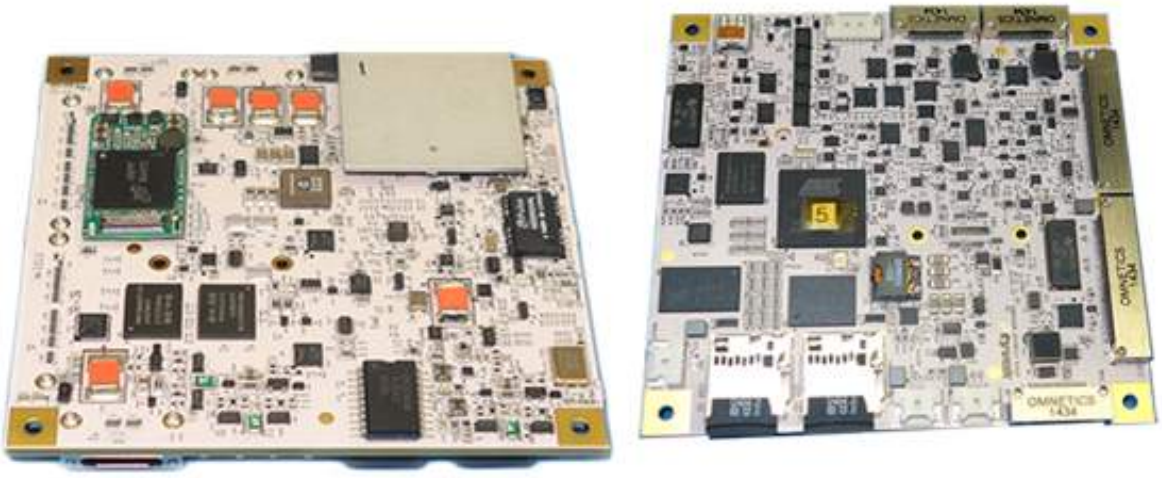

Figure 4-28: Reference: http://www.tyvak.eu/irm.html

The TT&C SBC is the manager of the schedule, systems monitoring and facilitates data transfer around the spacecraft. In the case of ADCS data, information via the radio, the BCT XACT system, are ported to the DiGiTaL/GNC system for position knowledge and thruster control. Data is also returned to the TT&C SBC for storage and distribution.

It is recommended that the two Tyvak SBC's (TT&C and DiGiTal) be connected via SpaceWire for high data throughput, while the crosslink radio, downlink radio, ADCS and electric power system (EPS) subsystems are equipped with RS-422 connectivity.

High level system architecture leading to board necessity and selection for cost, size, weight and power were of primary focus for this study. Additional trade analysis and control strategy will be detailed in Phase A studies of the mission.

4.2.4.1.6 Electrical Power System

The mDOT EPS performs the following functions: (1) capture, store, and distribute power for Spacecraft bus and payload, (2) manage solar array power capture, (3) manage battery power storage, and (4) switch and distribute power to subsystems/ components.

mDOT's power requirements were compiled from all powered subsystems and analyzed by operational mode. The most demanding mode is found to be during a science Observation. The remaining modes were assessed to be less demanding than Observations. The Commissioning and Formation Acquisition phases also require thruster burns which are less than 5 minutes in duration (same duration as the burns during Observations) followed by a drift period. Decommissioning in the LEO orbit is not a power concern.

For analysis, the LTAN noon/midnight orbit was assessed (worst case for power considerations). For this mode the spacecraft uses body-mounted solar cells capable of generating at least 192 W (assuming Peak Power Tracking) of power at end-of-life (EOL); 345 Wh of battery storage capacity (EOL) is provided. SpectroLab provides solar cells which will be installed onto the exterior of the spacecraft body, 35 cells per surface (8 sides - 280 total cells). This solution allows for pointing in all directions while still receiving

adequate power while in sun. The panels are equipped with UTJ solar cells with proven 28.3% efficiency. mDOT uses 32x LG INR 18650HG2 3000 mAh Li-ion batteries, with four series and eight parallel connectivity. The maximum depth-of-discharge (DOD) is 20% due to the LEO orbit selected, as the orbit cycle count is < 6,500 for the entire 1.1-year mission; future refinement of the number of charge/discharge cycles could allow for a less-conservative DOD.

mDOT EPS boards leverage the design used on BioSentinel, which is an Ames Research Center mission scheduled to launch in 2020 on EM-1. The power management card controls PPT for the solar arrays, monitors over current, and manages battery usage. The power distribution card is a switch board that controls power switching, DC-DC conversion, and power regulation, among others. For mDOT components, the EPS must supply 12 V bus voltage and 3.3 V of regulated voltage. Additionally, each of the batteries in series has an individual management card. For the current battery design, there are eight parallel battery strings; thus, eight battery management cards. Figure 4-29 shows the power distribution connectivity of the Spacecraft at EOL. The bus power is distributed to the ADCS XACT, TT&C Tyvak SBC, DiGiTaL/GNC Tyvak SBC, the Busek/ECAPS 5 N thrusters, and the Cesium radio. Pulse power is provided for deployment mechanisms.

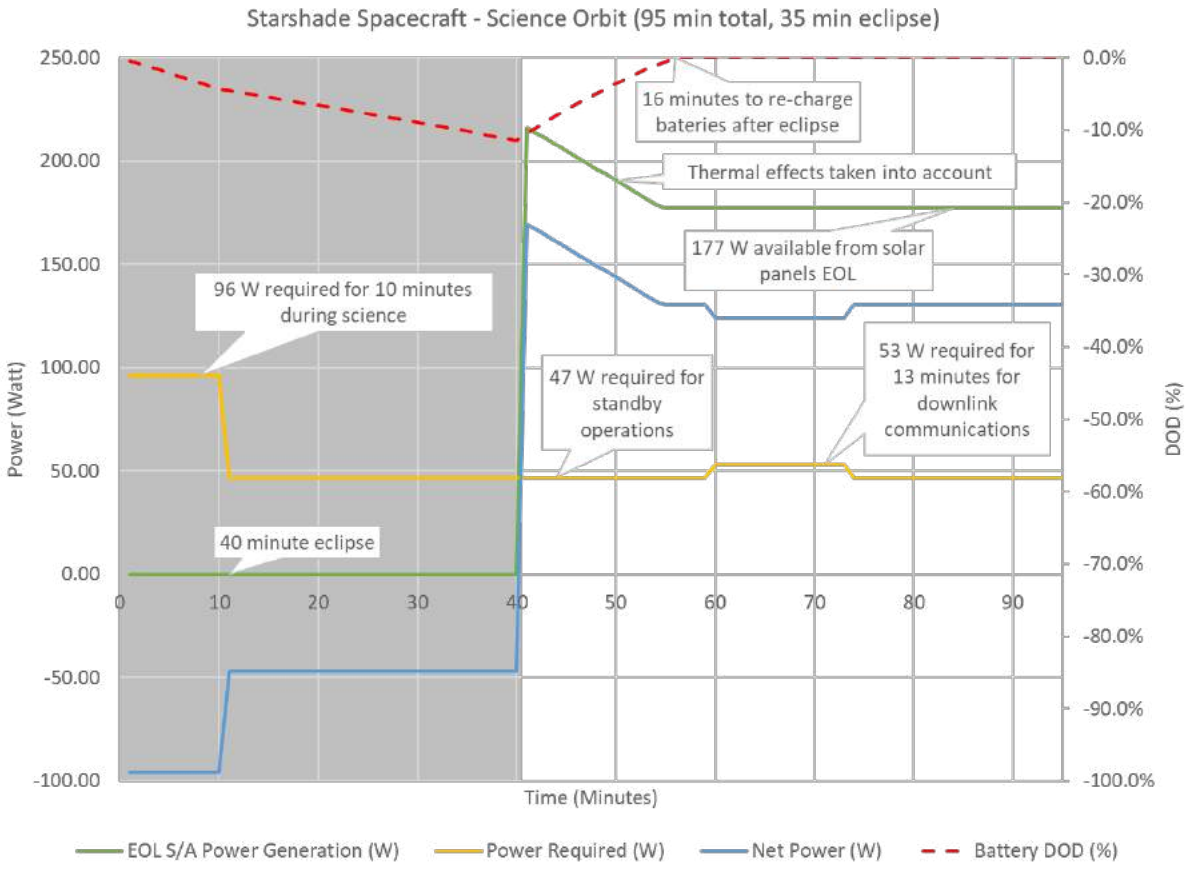

Figure 4-29: Science observation power.

In this profile, the DOD is <20% with margin of 53%. See Table 4-9 below.

Table 4-9: Tyvak SBC.

[6]

	Value
EOL	1.1 yr
EPS Efficiency	80%
Charge Efficiency	90%
Discharge Efficiency	90%
DOD Max Allowed	20%
DOD Max Reached	**11%**
OAP - Solar	**112.5 W**
OAP - Bus	**52.8 W**
Margin Solar/Bus	**53%**

4.2.4.1.7 Communications

The SS employs one communication system for both crosslink and telemetry, tracking and command (TT&C), as shown in Figure 4-30. The SS also includes a dedicated redundant system for emergency and safe mode TT&C based on the same hardware solution as the primary system. The nominal system works in S-Band and provides both TT&C, emergency and safe mode TT&C, and crosslink communication with the TS to exchange relative position information. The TS employs the same hardware solution for the crosslink and science data downlink, while the bus provides TT&C and redundant science data downlink capability. mDOT plans to use the KSAT ground station network (NEN) and the SG1 dish is the baseline for the link analysis.

6

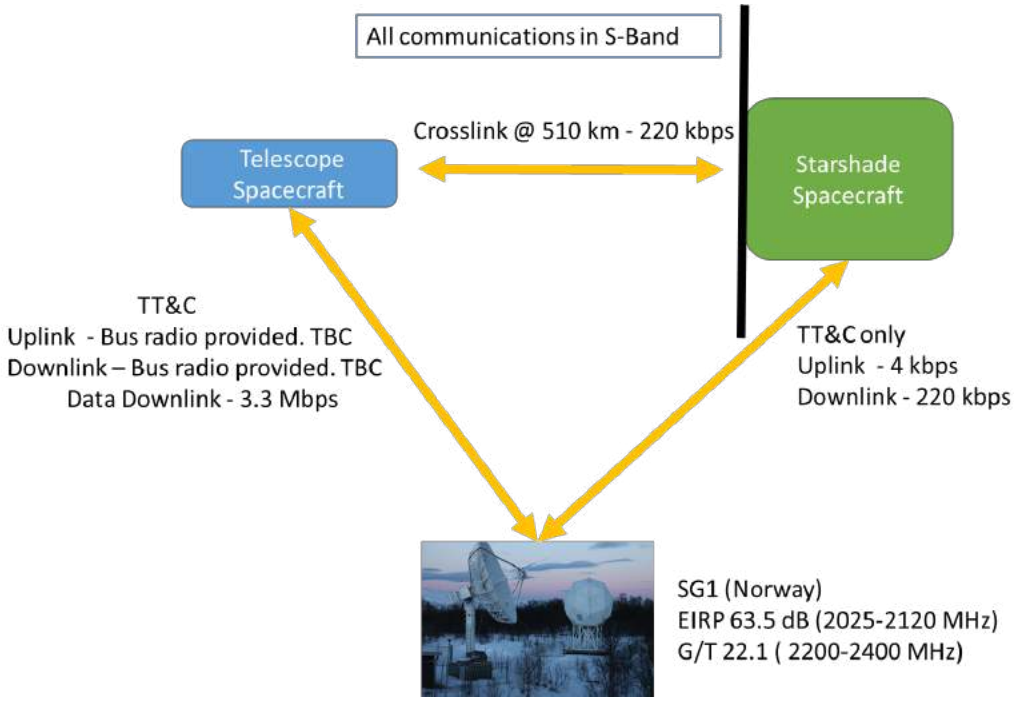

Figure 4-30: Radio communication links.

The S-Band system uses a Software Defined Radio (SDR) from CesiumAstro with an integrated active phased array antenna known as the Transmit/Receive Module (TRM). A Xilinx FPGA hosts an IP core, which contains a microcontroller that brings up all the components of the SDR and provides interfaces for the communication cores to two AD9375 transceivers as well as to the spacecraft computer. Each SDR can connect to up to four TRM. Each TRM includes 4 low noise amplifiers (LNAs) and 4 power amplifiers (PAs) with a combined output power level of 4 W. The TRM also contains one 4:1 combiner, one 4:1 divider and four Transmit/Receive switches. Each of the four antennas contains a 4-patch array. Each patch in the antenna is connected to one of the Transmit/Receive switches in the TRM module for receive or transmit. The 4 patches provide 8 dBi peak gain and 3-dB full beamwidth of 60 deg. Figure 4-31 shows a detailed block diagram for the Cesium SDR, TRM system. Cesium is expected to reach TRL 8 in May 2019 and it is currently the baseline solution for the NASA Ames Starling mission. https://www.nasa.gov/sites/default/files/atoms/files/336429-508-to5_nac_dec_2017_smallsats_tagged.pdf [accessed January 16, 2019]. Figure 4-32 shows a high-level flowchart for the SDR.

[6]

CESIUM PROPRIETARY: REMOVED

Figure 4-31: CommPack SDR design. *(CESIUM PROPRIETARY)*

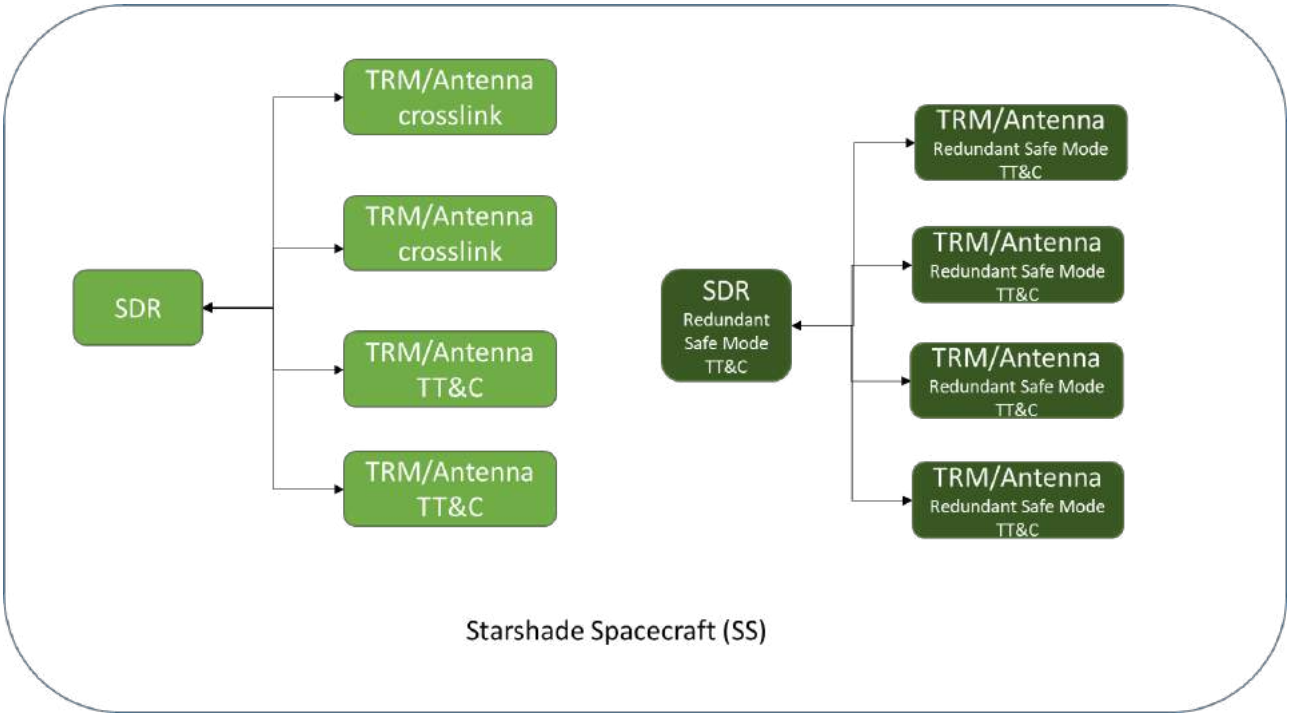

Figure 4-32: SDR flowchart.

4.2.4.1.7.1 Link Analysis

Initial analysis show that mDOT close both the TT&C and Science data RF downlink with >> 6 dB. The crosslink between the SS and the TS closes with 5.5 dB at max expected distance of 510 km. All the analysis for the RF links assume the use of the Cesium radio and the SG1 ground station in Norway

[6]

(KSAT/NEN). Table 4-10 gives details on the various link budgets and Appendix A.5 shows details for each link budget. In addition, the mDOT team also performed preliminary link analysis using the KSATLite ground stations, which consists of 3.7 m dishes (versus the 11.3 m of SG1) co-located with traditional KSAT dishes. While these results indicate that KSATLite assets may meet mDOT requirements, KSATLite is not integrated with NASA NEN, therefore a future trade will be performed to assess the use of KSAT vs KSATLite assets based upon cost, performance, and operational complexity.

Table 4-10: Data Rates and Link Margin Results.

S-band Patch **Ground Station SG-1 (KSAT/NEN)** **All values for Cesium SDR – 4 W RF out**	**Data Rate (kbps) - Link Margin (dB)**	
	Uplink	Downlink
Telemetry	----------	220 - 25
Command	4 - 26	
Science downlink		3290 – 13.5
Crosslink		220 – 5.5

4.2.4.1.7.2 Data Throughput Analysis

From the MTM (Table 4-1) the data volume of science data that needs to be downloaded after each Observation varies from 10 MB to 600 MB. Initial analysis show that a 3.3 Mbps data rate allows all science data generated in one Observation to be downlinked to a ground station in 1 to 5 passess (see Figure 4-30). mDOT has ~ 14 daily available passess with SG1 (TBR). The bandwith occupancy is estimated to be within the 5 MHz bandwidth limit (paragraph 15.4.1 Near Earth Network Users' Guide – 453-NENUG https://sbir.gsfc.nasa.gov/sites/default/files/453-NENUG%20R2.pdf [accessed January 16th 2019])

4.2.4.1.8 Formation Flying

Formation Flying requires 6 degree of freedom (DOF) maneuverability. i.e. 3 DOF rotation, 3 DOF translation. Table 4-11 shows that the functionalities of subsystems and corresponding role for the required rotation and translation for Formation Flight. XACT ADCS subsystem (in RED) introduced in Section 4.2.4.1.8.1 take a responsibility of attitude knowledge estimation, attitude control command, and driving reaction wheels, and deliver thruster command to thruster units; GNSS subsystem (in Yellow) provides GNSS solution and raw measurements; The guidance/navigation/control functionality required for Formation flying (Green) is addressed in Sections 4.2.4.1.8.2 and 4.2.4.1.8.3.

[6]

Table 4-11: Formation Flying roles and subsystem (Red-XACT, Yellow-GNSS, Green-Stanford GNC).

	Rotation-subsystem	Translation-subsystem
Sensor	ADCS	GNSS subsystem
Software	ADCS	DiGiTaL
Controller	ADCS	Formation Control
Actuator	Reaction Wheels	Thrusters

4.2.4.1.8.1 ADCS

ADCS provides the estimated attitude knowledge and implements control commands to maintain or change attitude to achieve desired pointing. ADCS design life spans from deployment from the ESPA Grande through end of mission.

The XACT (Gen3) is a complete ADCS subsystem designed, manufactured, and tested by Blue Canyon Technologies (BCT). It consists of the ADCS processor with integrated Inertial Measurement Units (IMUs) (gyroscope/accelerometer), two Nano Star Trackers (NST), two BCT sun sensors, four RW4 reaction wheels (1 wheel for redundancy), and three Magnetorquer rods. XACT system provides an interface to thruster so the thruster control command can be implemented through XACT. The ADCS processor closes the loop for the system by processing the NST data (with a lost-in-space solution if the star trackers do not find a fix), estimating the attitude from the sensors with a Kalman filter, commanding the reaction wheels, bridging thruster control command to propulsion units, and commanding momentum management operations. The RW4 reaction wheels have a stored wheel momentum of 4 Nms and maximum torque of 0.3 Nm. The NST have an attitude knowledge of less than 7 arcsec about all axes when placed orthogonally. As the mDOT attitude requirement of 1 degree is much looser than the performance typical ADCS system could provide, it is not treated as a driving requirement.

The ADCS provides 3-axis attitude pointing capability; sensor and actuator components are listed in Table 4-12.

6

Table 4-12: Starshade Spacecraft ADCS system components.

	Vendor/Model	Mass, kg	Note
Star tracker (x2)	Blue Canyon Nano star tracker	0.35	Accuracy [Roll/pitch/yaw]: [40/6/6] arcsec
Coarse Sun sensor (x2)	BCT MICD, DiGiTaL Strip Assembly	0.008	Accuracy: 5 degree, 1 sigma. Redundant to Star tracker in safe mode
Reaction wheels (x4)	BCT RW4	12.0	3 kg x 4
Magnetorquer Rod (x3)	Microcosm MT-140	15.9	5.3 kg x 3 axis

The sizing of ADCS hardware is selected based on the mission design, spacecraft body design, Earth sun-synchronous orbit environments, and corresponding constants (e.g. sunlit area, gravity constant, magnetic constant, solar reflection factor, drag coefficients, atmospheric density, etc). A comparatively high drag coefficient is assumed to consider the effect of asymmetry on the uncertainty of moment of inertia, where the velocity direction is perpendicular to the starshade petal structure during nominal operation periods. A conservative surface area of 1.705 m^2 subject to the disturbance environment is used, assuming solar panels are attached on the body, and no degradation effect of velocity is assumed. Only Reaction wheels (RW) are used for compensating the torque error generated by a center of mass offset. The assumed maximum uncertainty on the estimated center of mass is 0.03 meter. The parameters used for sizing estimation are shown in Table 4-13.

Table 4-13: Reaction Wheel Sizing Parameters.

Parameter	Value
Moment of Inertia: Ixx/Iyy/Izz	11.3/38.9/39.99 kg m^2
Altitude	600 km altitude, 98 degree inclination
Uncertainty on location of center of mass	0.03 m
Instant Sunlit Area	1.705 m^2
Drag Coefficient: Cd	2.5

Driving parameters for Disturbance Environment are provided in Table 4-14.

Table 4-14: Disturbance Environment.

6

Constants			Disturbance Torque Summary		
Solar Constant	1366	W/m^2	**Solar Radiation**	2.486E-07	Nm
Atmospheric Density	8E-13	Kg/m^3	**Atmospheric Drag**	9.469E-10	Nm
Averaged Velocity	7612.7	m/s	**Gravitation gradient**	4.77E-05	Nm
Magnetic Constant	7.8E15	tesla m^3	**Magnetic field**	2.277E-05	Nm
Earth Gravitational constant	3.98E14	M^3/s^2			
			SC Orbit Parameters		
Mechanical Design Requirement			**SC Period**	5.677E+03	Sec
Center of pressure (Cp)-to-Center of Gravity(Cg) offset	0.02	m			
Thruster Nozzle Misalignment	0.05	degree	**SC Dimensions**		
Cg uncertainty	0.03	m	**Lx**	1.000	M
			Ly	1.150	M
			Lz	1.400	M

The ADCS switches through a series of modes (Figure 4-33): orbit transfer/de-tumble, collision avoidance, formation acquisition, formation keeping, momentum management, communication/target pointing, and Sun-Pointing which correspond to fixed operations internal to the XACT unit.

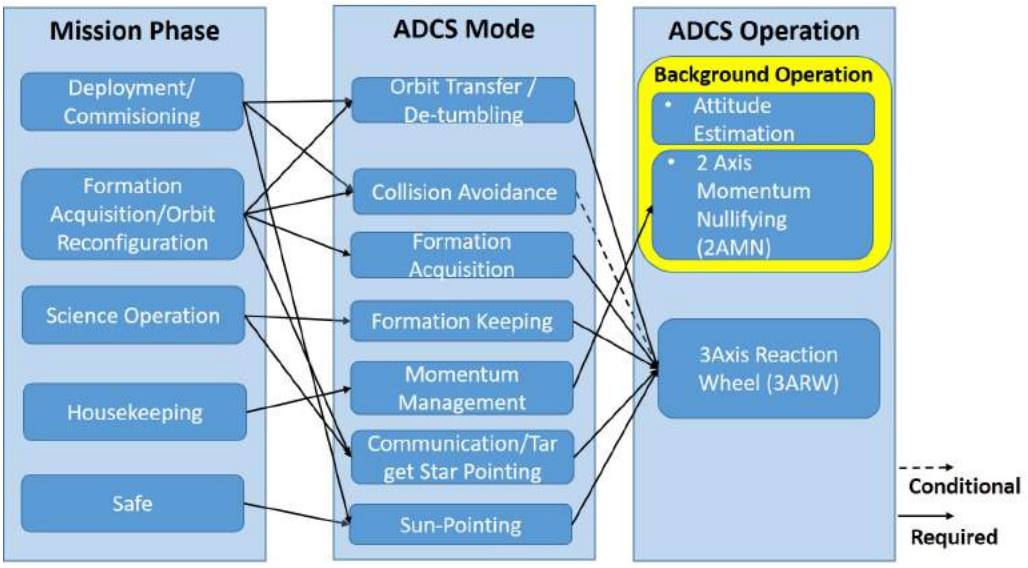

6

Figure 4-33: ADCS modes flowchart.

During Observation, the SS requires full control of both rotation and translation except cross-track thruster (5 DOF). ADCS keeps SS attitude so it points towards a target star by 3 Axis Reaction Wheels (ARW) and maintains its line of sight between the TS and the target star. Stored momentum of reaction wheels is managed through Magnetic Torquer (magnetorquer) rods. This momentum management operation runs as a background in all nominal mission phases (though it is inhibited during Science Phase Observations). As the orbit is Sun-synchronous close to a polar orbit, the Earth magnetic field provides enough change of field so the momentum can be nullified through the variation of local fields.

A block diagram of the ADCS architecture for the SS is shown in Figure 4-34. BCT ADCS system provides calibrating processes for all sensors and actuators on-ground and closes the attitude determination and control loop. The analysis performed for the selected ADCS shows ample margin in attitude knowledge, pointing accuracy, and minimization of jitter compared to the mission traceability requirements (Table 4-1). The BCT RW4 is designed to last 10 years and are currently rated for 4 years.

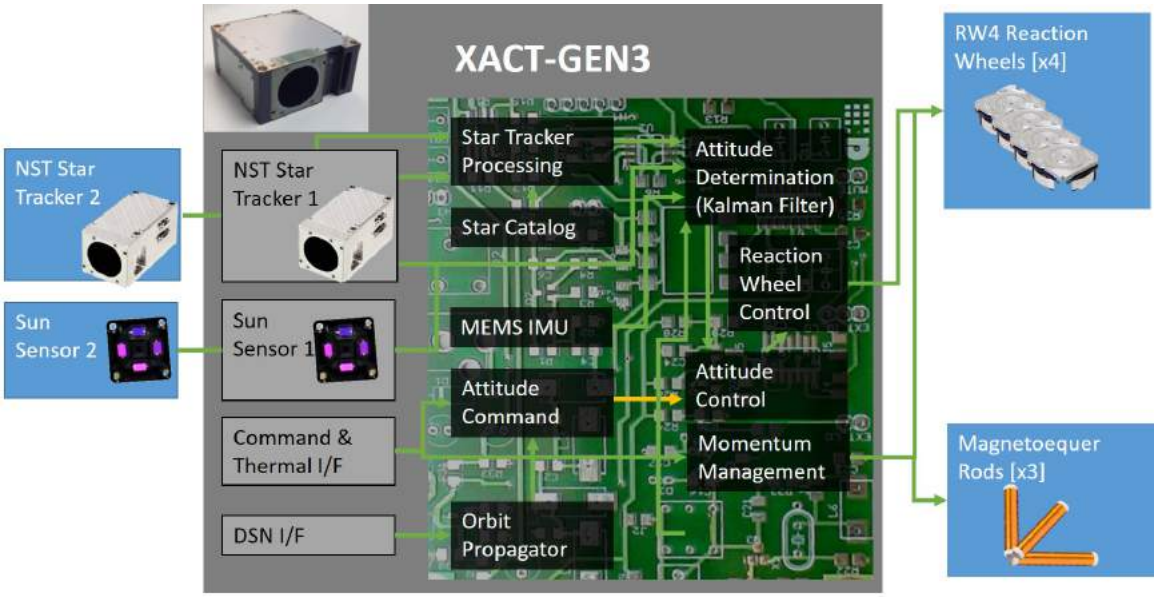

Figure 4-34: Block Diagram of ADCS subsystem.

4.2.4.1.8.2 DiGiTaL

The DiGiTaL navigation system serves two purposes on the starshade spacecraft: 1) estimation of the absolute orbit of the SS, and 2) estimation of the relative position and velocity of the telescope with respect to the starshade. DiGiTal includes a hardware layer (GNSS receiver and antennas) and a software layer.

The selected GNSS receiver is the Novatel OEM 729 Dual frequency GNSS receiver. Novatel OEM series is one of the most well-known for CubeSat and SmallSat missions such as CanX-2 and E-POP. Novatel OEM 7 offers Dual frequency (L1/L2) tracking capability so it is used for estimation/mitigation of Ionospheric delay error for long baseline precise positioning in the LEO environment. This sensor provides carrier-phase measurements with millimeter-level noise, enabling DiGiTaL's estimation and filtering algorithms to provide relative state estimates with ±2cm accuracy.

[6]

To ensure continuity and robustness of GNSS measurements, the SS is equipped with two GNSS antennas mounted on extension arms on the zenith and nadir faces of the spacecraft bus to ensure than each antenna has an unobstructed 120° FoV. Only the most zenith-pointing antenna is used for navigation purposes at any time. This antenna is through an RF switch based on attitude information provided by the spacecraft bus. This allows support of ADCS safe mode and tumbling operations.

Because the absolute orbit knowledge requirements are very benign, the absolute orbit is estimated directly from the position and velocity solutions from the GNSS receiver.

Instead, the pseudocode and carrier-phase measurements from the SS and TS (transmitted using the crosslink) are used by the DiGiTaL software to compute relative state estimates in real time with accuracy of 2 cm or better. This is accomplished using differential carrier-phase techniques similar to those used on the PRISMA mission (D'Amico, Ardaens, & DeFlorio, Autonomous formation flying based on GPS - PRISMA flight results, 2012). While carrier-phase measurements have millimeter-level noise, they are subject to an integer offset in the number of cycles. This offset must be computed for each measurement using integer ambiguity resolution (IAR). To meet the relative navigation requirements for mDOT, this must be accomplished onboard in real-time. To minimize the computation effort required for this task, DiGiTaL computes wide-line measurement types by fusing carrier-phase measurements from different frequencies and constellations (e.g. Galileo, Glonass, Beidou). These measurement types benefit from common error cancellation (e.g. ionosphere offset) and reduce the search space for the integer ambiguity resolution problem. Once an integer ambiguity solution is acquired, DiGiTaL provides relative state estimates with accuracy of 2cm or better. Figure 4-35 shows the state estimation error and formal 3-sigma covariance for the filter after activation of IAR as obtained with hardware-in-the-loop at Stanford.

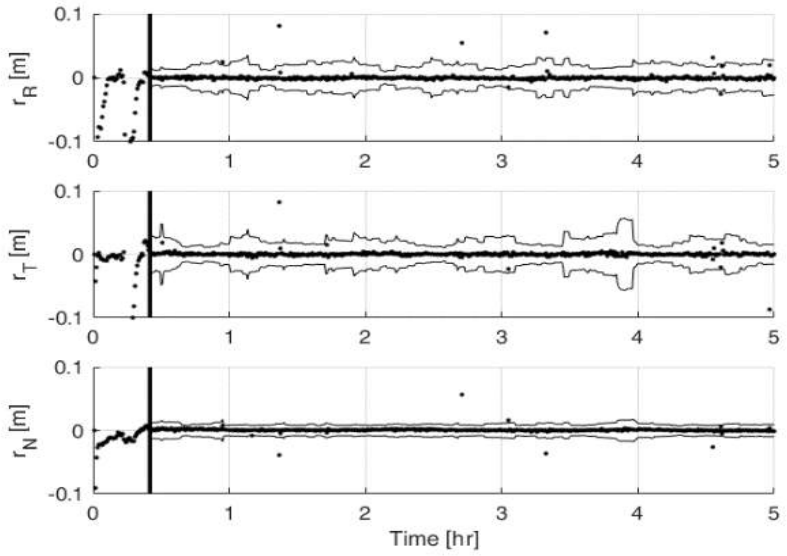

Figure 4-35: Estimation error and 3-sigma formal covariance for DiGiTaL relative position estimates after IAR fix (vertical black line).

4.2.4.1.8.3 Formation Control

The absolute and relative state estimated provided by DiGiTaL are used by the "Formation Control" algorithms to compute the translational maneuvers required to control the formation. Formation

[6]

Control is divided into two distinct modes: 1) Observation Mode, and 2) Reconfiguration Mode. Transitions between these modes are deterministically computed from the properties of Observation Sequences uploaded from the ground.

In Observation Mode, a closed-form state-space control logic is employed that simultaneously minimizes the number of executed maneuvers and minimizes propellant consumption. The number of maneuvers is minimized by planning the maneuvers such that the relative position in the plane perpendicular to the LOS crosses the full diameter of the shadow. These maneuvers act in direct opposition to the relative acceleration perpendicular to the LOS, ensuring that the formation is efficiently controlled. An example trajectory of the relative position in the plane perpendicular to the LOS is shown in Figure 4-36. This trajectory corresponds to the first in a sequence of ten observations of a target, resulting in a large relative acceleration in the plane perpendicular to the LOS and a cumulative delta-v cost of 3 m/s for the five minute observation. This trajectory includes 36 maneuvers with burn times ranging from 0.2 to 3.3 seconds. Because the maneuvers are planned in closed-form, this control logic runs in <1 second on the Tyvak processor baselined for mDOT.

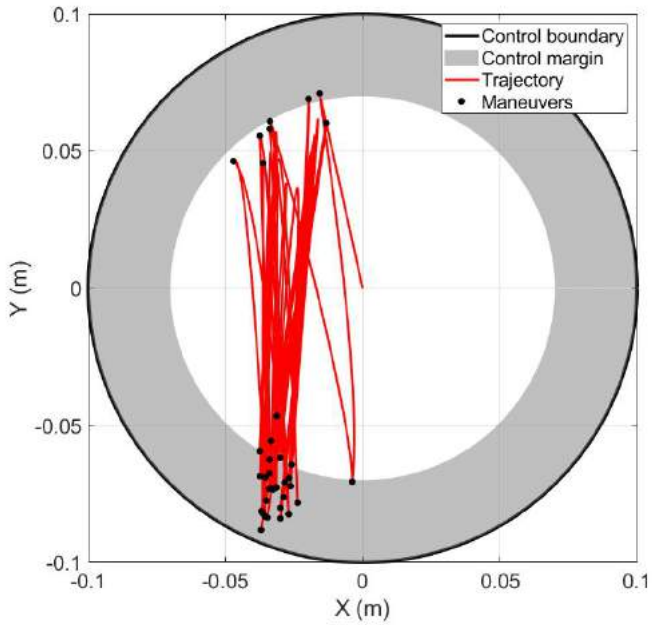

Figure 4-36: Trajectory in plane perpendicular to LOS using Observation Mode control logic.

In Reconfiguration Mode, a stochastic model predictive controller is used to plan a maneuver sequence that ensures that the formation is aligned with the target at the start of the next observation. This control logic is the same for reconfigurations to re-align with the same target or to align the formation with a different target. At each update step (10 minutes or slower), the state estimate and covariance are propagated to the start of the next observation by numerically integration the equations of motion including dominant perturbations in LEO including any previously planned maneuvers. If the desired state is within the 3-sigma covariance bound of the propagated state or the entire 3-sigma covariance bound is within the control window, the previous maneuver plan is kept and planned maneuvers are

executed until the next update. If neither of these conditions is satisfied, the maneuver plan is updated using a recently developed globally optimal impulsive maneuver planning algorithm (Koenig & D'Amico, Real-Time Algorithm for Globally Optimal Impulsive Control of Linear Time-Variant Systems, 2019). This is accomplished by first propagating the orbits of both spacecraft without any maneuvers. Next, the desired state of the SS is computed by adding the nominal relative state at the start of an observation to the propagated orbit of the TS. Finally, a maneuver sequence that drives the SS from the propagated state to the desired state is computed using the numerical algorithm in (Koenig & D'Amico, Real-Time Algorithm for Globally Optimal Impulsive Control of Linear Time-Variant Systems, 2019). Preliminary tests have found that this algorithm can be executed in <10 secons on the Tyvak processor baselined for mDOT. To enable observations to be performed over consecutive orbits, maneuver planning and execution are run autonomously on-board. Navigation and control data is downloaded to the ground in regular intervals for post-facto analysis.

A block diagram of the communication architecture for the guidance, navigation, and control subsystems for the SS and TS is shown in Figure 4-37.

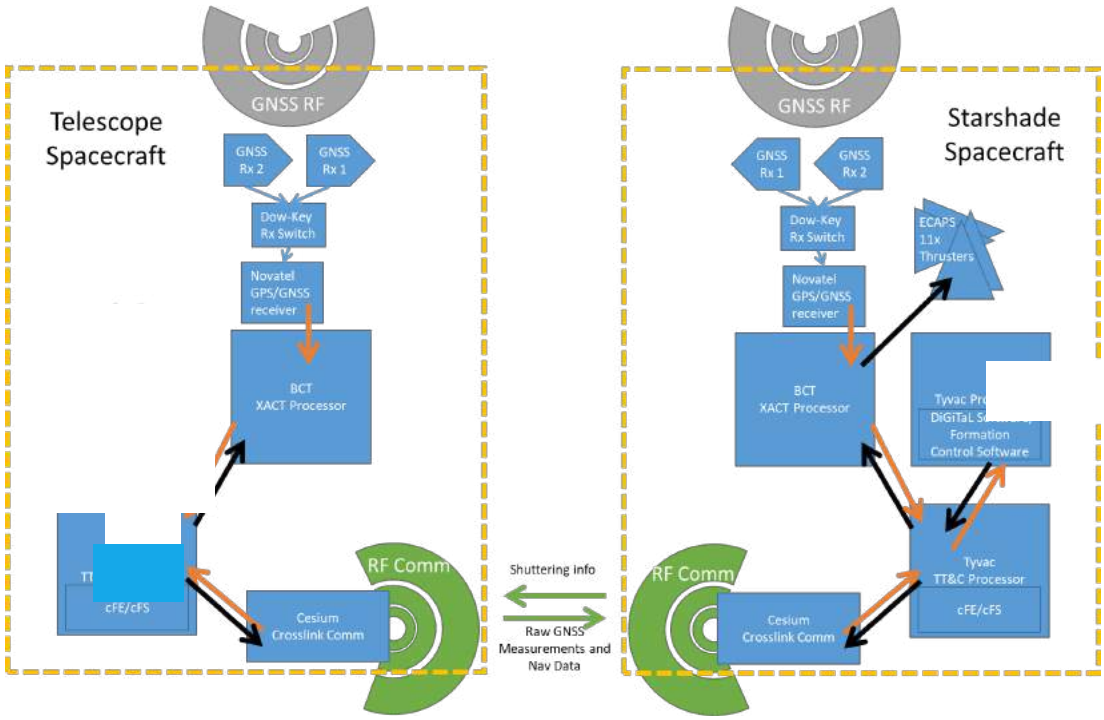

Figure 4-37: Communication flowchart for starshade and telescope spacecraft.

The information exchanged between each of these components on the SS is shown in Figure 4-38.

6

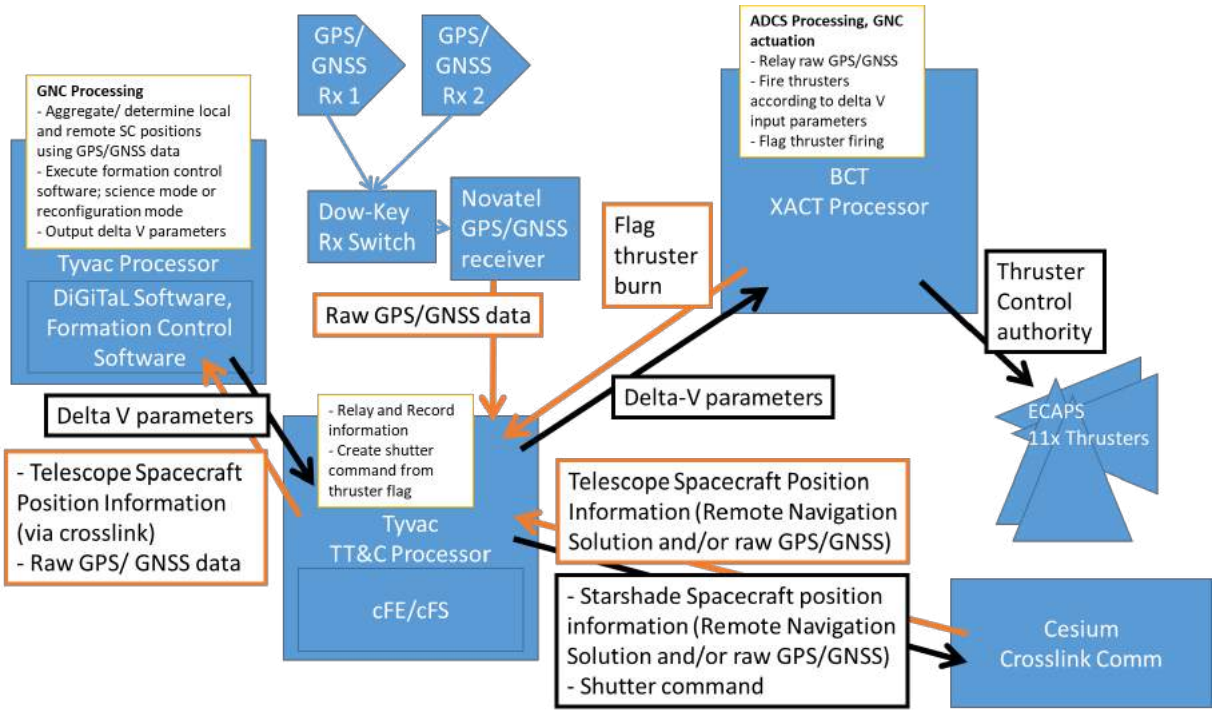

Figure 4-38: Information flow between starshade spacecraft subsystems.

4.2.4.1.9 Thermal

The components selected have LEO heritage and engineering best practices were followed in designing the ConOps with respect to thermal and power management. The baseline SS design includes allocations for heaters, temperature sensors, and coatings and coverings (e.g. MLI) to be further refined in later study.

4.2.4.1.10 Radiation

This mDOT radiation analysis includes an environmental assessment of the exposure conditions for the spacecraft trajectory and operational orbit, as well as a preliminary assessment of the component level susceptibility for high energy and total dose exposures.

Environment and Simulation Parameters

The radiation environment for mDOT yields a total ionizing dose (TID) of 4 kRad under 2 mm Aluminum shielding during the 1 year mission lifetime. With a radiation design margin (RDM) of 2 (RDM=2), it is advisable to design the spacecraft to withstand 8 kRad TID exposure.

The radiation environment is modeled during solar maximum using SPENVIS, ESA's Space Environment Information System, which incorporates many modeling tools including: SHIELDOSE, CRÈME 96, AE8, AP9, ESP-PSYCHIC, and the ISO-15390 standard model. The simulation parameters model the radiation environment with an approximate launch date of 2024 and the orbit at 600 km altitude above Earth for a 1 year mission duration.

Table 4-15:Radiation exposure summary.

6

Mission start	Approximate Orbit	Duration	Shielding	Exposure	TID
Jan 2024	600 km (LEO, SSO)	1 year	2 mm Aluminum	4 kRad	8 kRad (RDM =2)

4.2.4.1.10.1.1 mDOT Mission Total Ionizing Dose (TID)

Table 4-16 and Figure 4-39 show the total ionizing dose (TID) absorbed by the spacecraft under varying thickness of aluminum shielding; note that 1/8-inch (3 mm) aluminum panels are currently modeled for the spacecraft). Values for TID with a radiation design margin (RDM) of 2 that are less than 10 kRad are marked in green. A TID between 10 kRad and 50 kRad is shown in yellow, and the red values mark the range of shielding inadvisable for design.

Table 4-16: Total ionizing dose over mission lifetime vs. shielding.

Shielding (Al absorber thickness)			**Total Ionizing Dose (TID)** 1 year Mission at 600 km		
mm	**mils**	**g cm^{-2}**	**rad**	**TID kRad**	**TID kRad RDM = 2**
0.05	1.968	0.014	2.23E+05	223	446
0.1	3.937	0.027	1.19E+05	119	238
0.2	7.874	0.054	6.41E+04	64.1	128.2
0.3	11.811	0.081	4.41E+04	44.1	88.2
0.4	15.748	0.108	3.35E+04	33.5	67.0
0.5	19.685	0.135	2.69E+04	26.9	53.8
0.6	23.622	0.162	2.22E+04	22.2	44.4
0.8	31.496	0.216	1.61E+04	16.1	32.2
1	39.37	0.27	1.23E+04	12.3	24.6
1.5	59.055	0.405	6.82E+03	6.82	13.64
2	78.74	0.54	4.00E+03	4.00	8.00
2.5	98.425	0.675	2.41E+03	2.41	4.82
3	118.11	0.81	1.49E+03	1.49	2.98

[6]

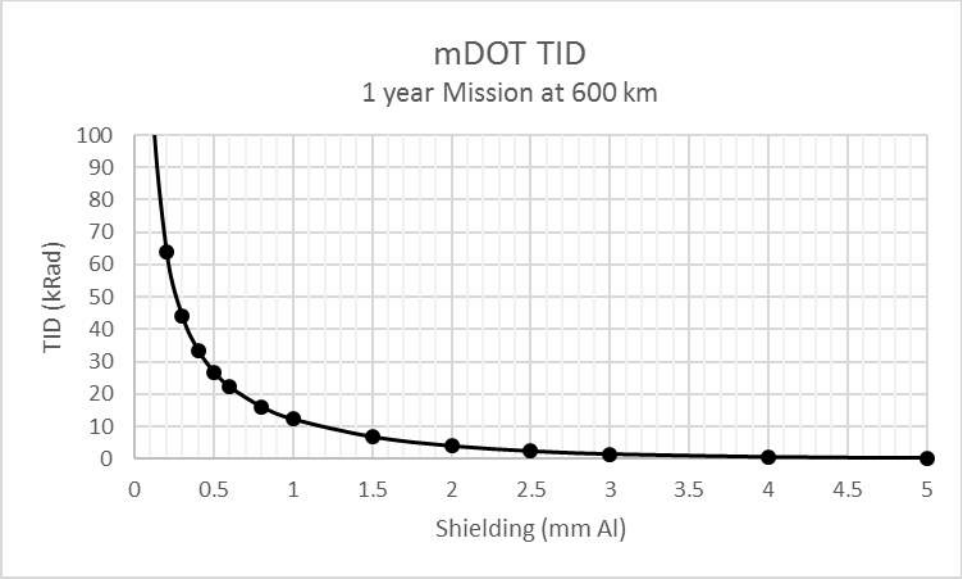

Figure 4-39: Total ionizing dose vs. shielding thickness.

4.2.4.1.11 Flight Software

The current Flight Software (FSW) strategy maximizes off-the-shelf existing flight package architecture and code re-use for schedule, cost reduction and high TRL claims. mDOT FSW is based on the NASA standard core Flight System (cFS) open-source software developed by GSFC. cFS is a platform- and project-independent reusable software framework, with a set of reusable software applications. The core Flight Executive (cFE), including the platform abstraction layer, was first used on the Lunar Reconnaissance Orbiter (LRO) launched in 2009, and the initial suite of cFS applications was first used on the Global Precipitation Measurement (GPM) spacecraft launched in 2014. This approach for mDOT emulates the LADEE (EOM 2014), BioSentinel (in development), and Starling (in development) FSW strategy. Items such as cFE, Target Language Compiler (TLC), Scheduler, Housekeeping, Health and Safety, File Manager, and others reuse 100% of existing code. Many hardware device drivers with ARC heritage are also reused. The BCT XACT has been integrated from BioSentinel and the I/O device drivers can be reused with minimal modification. New software that will be developed will be plugins to the DiGiTaL/GNC embedded software that will augment the ADCS solution. Note that the navigation algorithms for DiGiTaL/GNC are written in C/C++, however wrapped in Simulink S-Functions for ease of integration into overall Ames spacecraft simulation environment. Minimal vehicle-specific code changes will be needed to the telemetry and command databases, Safe Mode, thermal control, and power control. Due to constraints of autonomous maneuvers for alignment, operators will not be in the loop during science operations, thus mDOT FSW must be robust and highly autonomous for operations.

Although the autonomous nature of this mission is demanding, the teaming of NASA Ames and Stanford Space Rendezvous Lab is best suited for the task. The NASA Ames team has been working with cFE/cFS for more than 10 years with a specific buildout for ADCS solution using Blue Canyon hardware (for BioSentenial - ongoing). This software build required in-depth knowledge of the ADCS hardware that will also be used for mDOT. The Stanford group adds additional knowledge of ADCS systems as well as algorithmic development for the DiGiTaL system software and formation control software needed to perform the mission.

[6]

FSW software requirements and decisions are preliminary and will be revisited in phase A studies.

4.2.4.2 Telescope Observer Spacecraft

The TS is a 6U CubeSat that is carried and deployed by the SS. Blue Canyon Technologies (BCT) was contacted by the study team and provided a cost estimate for a LEO spacecraft bus which meets the top level mission requirements (see Figure 4-40 and Table 4-17). They are currently considering modification of either their 21ASM1950 (BCT structure with simplified avionics) or the BCT 6U RAVAN bus (with simplified assembly). The 6U FlexBus platform should also be assessed for suitability for mDOT mission needs. Future discussions with BCT will formally define the interfaces which will support the telescope and DiGiTaL payloads into their platform. The requirements on the TS bus are well within reasonable limits for current LEO CubeSat capabilities, and so procurement of a suitable bus is considered a low-risk item by the study team.

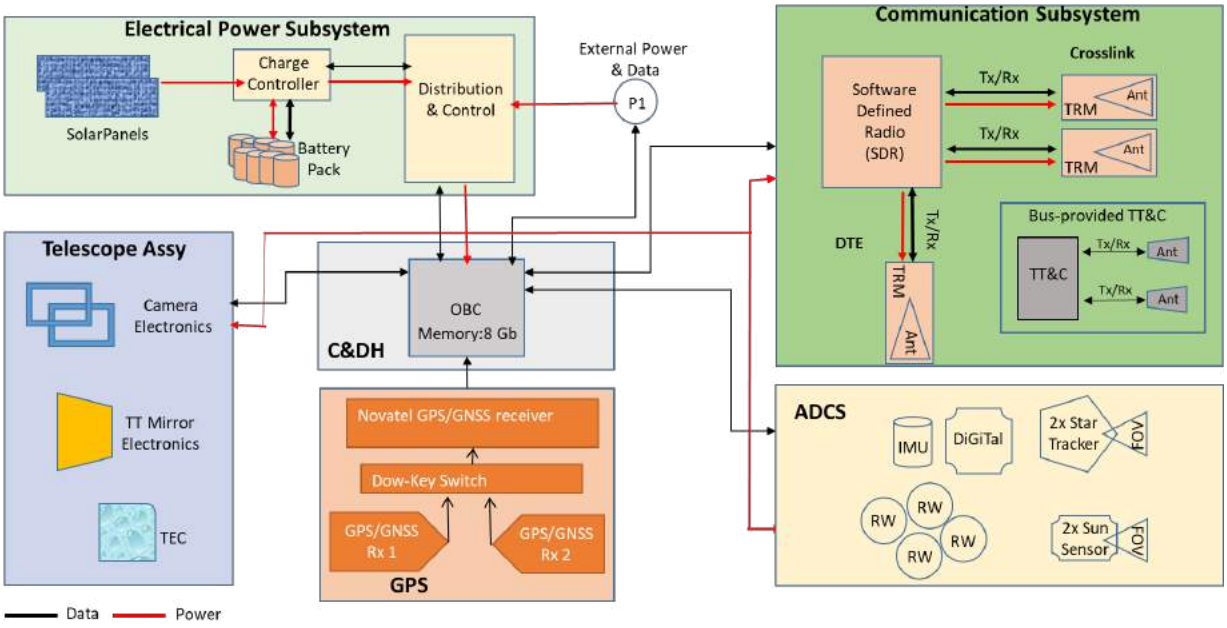

Figure 4-40: Telescope Spacecraft Functional Block Diagram.

4.2.4.2.1 Flight System

The TS has no propulsion system, thus it relies on its ADCS reaction wheels for total attitude control and the magnetorquers for wheel desaturation. The telescope assembly occupies 4U volume in an L-shape configuration (see Figure 4-41) which leaves 2U volume for housing spacecraft avionics. Solar cells are body-mounted on the spacecraft sun-facing panels and are augmented by a deployable solar panel(s). The deployable panels may be eliminated if TS power margins are found to be adequate without them. Crosslink patch antennas are mounted on the aperture side and on the anti-aperture side. A patch antenna is mounted on the Earth-facing panel for DTE using NEN (KSAT). Like the SS, the TS is also equipped with GNSS-capable DiGiTaL systems for enhanced position determination. Data volume sufficient for three Target Stars is provided, assuming 600 MB per Observation and two revisits per Target, although data is intended to be downlinked after all Same Target Observations for a given Target have been completed.

[6]

Table 4-17: Telescope spacecraft vendor requirements summary.

Resource	Value	Note
Volume for Telescope	4U in L-shape	see Figure 4-41
DiGiTaL antenna placement	2x GNSS antennas, 1x GNSS receiver, 1 RF switch	GNSS antennas shall be mounted one on Zenith and one on Nadir
Crosslink Radio System	1 SDR, 3 antennas	SDR: 5 x 8.5 x 1.4 cm Each Antenna: 10 x 10 x 2cm
Payload Power	45 W while in eclipse (15 minutes/orbit), 10 W daylit	Duty Cycle for Science Observations
Pointing Accuracy	± 0.45 deg, all axes	Note capability of bus is ~0.007 deg
Design Lifetime	18 months	Nominal mission duration 1.1 years
Orbit	SSO, 600 km, 98 deg inclination	LTAN: noon-midnight
Propulsion	None needed	
Science Data Volume	4 GB	Assuming half of an 8GB SD card for science data. 1 Target x 2 Observations/each x 600 MB = 1.2 GB data per Target

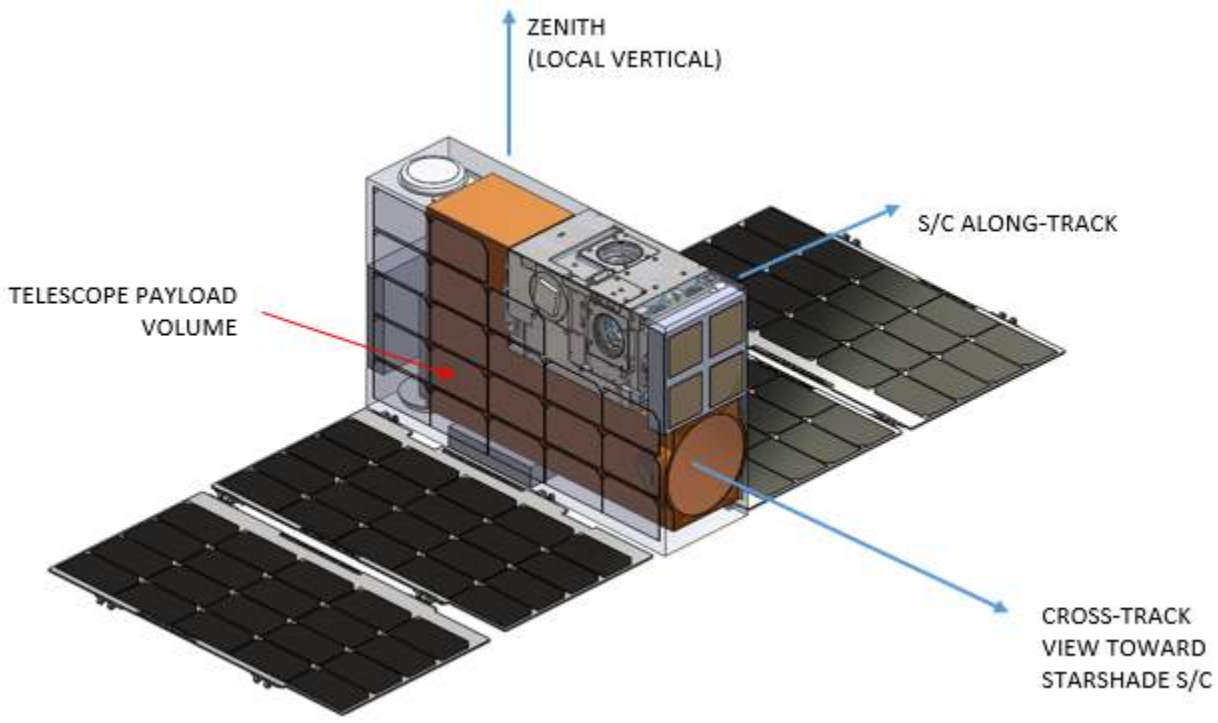

Figure 4-41: Telescope Spacecraft Bus Concept, Isometric View.

6

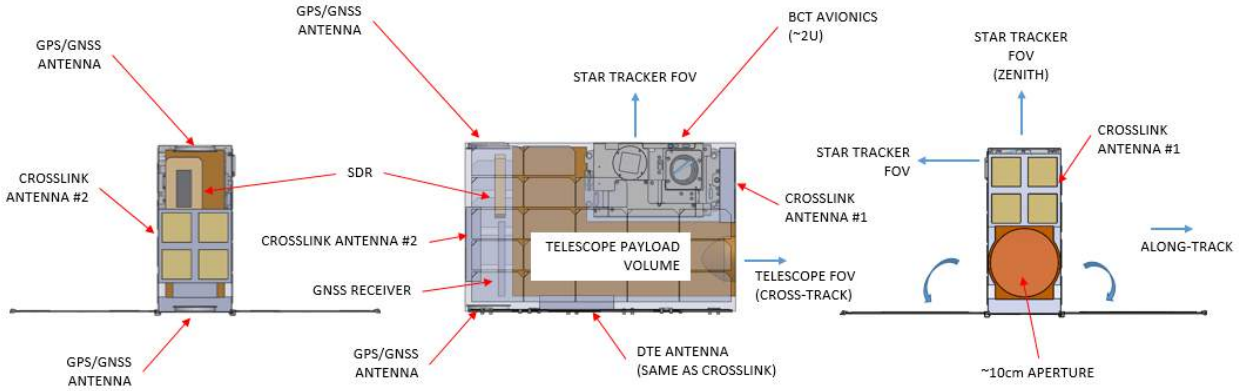

Figure 4-42: Telescope Spacecraft Bus Concept, Side Views.

Notional dimensions are shown in Figure 4-43.

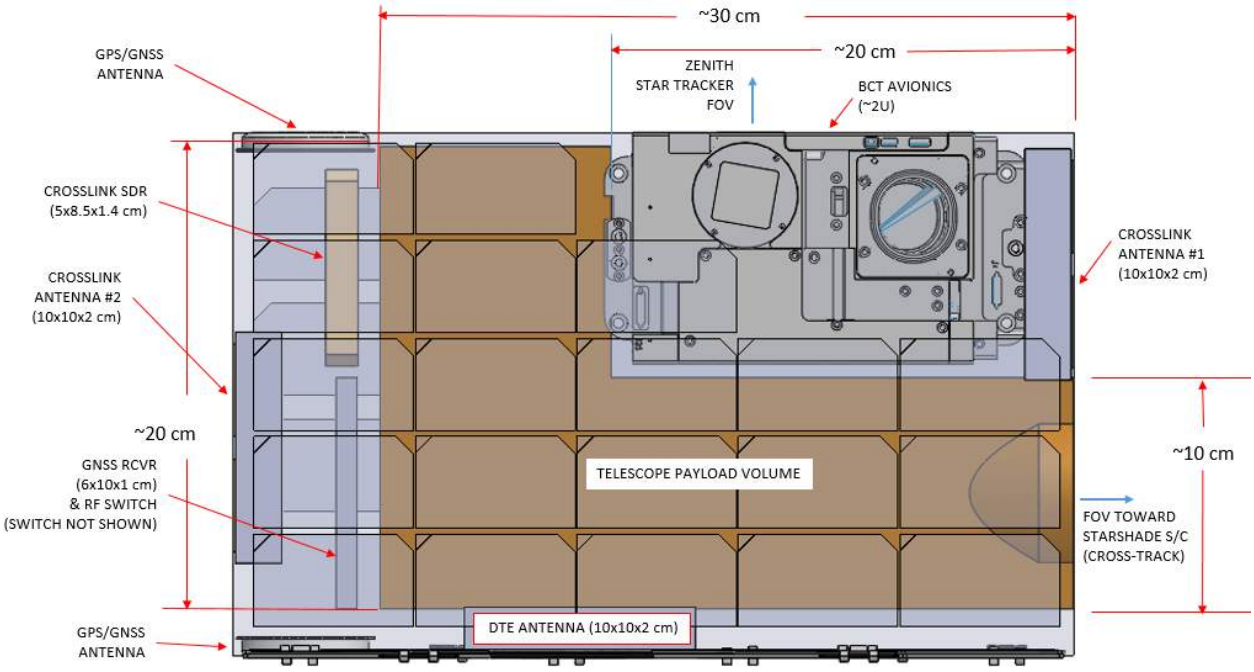

Figure 4-43: Telescope Spacecraft Bus Concept with Dimensions.

Table 4-18 provides an overview of the expected Telescope Spacecraft subsystems. BCT has assessed the overall system TRL at 7/8 after accounting for payload interface modifications.

[6]

Table 4-18: Telescope spacecraft major components.

Subsystem	Major Subsystem Component
Payload	Telescope Assembly with 2 cameras, tip/tilt mirror, and TEC
Structure	6U from BCT Telescope Assembly to occupy 4U in L-shape form
C&DH	Tyvak SBC with Tyvak Linux BSP Operating System ARM Cortex A8+ DSP Coprocessor 512 MB RAM NAND-Flash 8 GB SD-card
Electrical Power System	BCT to provide
Communication	Cesium SDR S-band with Tx/Rx Module (TRM) 3 S-band patch antennas (2 for crosslink, 1 for downlink) Xilinx FPGA host
ADCS	BCT XACT
Thermal	Deferred for future proposal effort
Propulsion	None
Flight Software	BCT, DiGiTaL

4.2.4.2.2 Communications

The 6U TS plans to use a Cesium S-Band system to support TT&C and science data downlink with KSAT , downlink to SS of GNSS data and uplink from SS of camera shuttering information. The Cesium telecommunication system uses the same hardware configuration as the SS. The Bus provided TT&C capabilities provides redundant science downlink capabilities with KSAT.

The functional block diagram for the TS communications subsystem is shown in Figure 4-44.

6

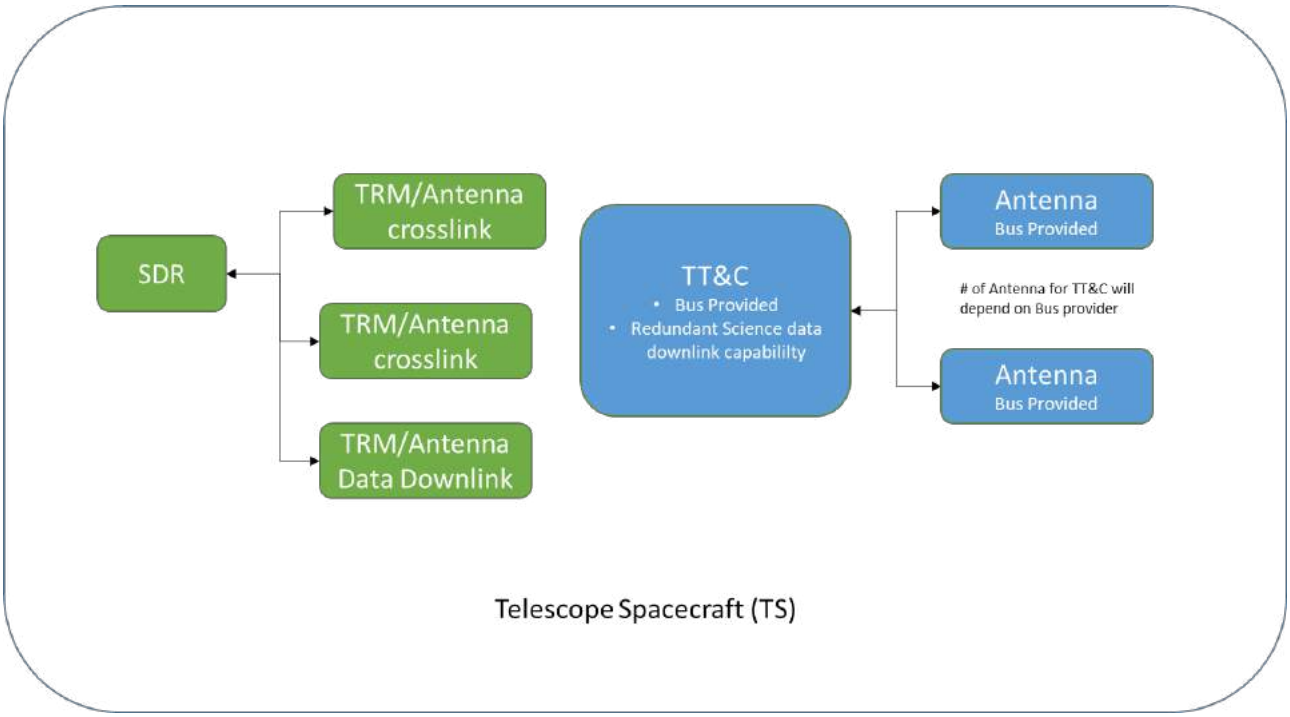

Figure 4-44: Telescope spacecraft communications block diagram.

4.2.4.2.3 Navigation

In the mDOT concept study, TS is a reference satellite and formation flying is implemented by SS. The role of TS for Formation Flying is to collect and transfer its GNSS measurements to SS. TS requires 3 DOF rotational maneuver capability to provide a field of view to Telescope so target stars in view of Telescope. However, no translational or control motion is required. Typical ADCS system offers much higher level of accuracy than ±1 degree of attitude requirement, BCT BUS's default ADCS, XACT, is used for this study.

To facilitate the use of DiGiTaL on the starshade for relative navigation with centimeter-level accuracy, the TS is equipped with a the Novatel OEM 729 Dual frequency GNSS receiver and two GNSS antennas on opposite faces of the spacecraft bus. As on the SS, an RF switch is used to selected the most zenith-pointing antenna using attitude data from the spacecraft bus. The raw position and velocity solution provided by the receiver is used for scheduling bus operations (power collection, downlink, etc). The pseudocode and carrier-phase measurements are transmitted to the SS using the crosslink as shown in Figure 4-37.

4.3 Development Approach

mDOT's development approach leverages ARC's significant experience in developing low-cost, cost-effective small Spacecraft missions and is based on NPRs 7120.5E (NASA Space Flight Program and Project Management Requirements), 7123.1B (NASA Systems Engineering Processes and Requirements), and GSFC-STD 1000 Rev G (Rules for the Design, Development, Verification, and Operation of Flight Systems, aka GOLD Rules), tailored for a Class D mission (as defined per NPR 8705.4, Risk Classification for NASA Payloads). Based on this classification, mDOT uses selectively redundant design approaches to mitigate critical single point failures, but otherwise permits the use of single string design.

[6]

4.3.1 System Engineering

mDOT's Project System Engineer (PSE) serves as the technical authority through all mission phases and chairs the Systems Engineering Team (SET). The SET manages the SE effort, including developing requirements, ICDs, and the Verification and Validation Plan; tracking technical performance measures (TPMs); and performing trade studies and analysis. Payload-to-Spacecraft ICDs are defined in Phase A, allowing independent testing of the instrument and Spacecraft prior to integration. The Spacecraft-to-host ICD is defined early in Phase B to establish critical interfaces with the host Spacecraft. Lower-level ICDs are developed as needed between critical HW and SW elements to ensure compatibility prior to integration. mDOT's Spacecraft team implements Spacecraft design using OTS components and systems wherever possible. The mission environments, both external and internal, are characterized to ensure adequate design margins are incorporated for radiation effects, electrical system grounding and noise, and EMI/EMC control for both on-orbit and launch environments. Configuration Management uses MINX, a secure web-based document management system successfully used on LADEE.

mDOT's SET implements the mission science requirements identified in the STM. The instrument and mission requirements listed in the STM (Table 2-1) flow down to requirements on flight and ground segments as shown in the MTM (Table 4-1). The mission requirements in the MTM are used to derive mission system specifications and ICDs, particularly the payload-to-Spacecraft ICDs. The Dynamic Object Oriented Requirement System (DOORS) tool is used for requirements tracking, flow-down, documentation, and verification. The instrument concept proposed by mDOT is modeled to validate that the technical performance meet the science objectives. Science constraints on the operations concept have been included to ensure the science operations produce the required measurements. Throughout the formulation, implementation and development phases, the mission architecture, operations concept, and models will be cross-validated to ensure consistency in meeting mission requirements.

6

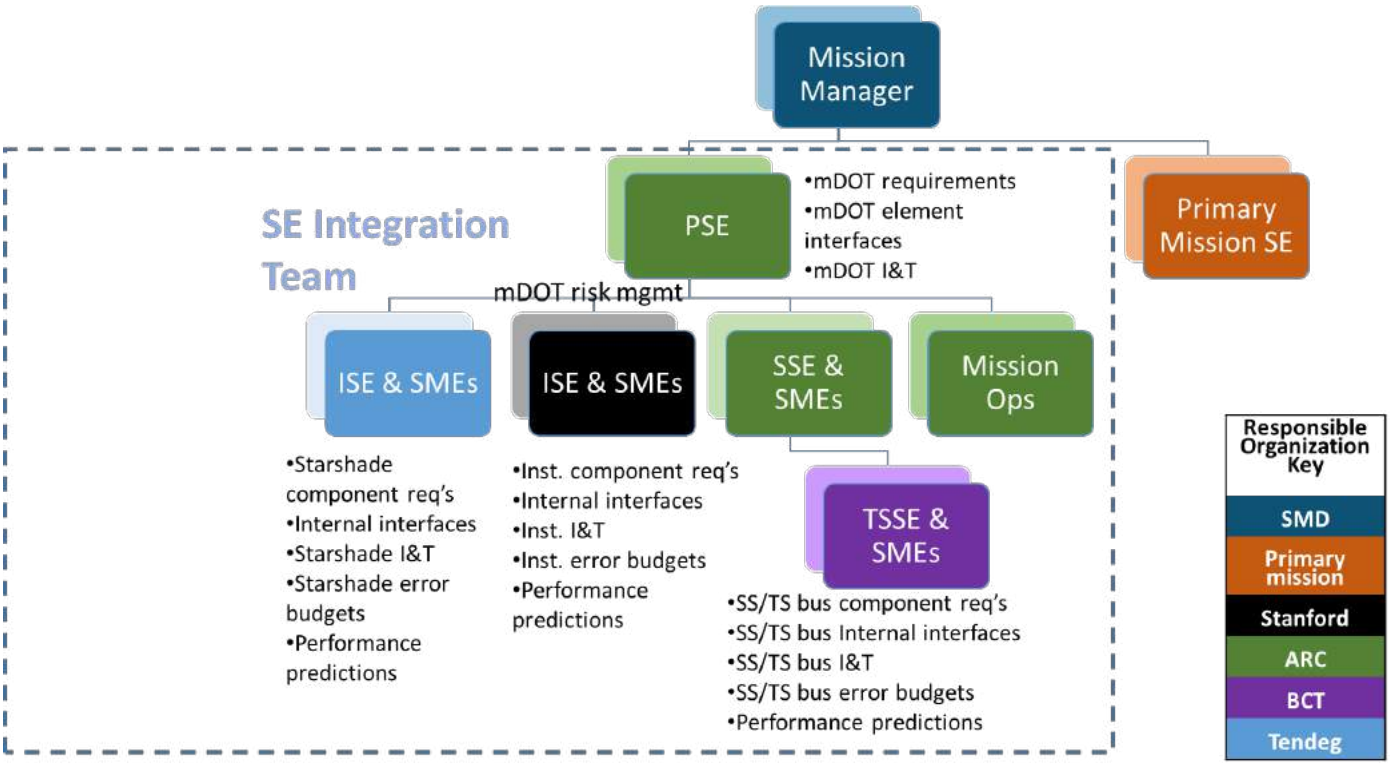

Figure 4-45: mDOT systems engineering roles.

4.3.2 Assembly Integration and Testing

4.3.2.1 Instrument AI&T

After the pre-ship review, the first Flight Model (FM) is shipped to NASA ARC for AI&T to the spacecraft, while the second FM remains at Stanford to serve as a spare.

The starshade assembly will undergo metrology before shipping to validate its deployed shape, using photogrammetry and a precision coordinate measuring machine. A key trade is the need for a deployment test after integration into the SS Bus; that could be conducted using a coordinate measuring machine and pre-defined reference points on each petal.

The telescope assembly is sufficiently compact that it can undergo optical end-to-end testing using a collimated beam produced by a simple optical bench or a commercial interferometer; the Stanford group has a Zygo interferometer with a 2" beam and can procure a suitable beam expander. End to end optical validation will insure the telescope meets image quality specifications.

Figure 4-45 illustrates the AI&T flow.

4.3.2.2 mDOT Assembly, Integration, Test, and Verification

The mDOT team has an assembly, integration, and test plan based on past SmallSat missions. The ARC track record of success in building, integrating, verifying, and flying small missions such as GeneSat, PharmaSat, O/OREOS, and LADEE gives mDOT a legacy of proven facilities, test partners, and assembly techniques. The mDOT plan benefits from ARC's background in work with geographically dispersed

[6]

partners for LCROSS and ISS Payloads and its practice in adapting NASA's verification process to small-scale efforts.

The mDOT AI&T plan covers the following elements: facilities, integration flow, verification, and approach to special processes.

4.3.2.3 Facilities

Our experience in SmallSat integration combined with the portable size of mDOT subsystems dictates that internal interfaces are developed by an experienced team with direct access to all hardware.

EMI/EMC is performed at a Santa Clara-based commercial vendor; while flatsat, mass and cm, calibration, and alignment testing are completed on-site at ARC. Ground station pre-compatibility is performed in cooperation with the ARC MMOC.

SmallSat-scale cleanrooms and benches, thermal vacuum chambers, and vibration test platforms are available at ARC. Multiple onsite facilities ensure flight surveying, testing, and troubleshooting can be accommodated at the same time as other ARC SmallSat efforts. Geographic proximity allows mission oversight personnel such as the CSO to supervise testing without having to travel.

4.3.2.4 Flow

An assessment has been performed of the minimum testing required, and the mDOT AI&T flow is in line with the study guidelines. Figure 4-46 and Figure 4-47 shows the order of assembly and test for the TS and SS, respectively. Following NASA GSFC STD-1000G, Rules for the Design, Development, Verification, and Operation of Flight Systems, mDOT has allowed schedule margin of 2 months per year for testing and adapting external interfaces. As mDOT is a hosted payload, discussions with the selected launch services provider and requirements imposed upon mDOT by the provider may drive future changes to this notional flow.

In addition to the best practices listed in Section 6, this flow was informed by ARC experience in hardware transfer and oversight with local offsite facilities as well as input from partners (Stanford, Tendeg, and BCT).

BCT in (Boulder, CO) leads AI&T for the TS (see Figure 4-46). Stanford delivers the tested telescope assembly and DiGiTaL to BCT for integration into the TS. System-level verification and bakeout of the TS is performed at BCT prior to integration into the SS. The TS is then hand delivered to ARC for integration into the Deployer hosted on the SS.

ARC leads AI&T for the SS (see Figure 4-47). Tendeg assembles, tests, and aligns the starshade assembly in (Louisville, CO) and ships it to ARC for integration into the SS bus. Stanford in (Palo Alto, CA) assembles, tests, and provides a flatsat of the complete DiGiTaL system to ARC. ARC assembles and integrates the SS bus. System-level bakeout and vibration testing is performed with a mass simulator in place of the TS. Following solar array deployment verification, the ESPA ring adapter is installed. The delivered TS is integrated into the SS. As a packaged system, the SS including TS then undergo final workmanship vibration testing (with access through an access port allowing for basic functional testing of the TS post-vibe).

6

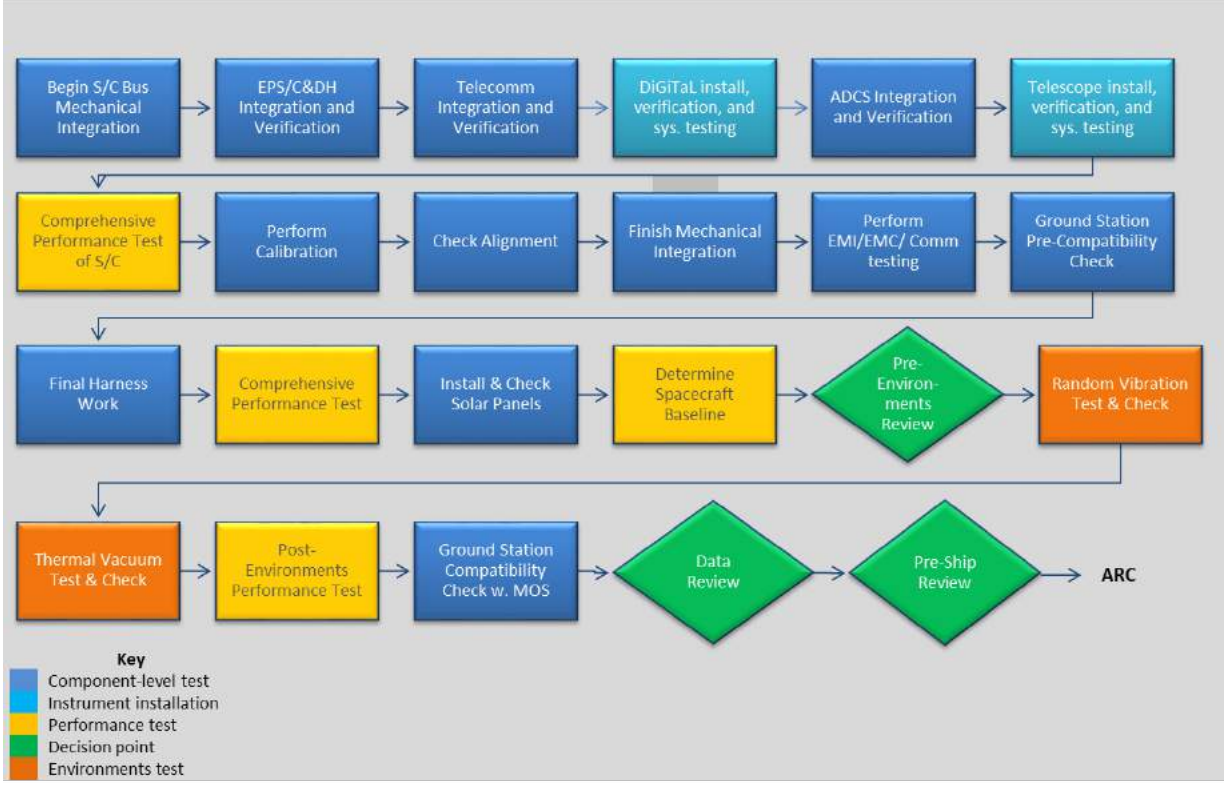

Figure 4-46: Telescope Spacecraft AI&T Flow, performed at BCT.

6

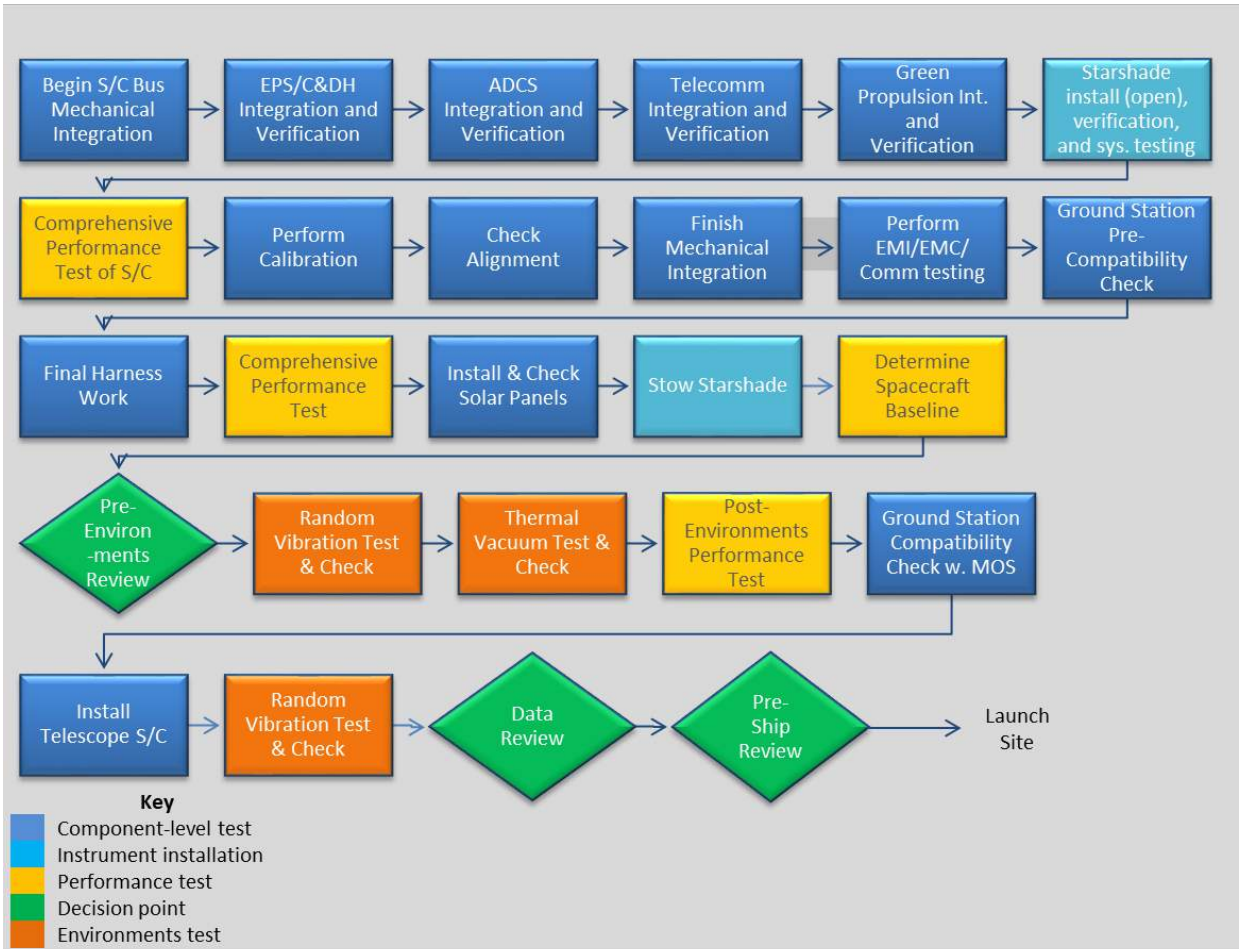

Figure 4-47: mDOT Starshade Spacecraft Assembly, Integration, and Test (AI&T) flow is a tailored form of ARC's flight-proven Class D process.

4.3.2.5 Verification

As detailed in Section 4.3.1, mDOT will be held to Class D verification standards. See Figure 4-46 and Figure 4-47 for planned verification activities.

4.3.3 Future Trades and Studies

4.3.3.1 Trades Performed

- Use of KSATLite (3.7 meter) dishes for Command and Science Downlink vs. KSAT (KSAT baselined)
- SS with Solar Array (or cells on the starshade) vs. Body-mounted cells only (body-mounted is baselined largely due to interface simplification but also for fewer disturbance torques)
- Two medium versus one large propellant tank (one tank is baselined for simplified propellant management, though two tanks would have allowed a greater propellant mass)
- 6am/6pm LTAN versus Noon/Midnight LTAN. Noon/Midnight LTAN was selected as baseline due to spacecraft operational simplicity and that Observation has to be performed in eclipse. One major prohibition imposed by mDOT is for the SS to not generate any significant light source that could be imaged by the TS during the observation period. The light source could be

any sunlight reflected off the SS (either reflective surfaces or the starshade itself) or thruster plume glow. This prohibition is not met by the 6AM/6PM LTAN where the starshade, having reflective thruster nozzle and patch antenna mounted on its surface facing the TS, is oriented towards the sun. Using the same 6AM/6PM LTAN but with the sun on the back side of the starshade would not work either since sunlight could violate the telescope FOV. In addition, Earthshine could be a significant source of scattered light when observing relatively faint targets. Any LTAN that can avoid unwanted light source(s) from being generated by the SS and at the same time not have the sunlight entering the telescope boresight would satisfy the requirements. These constraints can always be satisfied when star observation is performed in Earth's shadow or eclipse. Thus, any LTAN orbit with eclipse at the equator lasting more than 5 minutes is feasible. However, for many orbits the analysis showed that the SS would have to occasionally rotate about its Normal axis to expose solar panel to sunlight after observation, then reverse the rotation for the next observation. These body rotations are not required with Noon/Midnight LTAN. Thus, a pragmatic choice of Noon/Midnight local time has been made for a baseline mDOT mission.

- Hybrid propulsion (electric and monopropellant) vs all green propellant-based system. Selected the green propellant system for simplicity which does not require high power like the electric propulsion system.
- Single 10N bi-prop vs Paired 5N green thrusters. Selected the 5N thrusters because there are no 10N green thrusters available. 10N thrusters are available but are bi-propellant utilizing hydrazine
- Alternative propulsion systems ruled out to date include the Busek BGT-5 (insufficient thrust) and the Aerojet MR-111G (low TRL).
- Reentry options for the TS. A mass of 16kg, Cd, Cr, and Ck areas of 0.18 m^2, Cd of 2.2, and Cr of 1 were used and a resultant lifetime computed. At 500 km, the lifetime estimate for average solar flux levels is 3.6 years. At 600 km, the TS was found not to decay within 25 years. If the drag area is increased to 0.25 m^2, the lifetime starting at 600 km altitude was found to be 15.8 years. This means that the orbital debris standard can be satisfied by intelligently managing the drag area of the TS by orienting the largest face into the velocity direction and/or using the deployable solar arrays as an aerobrake.
- Reentry options for the SS. Similar to the TS, a preliminary orbital lifetime was computed for the SS. A mass of 184 kg, Cd, Cr, and Ck areas of 1 m^2, Cd of 2,2 and Cr of 1 were used and a resultant lifetime computed. At 600 km, the lifetime estimate for average solar flux levels was outside the 25 year limit. By modeling an average drag area of 7 m^2 (using the starshade as an aerobrake), the lifetime of the SS was reduced to 4.7 years. This can be further reduced by expending any remaining propellant to reduce the orbit altitude.

[6]

4.3.3.2 Recommended Trade Studies

Table 4-19: Recommended future trade studies.

Trade #	Subsystem	Future Trade	Rationale
1	Starshade Payload	Manufacturing options	The baseline starshade manufacture and deployment mechanism is relatively low-risk, moderate cost and mass, but does not scale to larger missions. We will explore lower-mass alternatives.
2	Starshade Spacecraft Propulsion	Switch to hydrazine-based propulsion system	Less expensive (but lower efficiency) than green propellant-based propulsion system. Extensive flight history.
3	Starshade Spacecraft Propulsion	Single propellant tank instead of two separate tanks	Current baseline simplifies plumbing since one tank supports all thrusters. Previous iteration used one tank for the N-thrusters and another tank for the T/R –thrusters. Tanks may not empty as planned, thus rendering a set of thrusters useless before end of mission.
4	Starshade Spacecraft Propulsion	Single 10N thruster vs a pair of 5N thrusters	Simplifies installation and occupies less volume than two 5N thrusters (however, it reduces redundancy). Current 10N thruster is bi-prop, but with flight heritage.
5	Telescope Spacecraft Propulsion	Add propulsion system to starshade spacecraft	This could reduce total system mass because less propellant can be used to achieve the same total delta-v because the TS has less mass than the SS.
6	CD&H	Single spacecraft to download science and housekeeping data and for receiving updated command tables. Current baseline requires each spacecraft to communicate to the ground.	This could save cost since only one spacecraft could download everything and receives all updated commands. Also, this improves the robustness of the system: SS can download TS housekeeping/science data or vice versa.

[6]

7	Communications	Reinvestigate use of KSAT vs. KSATlite	As the science implementation approach matures, the data volume requirements may change. Reassessing the use of KSATlite with respect to link analysis but also cost and operational complexity may be warranted.
8	Communications	Single-string vs. redundant communication systems	The current design baselines redundant communication systems; single vs. redundant systems should be traded with respect to cost and project risk posture.
9	C&DH	Single vs. Double onboard computers (for hosting DiGiTaL and GNC software)	Minimizing hardware is desired for mass and interface considerations.
10	C&DH	Onboard SBC hardware selection	The Tyvak system is selected for the purposes of this report since this is the test bed hardware for the setup at the Space Rendezvous Lab at Stanford. Other SBC hardware options are available that may simplify other areas of development, they are: 1) BioSentinel-legacy SBC from SDL (works with cFE/cFS, Ames has familiarity), 2) SBC from Cesium (simplified radio interface), or 3) SBC from Blue Canyon (the FSW would be similar between the telescope and the starshade, thus decreasing complexity).
11	AI&T	Integration of TS prior to or subsequent to SS environmental test	To facilitate functional test of the TS while it is installed in the Deployer, access considerations must be made. If these accesses are undesirable, the TS can be fully environmentally tested prior to installation in the SS, but as a standalone system.
12	ADCS	GNSS RF Switch options	The selected switch is geometrically large, but the only space-rated suitable switch. There may be a preference to select and test another switch for form factor purposes.

[6]

13	Telescope instrument	Image stabilitization approaches	To achieve sensitivity and angular resolution we require sub-arcsecond pointing stability. In the baseline this is achieved with an image stabilization mirror fed by a separate camera channel. Newer spacecraft buses may have the control capability using just their reaction wheels to achieve nearly the same pointing stability if given sufficiently precise information. Feeding back sensor information to the reaction wheels to remove the tip/tilt platform should be explored.
13	Spacecraft Bus Provider	Tyvak vs. ARC/BCT	An additional commercial spacecraft bus provider (Tyvak) expressed interest in partnering to supply the TS and SS bus provider late in the study; a more commercial bus could reduce costs but must be studied. Exploring cost and capabilities should be further investigated.

4.3.3.3 Future Work

This study identified several areas of particular interest for the mDOT mission. Should additional funding be made available, the study team recommends the following as high-priority follow-on tasks:

- To assess other comm system (radio/ antenna/frequency band) options for crosslink and/or TT&C (S-band baselined)
- The GNC Software architecture for the SS and TS is preliminary and will be revisited in Phase A studies.
- To assess Cesium radio capabilities once TRL 8 is achieved (exp. Summer 2019), in particular for data rate capabilities (and update the link analysis and suitability for mDOT)
- Define SW tasks with greater fidelity and assign responsibility.
- Higher-fidelity simulation of maneuvers and propellant consumption for the mission phases; it is anticipated that this will refine the required delta-V and allow for propellant tank size reduction.
- Analyze thruster plumes and heat zones, and modify thruster arrangement to minimize impacts
- Perform thermal analysis and define resulting thermal management approach
- Based upon specific launch opportunities identified, the appropriateness of the LTAN assumption should be assessed. It is expected that the propellant budget can be adjusted to allow for small adjustments to the LTAN if necessary.
- Coordination between ARC and Tendeg will determine the best approach for transport of the starshade and the detailed integration flow (e.g. whether to unfold the starshade at ARC prior to integration with the bus)

[6]

- Refine minimum separation model to account for number and duration of observations for each target (to reduce minimum angular separation between pointing vector to target and cross-track direction)

4.3.4 Risk Assessment and Mitigation Plans

The risk matrix below provides a snapshot of the baseline mDOT identified risks with respect to their severity to the overall mission. The table below shows mDOT's preliminary risk assessment generated through risk identification and using project evaluations, and technical assessments.

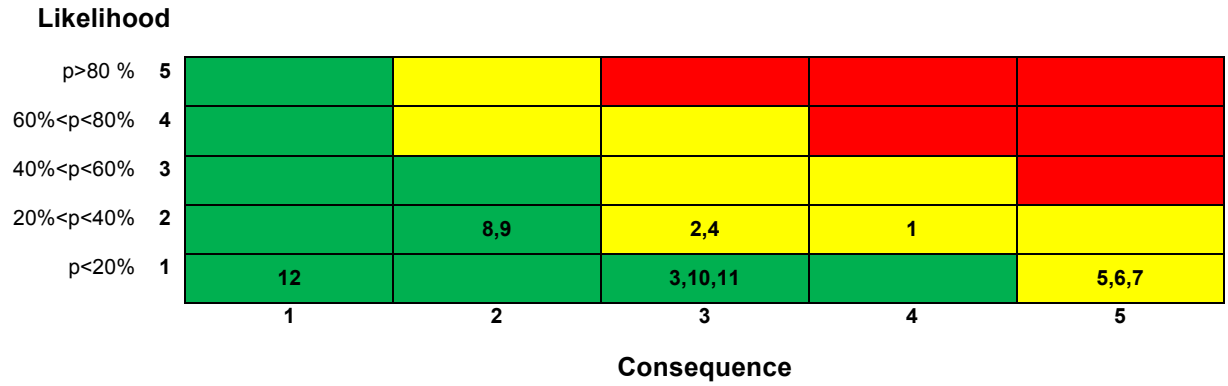

Figure 4-48: 5x5 risk matrix.

Table 4-20: List of risk elements.

Unique ID	LxC	Risk Title	Description	Mitigation
1	2x4	Starshade Deployment Failure	Given that the starshade mechanism is a new design, there is a probability of incomplete deployment, adversely impacting science capability	Design a test system for deployment in 1-g environment to facilitate verification of the flight configuration If the motor senses partial deployment, it stops and switches to a standby mode and waits for ground command for corrective actions.

[6]

2	2x3	DiGiTaL/GNC failure	Given that the DiGiTaL computer goes into Safe Mode (locks up) for >5 minutes (TBC), there is a possibility that position knowledge accuracy will be degraded (below threshold), which can result in missed Observations or shortened total duration.	Include contingencies in science plan that re-allocate delta-v that would have been used in missed observations to other targets after control is re-established.
3	2x3	Propellant Quantity	Given that translational maneuvers are required to align the formation with each target, there is a possibility that the loaded propellant may get depleted early, which can result in not achieving the entire mission objectives.	Maximize propellant tank size and fill to capacity. Reduce SS mass. Perform Monte Carlo (3-sigma) analysis to estimate propellant usage. Include contingencies in science plan to account for deviations from predicted propellant expenditure.
4	2x3	Solar Array/ Instrument Contamination by Thruster Plume	Given that condensation of ex-haust products or heat effects forms on solar arrays and instrument surfaces, there is a possibility that solar array efficiency and sensor readings will be degraded, which can result in reduced mission life and compromised mission data.	Conduct plume impingement analysis. Investigate different propellant options and pick solution with acceptable thrust performance and minimized contamination impact. If possible, orient sensitive solar array and instrument surfaces away from thrusters.
5	1x5	Telescope Spacecraft Deployment Failure	Given that the TS is deployed from a 6U Dispenser, there is a possibility that the TS will not deploy or will recontact with the SS, which can result in mission loss.	Verification of Deployer using mass simulator during AI&T. Verification of final installation. Ensure Dispenser system provides sufficient ΔV to avoid recontact with Primary S/C (Analysis).

[6]

6	1x5	Recontact with ESPA Grande	Given that the SS will be ejected from the ESPA Grande, there is a possibility that the SS could recontact with the ESPA Grande, which can result in loss of mission.	Coordination with LV and analysis to determine appropriate wait time prior to starshade deployment and spacecraft power-up.
7	1x5	TS/SS Conjunction/ Collision	Given that the minimum separation between the TS and SS occurs over the poles, there is a possibility that loss of nominal control on either spacecraft could cause a collision, resulting in loss of mission (and orbital debris).	Exclude science targets with declinations within 0.35^0 of $\pm 8^o$, ensuring passive collision avoidance via e/i-vector separation. In the event of an extended navigation outage, the ground segment can command the SS to perform collision avoidance maneuvers.
8	2x2	Telescope Spacecraft Orbit Decay	Given that the TS has no propulsion system, there's a possibility that the TS may remain in orbit beyond 25 years after launch, resulting in non-compliance with the NASA Handbook for Limiting Orbital Debris (and International Standards).	At the end of mission life, orient the TS such that its largest surface area faces into the velocity vector to increase atmospheric drag forces.
9	2x2	Rideshare Opportunity	Given that the SS volume must protrude into the interior of the ESPA-Grande ring, there is a possibility that a rideshare opportunity will not be available when mDOT is ready to launch, resulting in a schedule slip while awaiting a suitable launch accommodation.	Early negotiation and coordination with the launch services provider to ensure early identification of options will minimize overall impacts on project schedule.
10	1x3	Starshade tolerance	Given that the starshade must be accurately manufactured (0.1 mm edge shape tolerance) and deployed, there is a possibility it cannot maintain the same tolerance under operational environment, which can result in image data contamination	Extreme care in selecting materials, machining of parts, and testing of assembly under similar operational environment must be tightly controlled.

[6]

11	1x3	Plume Impingement	Given that plume impingement on the starshade occurs during an Observation, there is a possibility that exhaust gas degrades the shape of the petals over the mission, which can result in image data contamination.	May tilt the R/T thrusters away from the starshade and use the reaction wheels to compensate for the thruster-induced torque. Design the SS to have its CM and R/T thrusters as far away from the starshade as feasible.
12	1x1	Cesium SDR & TRM Hardware at TRL 6	Given that the Cesium radio hardware is not flight qualified yet, there is a possibility that it will not pass qualification testing before it is required for AI&T	Keep updates on incoming qualification testing (planned for May 2019); trade study for alternative comm systems.

[6]

4.4 Technology Needs, Gaps and Required Development

Most subsystems required for mDOT are currently at TRL 7 or higher. It is believed that all subsystems at lower TLR can be matured to TRL 6 or higher within two years through qualification testing on-ground and flight demonstrations on other missions. Current status and technology development plans for subsystems below TRL 6 are summarized in Table 4-21.

Table 4-21: Spacecraft technology development plan.

Item	TRL Referring to mDOT Mission Environment	Development Need	Developed as part of mDOT
Starshade Deployment Assembly	5	On-ground demonstration of starshade manufacture and deployment with acceptable errors	Testing assembly for starshade deployment and verification
Telescope Payload Assembly	5	Validation of telescope payload performance	Telescope testing environment
ECAPS Thrusters	5	Validate thruster performance in flight	None
DiGiTaL/GNC	5	Flight demonstration of autonomous precise relative navigation and control	Hardware-in-the-loop testing
Tx/Rx Module with Patch Antennas	5	On-ground qualification tests	None

Starshade Deployment Assembly

The deployment assembly (hub, motor, linkages, and hinges for petals) is a novel design developed by Tendeg specifically for the mDOT mission. While the materials and components for this design are similar to those used in full-scale starshade designs (Webb, et al., 2014), an on-ground test campaign is required to verify that the proposed design can be manufactured and deployed with acceptable errors.

Telescope Payload Assembly

The telescope payload is a modified version of the Planet Labs PS2 telescope, which now has extensive flight heritage (>100 units on orbit) in the Dove constellation. The modifications include introduction of a Mirrorcle S6180 mirror and secondary detector for image stabilization and a TEC for thermal control. A laboratory prototype of a two-sage attitude control system has been developed and tested at Stanford University (Beierle, Norton, Macintosh, & D'Amico, 2018). Further on-ground qualification testing is needed as part of mDOT to raise the TRL of the image stabilization to 6.

ECAPS Thrusters

[6]

The propulsion system uses HPGP 5N thrusters developed by Bradford ECAPS. The 5N thruster is based on a 1N version with LEO flight heritage from the Skysat 3-7 and PRISMA missions. Development and qualification of the 5N thrusters is coupled with the qualification program for the HPGP 22N thrusters.

The first flight-like HPGP 22N thruster was designed and built to substantiate the thruster design, build process, and testing to NASA GSFC PACE mission requirements. This test program was intended to bring the thruster TRL level from 5 to 6. The HPGP 5N and 22N thruster designs will be updated to incorporate the lessons learned during 22N thruster testing (completed in 2017). The HPGP 5N thruster is scheduled to be tested in 2018-2019 (Mulkey, Maynard, & Anflo, 2018). Successful completion of this test campaign should bring the 5N thruster TRL level to 6

Tx/Rx Module with Patch Antennas

The telecommunication system uses a Tx/Rx module and Patch Antennas developed by Cesium, the same manufacturer of the SDR. While the SDR is already at TRL 6, the Tx/Rx module is currently at TRL 5, progressing to TRL 6 upon completion of thermal testing of the existing high-fidelity engineering model. The Patch Antennas are currently at TRL 4, with Cesium in the process of starting manufacturing of the patch antenna's engineering model. The entire telecommunication system -SDR, Tx/Rx Module and Patch Antennas- is planned to complete qualification testing (TRL 8) by end of summer 2019.

DiGiTaL and Formation-Flying Algorithms

The DiGiTaL navigation and formation-flying algorithms are under development at the Stanford's Space Rendezvous Laboratory under two NASA SSTP contracts in collaboration with NASA Ames and GSFC. DiGiTaL uses differential carrier-phase GNSS techniques similar to those deployed on the PRISMA mission (D'Amico, Ardaens, & DeFlorio, Autonomous formation flying based on GPS - PRISMA flight results, 2012) which achieved 10cm (3D, rms) relative positioning accuracies at separations from 2m to 50km. However, DiGiTaL aims at centimeter-level relative positioning accuracy (1D, rms) in real-time through improved integer ambiguity resolution algorithms at separations up to 505km. The mDOT mission requires a formation at 500 km separation to autonomously maintain alignment with an inertial target with centimeter-level accuracy and conduct formation reconfigurations to re-align the formation for repeated observations of the same target. To date, these capabilities have only been partially flown and verified in space. The Stanford's Space Rendezvous Laboratory has experience with these algorithms from the flown GRACE, TanDEM-X, PRISMA, BIROS missions. Improved algorithms are currently in development as part of the Autonomous Nanosatellite Swarming using Radio-Frequency and Optical Navigation (ANS) (Stacey & D'Amico, 2018) SSTP contract in collaboration with NASA Ames Research Center. It is expected that the TRL of DiGiTaL and formation-flying algorithms will be raised to 7 within two years, through the current Stanford's research&development program and scheduled flight demonstrations on the Dwarf and Starling1 missions (Sanchez, et al., 2018) which are scheduled for launch in 2020 and 2021 respectively.

5 Management and Organization

A nominal program would be managed by Stanford with extensive collaboration with NASA Ames, a smallsat vendor, and Tendeg. Through the SLAC National Accelerator Laboratory, Stanford has extensive experience with managing projects at the $30M-$500M level, including the camera for the Large Synoptic Survey Telescope and instruments for the Fermi gamma-ray space telescope.

[6]

PI Bruce Macintosh has led large ground-based programs, in particular the Gemini Planet Imager high-contrast instrument, which was a 8-year program with a distributed international engineering team peaking at 50 FTEs.

Co-I Simone D'Aminco would serve as project engineer.

SLAC would identify and provide a dedicated project manager and systems engineer. Subsystem lead engineers would be identified at each major participating institution.

6 Schedule

Within the scope of this study we did not develop a full work-breakdown-structure based schedule. The schedule below is presented based on previous mission concepts assuming a January 2020 Phase A start

Table 6-1: Schedule table.

mDOT Milestones or phase	Date or start date	Duration
Phase A	1/2020	9 months
Phase B	1/2021	12 months
SRR	3/2021	
PDR	11/2021	
Phase C	1/2022	12 months
Petal prototype validation	2/2022	
CDR	9/2022	
Phase D	1/2023	12 months
Launch	1/2024	
Phase E	1/2024	13 months
Phase F	2/2025	3 months

7 Cost Estimate and Cost Estimating Methodology

The total mission cost for the mDOT Mission is $50.4M, including cost reserves during Phase A Concept Study of 15%, development (phase B-D) of 42%, and 15% of operation (phase E) and closeout (phase F) for a total of 40% reserve. Table 7-1 summarizes the mDOT Total Mission Cost during all mission phases.

[6]

In discussions with Tyvak, a smallsat vendor, they believed the parametric methodology singificantly overestimated cost and developed a first-order bottom-up cost using of off-the-shelf hardware including a 30% reserve that would reduce cost to $35M.

Table 7-1: Cost table ($M).

RY $M	Estimates	Methodology
Phase A		
Concept Study	$ 0.8	Grassroots
Phase A Total	**$ 0.8**	
Phase B/C/D	$ -	
Mission PM/SE/SM&A	$ 3.7	Analogous
Science	$ 0.8	Grassroots
Starshade Spacecraft	$ -	
Starshade	$ 3.6	Ames ROM*
Subsystems	$ 16.1	Parametric SEER-H + Stanford R&D
Telescope Spacecraft	$ 3.5	Ames ROM*
I&T	$ 1.8	Parametric: SEER-H
MOS/GDS	$ 3.7	Analogous
Phase B/C/D Total	**$ 33.2**	
Phase E/F	**$ -**	
Implementations & Closeout	$ 1.4	Analogous
NEN	$ 0.6	NEN Rates
Phase E/F Total	**$ 2.0**	
Reserve	**$ 14.3**	
Total mDot PI-Managed Mission Costs	$ 50.4	
	$ 36.1	Total less reserve
	40%	Reserve

**Ames ROM estimate, pending vendor quote (3.7.2018)*

Please see Appendix A.10 for cost variance explanations.

7.1 Cost Ground Rules and Assumptions

The mDOT costs are estimated based on Class D of the NASA payload risk classification. NASA Center Management & Operations (CM&O) cost will be included in the estimation based upon further requirements. All costs are in FY19$. Launch vehicle is not costed in this estimation as mDOT is a secondary payload and only requires a spacecraft integration cost onto the primary spacecraft in Phase D.

7.2 Cost Methodology and Approach

Cost models and methodologies are used, where appropriate, as shown in table 7.0 and described below.

Phase A

[6]

High-level grassroots cost estimates developed by the cost team with input received from the principal investigators were used to estimate Phase A, which has an expected duration of nine months.

PM, SE, SMA

Analogous methodology was used to estimate project management, systems engineering, and safety & mission assurance costs. TESS and Kepler were chosen for the analogous cost estimates because of their similarity to mDOT as telescope spacecrafts studying exoplanets.

Science

Science costs are based on a high-level grassroots estimate developed by the principal investigators for an expected total mission duration of 1.1 years.

Spacecraft, Instrument, System I&T, MOS/GDS

The SS subsystems cost of $16.1M is primarily developed using a parametric cost estimation approach as the methodology with SEER-H, which includes additional R&D costs provided by Stanford. I&T costs of $1,819K were also estimated using a parametric approach with SEER-H.

Vendor quotes from Blue Canyon Technologies (BCT) and Tendeg (will be) used to estimate the cost of the starshade instrument and CubeSat telescope spacecraft, respectively.

Analogy methodology based on TESS and Kepler were used to estimate MOS/GDS costs.

Phase E/F

Near Earth Network (NEN) costs in Phases E were estimated based on cost guidance from SCaN (Space Communication and Navigation) of an average of 1-2 contact per day for the entire mission lifetime.

Analogous methodology based on TESS and Kepler was used to estimate the implementation/closeout costs.

COST RISK AND RESERVES

Included in the mDOT cost is the cost reserve of $14.3M (FY19$), or 40%, with cost reserve allocations as follows: 15% during Phase A Concept Study, 42% in development (Phases B-D), and 15% in operation (Phase E) and closeout (Phase F). These allocations are based on historical development and operations risks.

The total cost reserve of $14.3M includes encumbered cost reserve of $5.8M (15%) and unencumbered cost reserve of $8.5M (25%). The encumbered reserve was derived from the risk assessment matrix identified in Table 4-20 in Section 4.3.4 These risks were quantified based on likelihood (L) and cost impact (CI) in Table 7-2.

6

Table 7-2: Cost threat matrix ($M).

		Cost Impact (CI, % of PI-Managed Investigation cost to complete Phase A/B/C/D or E/F not including unencumbered cost reserve)				
		Minimal (1% < CI <= 2.5%)	Very Minimal (2.5% < CI <= 5%)	Limited (5% < CI <= 10%)	Moderate (10% < CI <= 15%)	Significant (15% < CI <= 20%)
Likelihood (L, %)	Almost Certain(L > 80%)					
	Very Likely (60% < L <= 80%)					
	Likely (40% < L <= 60%)					
	Possible (20% < L <= 60%)		$0.64	$3.19	$1.04	
	Unlikely (L<=20%)	$0.02				$0.91

The cost breakout of each individual risk identified in Section 4.3.4 is shown in the following chart:

Table 7-3: List of cost risks.

Unique ID	LxCI	Mission Cost (Phases A-D)	Cost Risks ($M)
1	3.1%	$ 34.1	$ 1.0
2	1.9%	$ 34.1	$ 0.6
3	1.9%	$ 34.1	$ 0.6
4	1.9%	$ 34.1	$ 0.6
5	1.9%	$ 34.1	$ 0.6
6	1.9%	$ 34.1	$ 0.6
7	0.9%	$ 34.1	$ 0.3
8	0.9%	$ 34.1	$ 0.3
9	0.9%	$ 34.1	$ 0.3
10	0.9%	$ 34.1	$ 0.3
11	0.9%	$ 34.1	$ 0.3
12	0.1%	$ 34.1	$ 0.0
		Encumbered Cost Reserve:	**$ 5.8**
		Unencumbered Cost Reserve (25%):	$ 8.5
		Total Cost Reserve	**$ 14.3**

7.3 Work Breakdown Structure

Macintosh

WBS:

[6]

Table 7-4: Work breakdown structure.

WBS Element	Title
1.0	Project Management
2.0	Systems Engineering
3.0	Safety and Mission Assurance
4.0	Science/Technology
5.0	Payload
5.1	Payload Management
5.2	Payload Systems Engineering
5.3	Payload Quality Control
5.4	System Architecture
5.5	Starshade
5.6	Optics Instrument
5.7	Instrument I&T
6.0	Spacecraft
6.1	Structures
6.2	Thermal
6.3	Electrical Power
6.4	Command and Data Handling
6.5	Telecommunications
6.6	Attitude and Determination Control
6.7	Propulsion
6.8	Flight Software
6.9	Spacecraft AI&T
6.10	Spacecraft Ground Support Equipment
7.0	Mission Operations
8.0	Launch Services

6

9.0	Ground Data Systems
10.0	System Integration and Testing

6

A.1 Master Equipment List

Subsystem	Name	Type	Model	Quantity	Unit Mass (kg)	Contingency (%)	Installed Mass/ CBE Mass (kg)	MEV/ Total Mass (kg)	Acquisition Category
Payload	Starshade	Instruments.Mechanical	Starshade, Release Mechanism, & Motors	1	23.2	20%	23.2	27.84	Mod-Major
	Deployer	Structure.Mechanical	ISIS DuoPack CubeSat Deployer	4	1	10%	4	4.40	Space-Procure to Print
	Telescope NanoSat (will be deployed)	Rideshare Payload	**mDOT 6U Telescope NanoSat**	1	12	0%	12	12	Mod-Average
			BCT 6U NanoSat Bus	*1*					
			Telescope Optics subassembly (10 cm aperture)	*1*					
			Telescope camera	*2*					
			Tip/Tilt Mirror	*1*					
			Telescope control electronics	*1*					
			Thermal Electric Cooler	*1*					
	Subsystem Totals			**37.2**		**19%**	**39.20**	**44.24**	
ADCS	Reaction Wheels	Actuators.Wheels	BCT RW4	4	3	3%	12.00	12.36	Space-Procure to Print
	XACT	IntegratedUnits	XACT Gen3; includes Flight Processor, 1x Nano Star Tracker (ST1), 1x SS, &1x IMU (Accelerometer & Gyroscope)	1	0.51	3%	0.51	0.51	Mod-Minor
	Star Tracker	Sensors.Star	Additional Blue Canyon Nano Star Tracker (ST2)	1	0.35	3%	0.35	0.36	Space-Procure to Print
	Magnetorquer (prop face)	Actuators.Torquers	Microcosm MT140-2	3	5.3	3%	15.90	16.38	Space-Procure to Print
	Sun Sensor	Sensors.Sun	BCT MICD, SUN SENSOR, DIGITAL, ASSEMBLY	2	0.008	3%	0.02	0.02	Space-Procure to Print
	DiGiTaL GNSS Rx	Sensors.GPS	NovAtel OEM628 GNSS Receiver	1	0.037	3%	0.04	0.04	Space-Procure to Print
	GNSS antenna signal switch (DiGiTaL)	Sensors.GPS	Dow-Key 411HY SPDT	1	0.055	3%	0.06	0.06	Buy and Integrate
	Subsystem Totals			**13**		**3%**	**28.87**	**29.72**	
CnDH	Tyvak C&DH	Computers	Tyvak Endeavour C&DH Processor	1	0.1	20%	0.10	0.12	Mod-Minor
	DiGiTaL Avionics board	Computers	Tyvak Endeavour C&DH Processor	1	0.1	20%	0.10	0.12	Mod-Average
	Subsystem Totals			**2**		**20%**	**0.20**	**0.24**	
Power	EPS Stack	Integrated Power Management Systems	SDL BioSentinel EPSC	1	0.062	5%	0.06	0.07	Mod-Average
	Batteries	Batteries	LG INR 18650HG2 3000mAh	32	0.047	3%	1.50	1.55	Space-Procure to Print
	Body-Mounted Cells	SolarArrays	Spectrolab UTJ (3 mil glass)	280	0.006	5%	1.68	1.76	Mod-Average
	Solar Panel Substrate	Other	Solar Panel Substrate	8	1.5	20%	12.00	14.40	Buy and Integrate
	Subsystem Totals			**321**		**19%**	**15.25**	**17.78**	
Propulsion	Green Prop	Thrusters.Liquid	ECAPS 5N HPGP Thruster	11	0.48	5%	5.28	5.54	Buy and Integrate
	Green Prop	Other	Plumbing (notional)	1	2	25%	2.00	2.50	Buy and Integrate
	Green Prop	Tanks.Propellant	ATK PSI 80298-1 (77.9L propellant capacity)	1	13.6	10%	13.60	14.96	Buy and Integrate
	Subsystem Totals			**12**		**9%**	**20.88**	**23.00**	
Structures	Launch Adapter	Adapters.Launch	Planetary Systems, Standard Lightband, 24 inch diameter, SC Half	1	1.098	3%	1.10	1.13	Space-Procure to Print
	Primary Structure	Other	Notional primary structure allocation	1	26.74	25%	26.74	33.42	Make
	Secondary Structure	Other	Brackets, tabs, ballast	1	7.54	25%	7.54	9.43	Make
	Cabling	Other	Notional layout	1	7.00	25%	7.00	8.75	Make
	Subsystem Totals			**4**		**23%**	**42.38**	**52.73**	
Telecom	Crosslink, DTE, DiGiTaL Radio	Transponders	CesiumAstro SDR with active TRM	2	0.187	10%	0.37	0.41	Buy and Integrate
	GNSS antenna (DiGiTaL)	Antennae.Local	Tallysman TW3972E GNSS Antenna	2	0.075	3%	0.15	0.15	Buy and Integrate
	DTE Antenna	Other	CesiumAstro Antenna with TRM module (active version)	8	0.1	10%	0.80	0.88	Buy and Integrate
	Subsystem Totals			**12**		**9%**	**1.32**	**1.45**	
Thermal	Heater	Heaters	Minco HK5951 (notional/TBR)	6	0.09	15%	0.54	0.62	Buy and Integrate
	MLI	Other	Coatings, 1 kg	1	1	15%	1.00	1.15	Mod-Minor
	Sensors, Misc	Sensors.Temperature	AD 590	32	0.005	2%	0.16	0.16	Buy and Integrate
	Subsystem Totals			**35**		**13%**	**1.70**	**1.93**	
Total Dry Mass-Before TS Deployment							**149.8**	**185.7**	
Propulsion	*Green Prop*	*Liquid Propellant*	*LMP-103S (ADN)*	--	--	--	95.80	81.20	Buy and Integrate
Total Wet Mass-Before TS Deployment							**245.6**	**266.9**	
Total Dry Mass-After TS Deployment							**137.8**	**173.7**	

6

A.2 Acronyms and Abbreviations

Acronyms or Abbreviations

2ATC	2 Axis Thruster Control
3ARW	3 Axis Reaction Wheels
ADCS	Attitude Determination and Control System
AI&T	Assembly, Integration, and Test
AO	Announcements of Opportunity
AOS	Acquisition of Signal
arcmin	Arc minute
arcsec	Arc second
ATC	Axis Thruster Control
BCT	Blue Canyon Technologies
C&DH	Command and Data Handling
CAD	Computer Aided Design
CBE	Current Best Estimate
cFE	core Flight Executive
cFS	core Flight System
Cg	Center of gravity
cm	Centimeter
CM	Center of Mass
CM&O	NASA Center Management & Operations
CMMI	Capability Maturity Model Integration
CMOS	complementary metal-oxide semiconductor
ConOps	Concept of Operation
COTS	Commercial off-the-shelf
Cp	Center of pressure
CSCI	Computer Software Configuration Item
CSO	

[6]

dB	decibel
DC	Direct Current
DD	Displacement Damage
DiGiTal	Distributed multi-GNSS Timing and Localization
DOF	Degrees of Freedom
DOD	Depth-of-Discharge
DOORS	Dynamic Object Oriented Requirement System
ELDRS	Enhanced Low Dose Rate Sensitivity
EM-1	Exploration Mission-1
EMI/EMC	Electromagnetic Interference/ Electromagnetic Compatibility
EOL	End of life
EPS	Electrical Power System
ESPA	Evolved Expendable Launch Vehicle (EELV) Secondary Payload Adapter
FOV	Field-of-view
FPGA	Field-Programmable Gate Array
FSW	Flight software
g	Gravity (acceleration)
GCR	Galactic Cosmic Rays
GDS	Ground Data System
GNC	Guidance, Navigation, and Control
GNSS	Global Navigation Satellite System
GOTS	Government off-the-shelf
GPS	Global Positioning Satellites
GSFC	Goddard Space Flight Center
HPGP	High Performance Green Propulsion
HW	Hardware
Hz	Hertz
I&T	Integration and Test

6

IAR	Integer Ambiguity Resolution
ICD	Interface Control Document
IP	Internet Protocol
ISS	International Space Station
IRIS	Interface Region Imaging Spectrograph
kbps	Kilo-bits per second
km	Kilometer
kRAD	Kilo RAD
KSAT	Kongsberg Satellite Services AS – Ground station in Norway
LADEE	Lunar Atmosphere and Dust Environment Explorer
LCROSS	Lunar Crater Observation and Sensing Satellite
LEO	Low Earth Orbit
LEOP	Launch and Early Orbit Phase
LNA	Low Noise Amplifier
LOS	Line of sight
LRO	Lunar Reconnaissance Orbiter
LTAN	Local Time of the Ascending Node
m	Meter
mAH	Milli-Amp hour
MB	Mega-byte
Mbps	Mega-bits per second
mDOT	Miniaturized Distributed Occuter/Telescope
MHz	Mega-Hertz
MLI	Multi-layer insulation
mm	Millimeter
MMOC	Multi-Mission Operations Center (located at NASA Ames)
MTM	Mission Traceability Matrix
N	Normal

6

N	Newton force
N/A	Not applicable
NASA	National Aeronautics and Space Administration
NASA ARC	NASA Ames Research Center
NEN	Near Earth Network
NIEL	Non-ionizing Energy Loss
nm	Nanometer
Nm	Newton-meter
Nms	Newton-meter-second
NST	Nano Star Tracker
OAP	Orbit Average Power
PA	Power Amplifier
PI	Principal Investigator
PSE	Project System Engineer
R	Radial
R&D	Research and Development
RAAN	Right Ascension of Ascending Node
RAM	Random Access Memory
RC	Ritchey-Chrétien
RDM	radiation design margin
RF	Radio Frequency
RMS	Root Mean Squared
RW	Reaction Wheel
SBC	Single board Computer
SDR	Software Defined Radio
SEB	Single Event Burnout
SEE	Single Event Effects
SEGR	Single Event Gate Rupture

6

SEL	Single Event Latchup
SET	Systems Engineering Team
SEU	Single Event Upset
SOC	Science Operation Center
SS	Starshade Spacecraft
SSO	Sun-synchronous orbit
STM	Science Traceability Matrix
SW	Software
T	Tangential
TBC	To be confirmed
TBD	To be determined
TID	total ionizing dose
TPM	Technical Performance Measures
TRL	Technology Readiness Level
TRM	Transmit/Receive Module
TS	Telescope Spacecraft
TT&C	Telemetry, Tracking, and Command
U	Unit volume = 10cm x 10cm x 10cm unit volume
UV	Ultra-violet
V	Volt
W	Watt
WBS	Work Breakdown Structure
Whr	Watt-hour

6

A.3 References

Beierle, C., Norton, A., Macintosh, B., & D'Amico, S. (2018). Two-Stage Attitude Control for Direct Imaging of Exoplanets with a CubeSat Telescope. *SPIE Astronomical Telescopes + Instrumentation.*

D'Amico, S., & Montenbruck, O. (2006). Proximity Operations of Formation Flying Spacecraft using an Eccentricity/Inclination Vector Separation. *Jornal of Guidance, Control, and Dynamics , 29* (3), 554-563.

D'Amico, S., Ardaens, J.-S., & DeFlorio, S. (2012). Autonomous formation flying based on GPS - PRISMA flight results. *Acta Astronautica , 82* (1), 69-79.

Giralo, V., & D'Amico, S. (2018). Distributed Multi-GNSS Timing and Localization for Nanosatellites. *ION GNSS+.*

Glassman, T., Lo, A. S., Arenberg, J., Cash, W., & Noecker, C. (2009). Starshade Scaling Relations. *Techniques and Instrumentation for Detection of Exoplanets.*

Koenig, A. (2019). *Formation Design of Distributed Telescopes in Earth Orbit for Astrophysics Applications.* Stanford University, PhD Thesis.

Koenig, A. W., & D'Amico, S. (2019). Real-Time Algorithm for Globally Optimal Impulsive Control of Linear Time-Variant Systems. *IEEE Transactions on Automatic Control* .

Koenig, A. W., D'Amico, S., Macintosh, B., & Titus, C. J. (2015). A Pareto-Optimal Characterization of Miniaturized Distributed Occulter/Telescope Systems. *SPIE Optics + Photonics.*

Koenig, A. W., Macintosh, B., & D'Amico, S. (2019). Formation Design of Distributed Telescopes in Earth Orbit for Astrophysics Applications. *Journal of Spacecraft and Rockets* .

Mulkey, H. W., Maynard, A. P., & Anflo, K. (2018). Green Propulsion Advancement and Infusion. *Space Propulsion Conference.*

Sanchez, H., McIntosh, D., Cannon, H., Pires, C., Sullivan, J., O'Connor, B., et al. (2018). Starling1: Swarm Technology Demonstration. *32nd Annual AIAA/USU Small Satellite Conference.*

Shaklan, S. B., Noecker, M. C., Glassman, T., Lo, A. S., Dumont, P. J., Kasdin, N. J., et al. (2010). Error budgeting and tolerancing of starshades for exoplanet detection. *Space Telescopes and Instrumentation 2010: Optical, Infrared, and Millimeter Wave.*

Stacey, N., & D'Amico, S. (2018). Autonomous Swarm Navigation and Asteroid Characterization. *AAS/AIAA Astrodynamics Specialist Conference.*

Webb, D., Kasdin, N. J., Lisman, D., Shaklan, S., Thomson, M., Cady, E., et al. (2014). Successful starshade petal deployment tolerance verification in support of NASA's technology development for exoplanet missions. *SPIE Astronomical Telescopes + Instrumentation.*

[6]

A.4 Design Changes Made During this Study

Early operational concept of mDOT used 6AM/6PM LTAN and was changed to Noon/Midnight based on spacecraft operational constraints (need to perform Observation in eclipse) and performance (SS does not rotate its body to expose solar panels to the sun). This LTAN change drove the solar array designs for the SS and TS.

The SS structure was changed from rectangular to octagonal shape due to the petal stowage geometry requirements. The starshade assembly hub is now hosting a thruster and a patch antenna.

The critical tolerances for starshade manufacturing and deployment have been relaxed. The critical mode tolerance (edge segment shape) has been increased from 0.005mm to 0.1mm.

The propulsion system was switched to an all-green propellant thruster system versus a combination of mono-propellant and electric thrusters. Eleven (11) 5N green thrusters from Bradford-ECAPS have replaced the two Busek BHT-200 electric thrusters and four (4) Aerojet Rocketdyne MR-103 1N hydrazine thrusters. These changes were made due to the higher control authority delivered by the 5N thrusters.

S-band patch antennas have replaced the earlier concept of using omni-directional UHF antennas for crosslink and ground communication.

Cesium S-band communication system have replaced the L3 Cadet Radio and the AstroDev Li-1 Radio.

Earlier concepts suggested that the SS bus rely upon a COTS or MOTS platform (e.g. Millennium Space Systems); the concept presented in this report has moved to a custom build due to its octagonal shape.

The 6U TS design remained mostly unchanged, except for the telescope assembly (including its two cameras, tip/tilt mirror, and cooling system) and now occupy 4U in an L-shape configuration.

6

A.5 Link Budgets

Transmitter					System		
	RF Transmit power	4	W		Frequency	2100	MHz
	Antenna Gain (peak)	8	dBi		Bandwidth expansion	100%	%
	Transmitter Circuit Loss	0.25	dB		Bit Information Rate, Rb	220000	bps
	Pointing Loss	3	dB		Protocol overhead	0%	%
					Telemetry		bps
Path					Desired BER	1.00E-06	
	Range	3000	km		Modulation	QPSK	
	Atmospheric Attenuation	0.15	dB		Coding	No Coding	
	Polarization Loss	0.25	dB		Required Eb/No	10.5	dB
					Implementation Loss	1	dB
Receiver					**Results**		
	Receiver Antenna Gain	45.1	dBi		C/No Margin	26.21	dB
	Receiver Antenna Size	11.3	m		Eb/No Margin	25.21	dB
	G/T	22.1	dB/K		Transmitted Baud Rate	110000.00	sps
	Rx Antenna to Receiver loss	2.5	dB		Transmitted Baud Rate	110.00	Ksps
	Antenna Name	SG1			Transmitted Baud Rate	0.11	Msps
					Occupied BW	154000.00	Hz
					Occupied BW	154.00	kHz
					Occupied BW	0.15	MHz

Telemetry downlink using 11.3m KSAT SG1

Transmitter	SG-1 KSAT - NEN				System		
	EIRP	63.5	dBW		Frequency	2050	MHz
	Transmitter RF Power	0	dBW		Bandwidth expansion	100%	%
	Antenna Gain (peak)	42.5	dBi		Bit Information Rate, Rb	4000	bps
	Transmitter Circuit Loss	0	dB		Protocol overhead	0%	%
	Pointing Loss	0.1	dB		Telemetry		bps
	Antenna Name	SG1			Desired BER	1.00E-06	
Path					Modulation	QPSK	
	Range	3000	km		Coding	No Coding	
	Atmospheric Attenuation	0.15	dB		Required Eb/No	10.5	dB
	Polarization Loss	0.25	dB		Implementation Loss	3	dB
					Results		
Receiver					C/No Margin	29.3	dB
	Receiver Antenna Gain	-20	dBi		Eb/No Margin	26.3	dB
	Receiver Antenna type	esium Patch			Transmitted Baud Rate	2000.00	sps
	G/T	-44.6	dB/K		Transmitted Baud Rate	2.00	Ksps
	Pointing Loss	3	dB		Transmitted Baud Rate	0.00	Msps
	Receiver Temperature System, Tsys	290	K		Occupied BW	2800.00	Hz
					Occupied BW	2.80	kHz
					Occupied BW	0.00	MHz

Command using 11.3m KSAT SG1

6

Transmitter	Cesium				**System**		
	RF Transmit power	4	W		Frequency	2300	MHz
	Antenna Gain (peak)	8	dBi		Bandwidth expansion	100%	%
	Transmitter Circuit Loss	0.25	dB		Bit Information Rate, Rb	220000	bps
	Pointing Loss	3	dB		Protocol overhead	0%	%
					Telemetry		bps
Path					Desired BER	1.00E-06	
	Range	510	km		Modulation	QPSK	
	Atmospheric Attenuation	0	dB		Coding	No Coding	
	Polarization Loss	0.25	dB		Required Eb/No	10.5	dB
					Implementation Loss	1	dB
Receiver	Cesium				**Results**		
	Receiver Antenna Gain	5	dBi		C/No Margin	6.49	dB
	Receiver Antenna Size	0	m		Eb/No Margin	5.49	dB
	G/T	-14.62	dB/K		Transmitted Baud Rate	110000.00	sps
	Rx Antenna to Receiver loss	0.25	dB		Transmitted Baud Rate	110.00	Ksps
	Antenna Name				Transmitted Baud Rate	0.11	Msps
					Occupied BW	154000.00	Hz
					Occupied BW	154.00	kHz
					Occupied BW	0.15	MHz

Crosslink

Transmitter	**Cesium**				**System**		
	RF Transmit power	4	W		Frequency	2100	MHz
	Antenna Gain (peak)	8	dBi		Bandwidth expansion	100%	%
	Transmitter Circuit Loss	0.25	dB		Bit Information Rate, Rb	3290000	bps
	Pointing Loss	3	dB		Protocol overhead	0%	%
					Telemetry		bps
Path					Desired BER	1.00E-06	
	Range	3000	km		Modulation	QPSK	
	Atmospheric Attenuation	0.15	dB		Coding	No Coding	
	Polarization Loss	0.25	dB		Required Eb/No	10.5	dB
					Implementation Loss	1	dB
Receiver					**Results**		
	Receiver Antenna Gain	45.1	dBi		C/No Margin	14.46	dB
	Receiver Antenna Size	11.3	m		Eb/No Margin	13.46	dB
	G/T	22.1	dB/K		Transmitted Baud Rate	1645000.00	sps
	Rx Antenna to Receiver loss	2.5	dB		Transmitted Baud Rate	1645.00	Ksps
	Antenna Name	SG1			Transmitted Baud Rate	1.65	Msps
					Occupied BW	2303000.00	Hz
					Occupied BW	2303.00	kHz
					Occupied BW	2.30	MHz

Science data downlink using 11.3m KSAT SG1

6

Transmitter	Cesium				System		
	RF Transmit power	4	W		Frequency	2100	MHz
	Antenna Gain (peak)	8	dBi		Bandwidth expansion	100%	%
	Transmitter Circuit Loss	0.25	dB		Bit Information Rate, Rb	3290000	bps
	Pointing Loss	3	dB		Protocol overhead	0%	%
					Telemetry		bps
Path					Desired BER	1.00E-06	
	Range	3000	km		Modulation	QPSK	
	Atmospheric Attenuation	0.15	dB		Coding	k=7, r=1/2 convolutional	
	Polarization Loss	0.25	dB		Required Eb/No	4.8	dB
					Implementation Loss	1	dB
Receiver					Results		
	Receiver Antenna Gain	15	dBi		C/No Margin	10.66	dB
	Receiver Antenna Size	3.7	m		Eb/No Margin	9.66	dB
	G/T	12.6	dB/K		Transmitted Baud Rate	3290000.00	sps
	Rx Antenna to Receiver loss	2.5	dB		Transmitted Baud Rate	3290.00	Ksps
	Antenna Name	KSAT_lite			Transmitted Baud Rate	3.29	Msps
					Occupied BW	4606000.00	Hz
					Occupied BW	4606.00	kHz
					Occupied BW	4.61	MHz

Science data downlink using 3.7m KSATLite dish (Svalbard – same location as SG1)

Transmitter					System		
	EIRP	44.8	dBW		Frequency	2050	MHz
	Transmitter RF Power	0	dBW		Bandwidth expansion	100%	%
	Antenna Gain (peak)	15	dBi		Bit Information Rate, Rb	4000	bps
	Transmitter Circuit Loss	0	dB		Protocol overhead	0%	%
	Pointing Loss	0.1	dB		Telemetry		bps
	Antenna Name	SG1			Desired BER	1.00E-06	
Path					Modulation	QPSK	
	Range	3000	km		Coding	No Coding	
	Atmospheric Attenuation	0.15	dB		Required Eb/No	10.5	dB
	Polarization Loss	0.25	dB		Implementation Loss	3	dB
					Results		
Receiver					C/No Margin	10.6	dB
	Receiver Antenna Gain	-20	dBi		Eb/No Margin	7.6	dB
	Receiver Antenna type	esium Patch			Transmitted Baud Rate	2000.00	sps
	G/T	-44.6	dB/K		Transmitted Baud Rate	2.00	Ksps
	Pointing Loss	3	dB		Transmitted Baud Rate	0.00	Msps
	Receiver Temperature System, Tsys	290	K		Occupied BW	2800.00	Hz
					Occupied BW	2.80	kHz
					Occupied BW	0.00	MHz

Command using 3.7m KSATLite dish (Svalbard – same location as SG1)

6

A.6 Requirements

Table A.6-1: Starshade spacecraft requirements.

Req Id	Starshade Spacecraft Requirements - Preliminary
	Starshade Spacecraft
SS-1	The Starshade Spacecraft shall be compatible with the ESPA Grande support ring structure as a secondary payload in terms of mass, volume, attachments, and environment
SS-2	The Starshade Spacecraft shall accommodate a 3.0m starshade payload in stowed configuration during integration, launch, and deployment events
SS-3	The Starshade Spacecraft shall provide a 6U cubesat dispenser for the Telescope Spacecraft
SS-4	The Starshade Spacecraft shall accommodate the Telescope Spacecraft during integration, launch, deployment from the ESPA, and separation events.
SS-5	After separation from the ESPA Grande, the Starshade Spacecraft shall maneuver to achieve 6AM/6PM LTAN orbit. mDOT SSO altitude will not change from the ESPA Grande transfer orbit altitude.
SS-6	Once separated from the ESPA Grande, the Starshade Spacecraft shall have the capability to perform checkout and commissioning while the Telescope Spacecraft is still in the 6U dispenser
SS-7	The Starshade Spacecraft shall have the capability to deploy the Telescope Spacecraft in the velocity direction.
SS-8	The Starshade Spacecraft shall perform maneuvers to achieve a cross-track separation distance of 500 km from the Telescope Spacecraft within 4 weeks after deployment
SS-9	The Starshade Spacecraft shall perform maneuvers to maintain safe separation from the Telescope Spacecraft throughout mission life
SS-10	The Starshade Spacecraft shall be able to communicate with the Telescope Spacecraft at a separation distance up to 600 km using S-band frequency
SS-11	The Starshade Spacecraft shall have the capability to send and receive data with the Telescope Spacecraft at a data rate of 220 kbps minimum
SS-12	The Starshade Spacecraft shall execute a ground command to deploy the starshade in the nominal deployed configuration
SS-13	The Starshade Spacecraft shall have 3-axis stability with 1 deg attitude control per axis
SS-14	The Starshade Spacecraft shall have the capability to point its starshade toward the Telescope Spacecraft throughout science observation period
SS-15	The Starshade Spacecraft shall have the capability to determine its orbit position to within 1 m accuracy using on-board GNSS-capable navigation system
SS-16	The Starshade Spacecraft shall have the capability to adjust its orbital position and attitude accordingly based on the received raw GNSS and navigation data from the Telescope Spacecraft
SS-17	The Starshade Spacecraft shall have the capability to control its cross-track distance from the Telescope Spacecraft to within 500 +/-5 km continuously during science observation period
SS-18	The Starshade Spacecraft shall have the capability to control its tangential and radial position to within 15 cm from the nominal line-of-sight between the Telescope Spacecraft and the target star throughout science observation

[6]

SS-19	The Starshade Spacecraft shall have the capability to communicate with Ground Station in S-band frequency
SS-20	The Starshade Spacecraft shall have the capability to store and downlink raw GNSS measurement and navigation data
SS-21	The Starshade Spacecraft shall have the capability to downlink to the Ground at data rates of 220 kbps minimum
SS-22	The Starshade Spacecraft shall have the capability to maintain starshade perpendicularity to line-of-sight between Telescope Spacecraft and target star to within 1 deg
SS-23	The Starshade Spacecraft shall have the capability to operate for not less than 1.1 years after separation from the launch vehicle
SS-24	The Starshade Spacecraft shall have the capability to support a up to five (5) Observations per target star for a total of 10 (TBR) target star
SS-25	The Starshade Spacecraft shall have the capability to accept and execute ground-based override commands.
SS-26	The Starshade Spacecraft shall have the capability execute Same Target Formation and Different Target Formation commands autonomously
SS-27	The Starshade Spacecraft shall have the capability to control formation relative motion during Observation to within +/- 15 cm lateral (perpendicular to line-of-sight) and to within +/-5 km longitudinal (along line-of-sight)
SS-28	The Starshade Spacecraft shall be capable of maintain starshade dimensional tolerance to within 5 mm in all critical parameters during Observation
SS-29	The Starshade Spacecraft shall have the capability to perform maneuvers for collision avoidance with the Telescope Spacecraft

Table A.6-2: Telescope spacecraft requirements.

Telescope Spacecraft Requirements - Preliminary	
TS-1	The Telescope Spacecraft shall fit within a 6U bus platform
TS-2	The Telescope Spacecraft shall fit within the 6U satellite dispenser
TS-3	The Telescope Spacecraft shall accommodate a payload telescope assembly with a total volume of 4U in L-shape configuration
TS-4	The Telescope Spacecraft shall have the capability to point telescope field-of-view (FOV) to an occulted target star for up to 5 minutes during Observation
TS-5	The Telescope Spacecraft shall have the pointing accuracy to 1 deg max
TS-6	The Telescope Spacecraft shall have the capability to communicate in S-band with the Starshade Spacecraft flying in formation located up to 600 km in cross-track direction
TS-7	The Telescope Spacecraft shall have the capability to transmit its current GNSS navigation measurement data to the Starshade Spacecraft in S-band at a data rate of 220 kbps
TS-8	The Telescope Spacecraft shall have the capability to determine its position to within 1m accuracy in real-time
TS-9	The Telescope Spacecraft shall have the capability to store the total accumulated science image data for each target star

[6]

TS-10	The Telescope Spacecraft shall have the capability ability to downlink the entire target star science data to KSAT ground station(s) before observing the next target star
TS-11	The Telescope Spacecraft shall have the capability accept and execute ground-based override commands
TS-12	The Telescope Spacecraft shall have the capability to protect the telescope assembly from sunlight intrusion into the telescope boresight
TS-13	The Telescope Spacecraft shall have the capability to operate for not less than 1.1 years after separation from the dispenser
TS-14	The Telescope Spacecraft shall have the capability to survive space environment at the 600 km altitude for not less than 1.1 years
TS-15	The Telescope Spacecraft shall have the capability to survive launch environment while stowed in the dispenser
TS-16	The Telescope Spacecraft shall have the capability to support up to five (5) Observations per target star for a total of 10 (TBR) target star
TS-17	The Telescope Spacecraft shall have the capability to store science image data up to 600 MB (TBR) for each target star.
TS-18	The Telescope Spacecraft shall have the capability to control absolute attitude with ±0.45deg accuracy
TS-19	The Telescope Spacecraft shall have the capability to store downlink science image data, DiGiTaL measurements data, and housekeeping data
TS-20	The Telescope Spacecraft shall have the capability to downlink downlink science image data, DiGiTaL measurements data, and housekeeping data at 3.3 Mbps minimum
TS-21	The Telescope Spacecraft shall have the capability to receive and store high-level guidance command for target pointing from the ground station
TS-22	The Telescope Spacecraft shall have the capability to store 600 MB minimum of total science data per target star.

6

A.7 Starshade Payload Structural and Thermal Analysis

A.7.1 Structural Analysis

Analysis Models

A stowed and deployed structural FEA were created to size the structural elements and determine response to excitations and loads. Petal geometry from CAD was used as baseline and sized from there. A notional octo-chassis composite structural panel was used for the spacecraft (SC) body, with an additional dummy mass to simulate the SC internals, with a total mass of 300 lbm. Model overviews can be seen in Figure A.7-1 and Figure A.7-2.

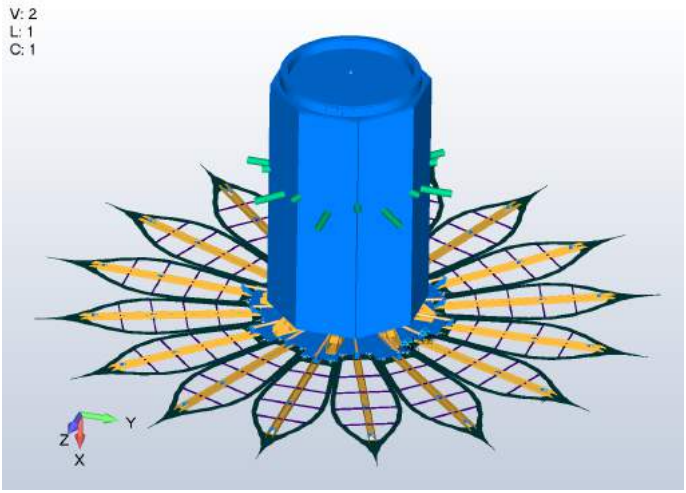

Figure A.7-1: Deployed finite element model.

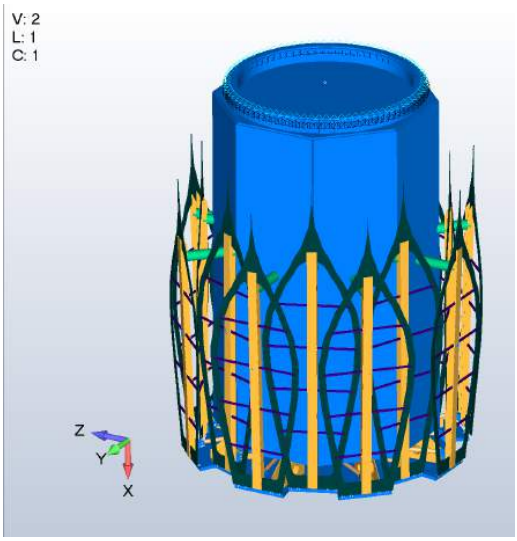

Figure A.7-2: Stowed finite element model.

Details of the structural elements are delineated below.

- Batten: 0.25” square carbon pultrusion, E=18Msi. Includes mass of 2x 1 mil Kapton layers for optical shield.
- Edge: 0.119” carbon edge stackup. E=11.9Msi

6

- Spine: 0.040” thick c-channel. E=11.9Msi
- Floor: HC Panel with 0.040” facesheets E=11.9Msi, 0.392” Hexcel 3.1pcf core.
- Chassis: HC Panel with 0.040” facesheets E=11.9Msi, 0.392” Hexcel 3.1pcf core.
- Hinges and Clevises: Ti-6Al-4V
- Strut Tubes: Carbon tubes 0.56” OD, 0.040” wall, E=18 Msi

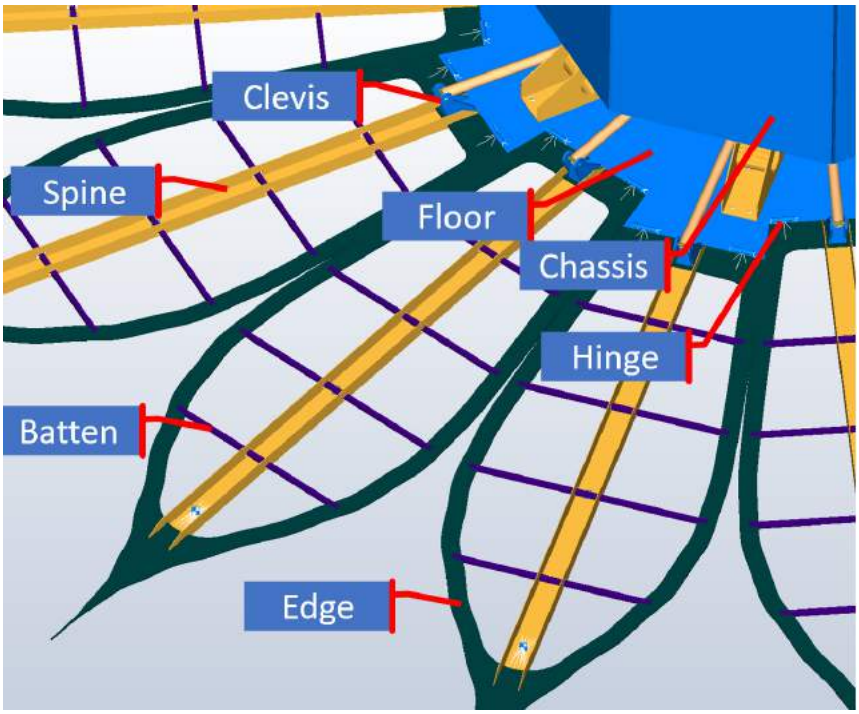

Figure A.7-3: Model details.

Stowed Results

In the stowed condition a free-free (no constraints) and constrained at the ESPA ring interface modal analysis was performed to assess the stiffness of the structure. In the ESPA ring fixed condition the first mode is at 45Hz. The modal effective mass fraction sums over the first 30 modes spanning up to 70Hz are shown in Figure A.7-4. The first 30 modes capture at least 85% of the effective mass fraction in all 6 DOF except translation along and rotation about the long axis of the chassis. This is expected, as those modes will be very high in frequency. A number of mode shapes, frequencies, and descriptions follow.

6

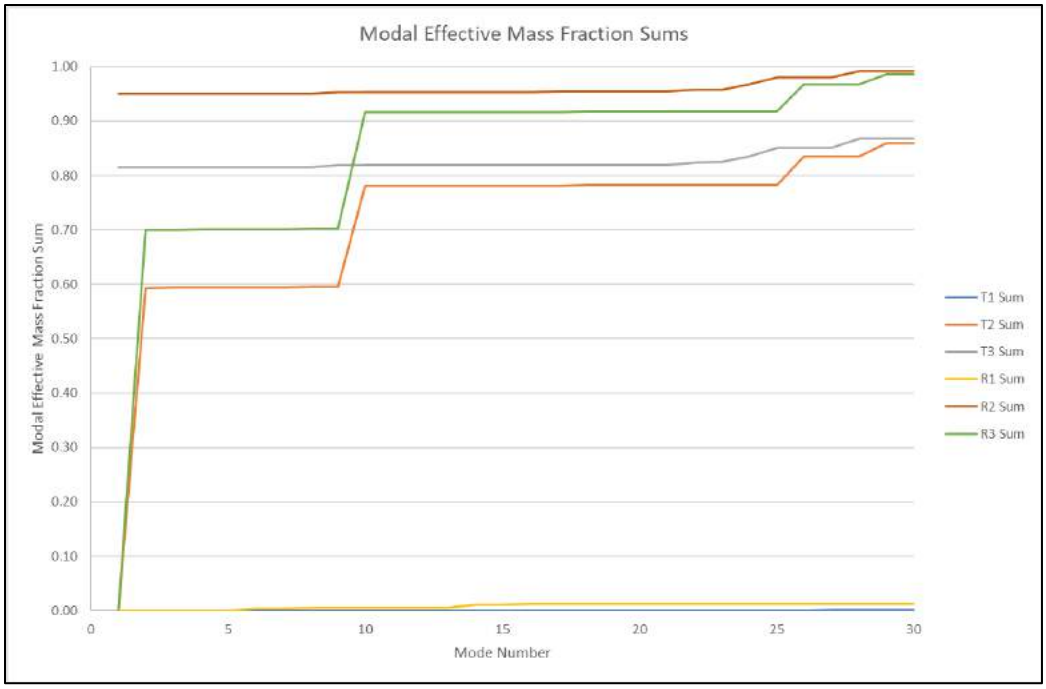

Figure A.7-4: Stowed, ESPA ring, modal effective mass fraction sum.

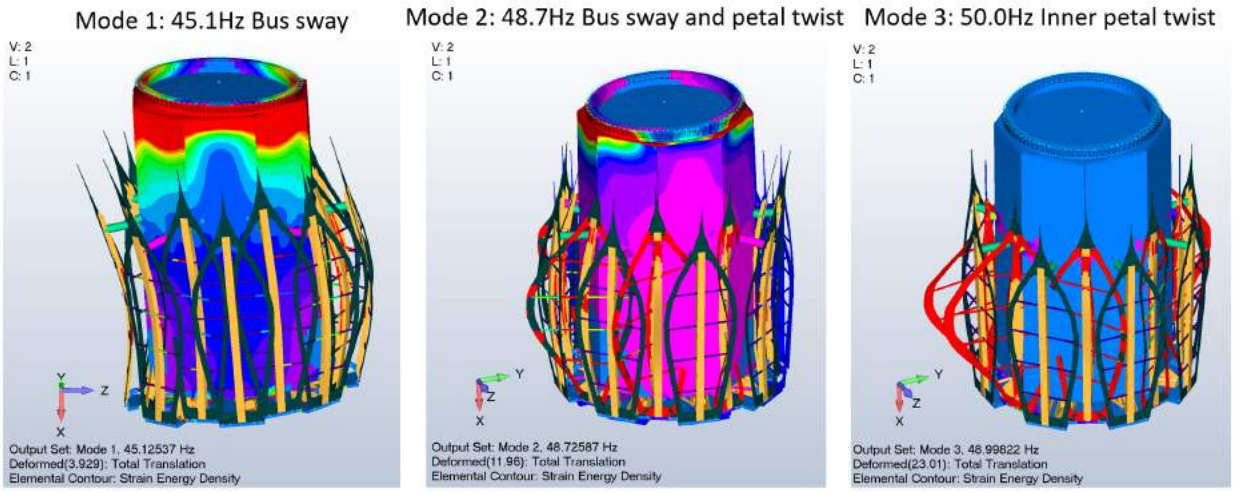

Figure A.7-5: Stowed, ESPA ring, modes 1-3.

6

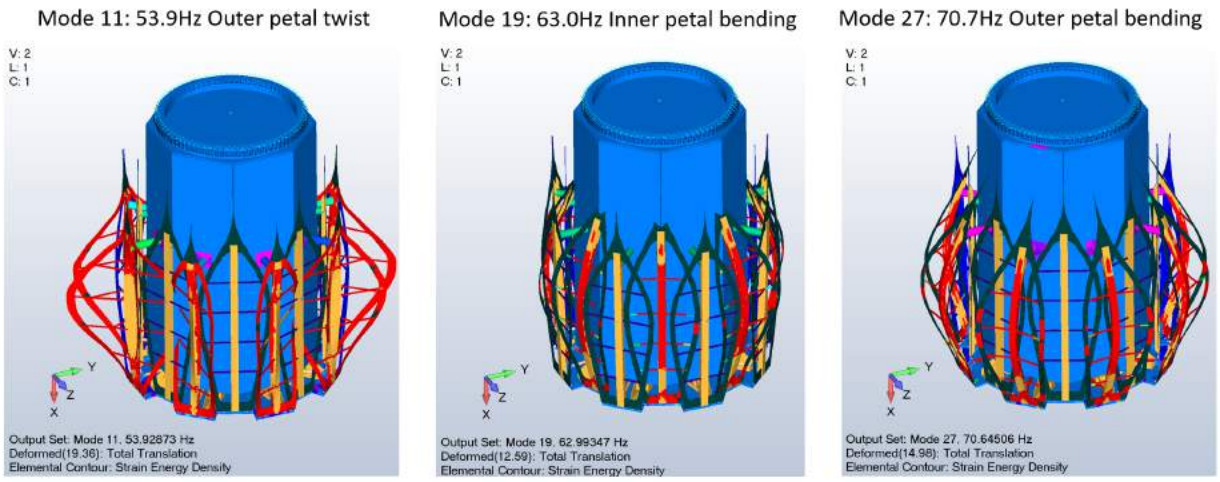

Figure A.7-6: Stowed, ESPA ring, modes 11, 19, 27.

A free-free (unconstrained) modal analysis was also performed to see how the spacecraft will behave when stowed (immediately following release from the launch vehicle). After the 1st 6 rigid body modes, the next set of mode shapes are shown, with each frequency region containing a myriad of similar combinations of petals that are active.

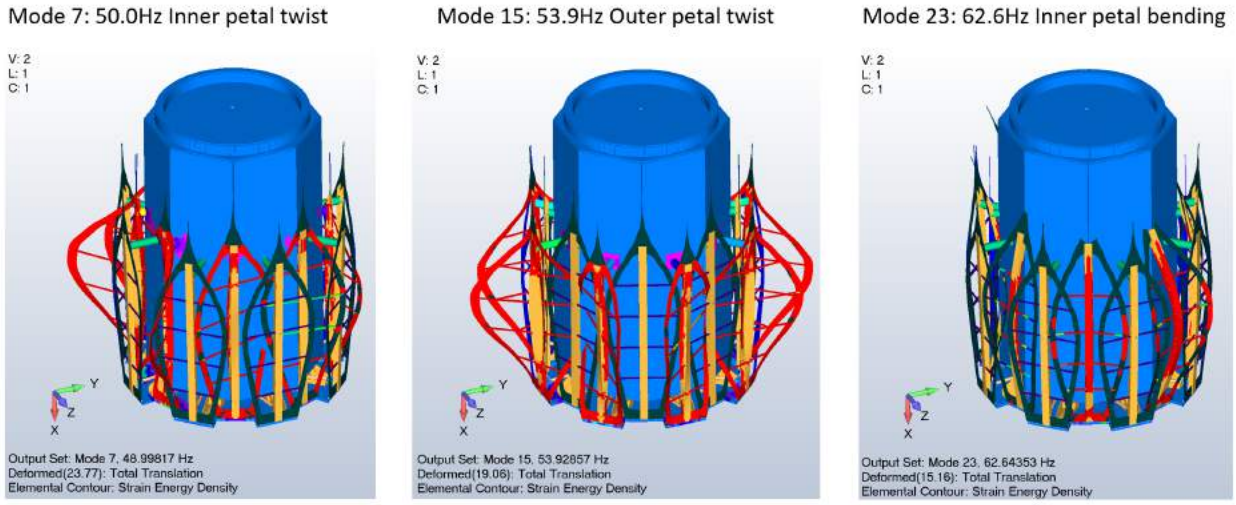

Figure A.7-7 Stowed, free-free, modes 7, 15, 23.

A 10G lateral (Y) load was applied as a worst-case enveloping G load. The Falcon 9 User Guide maximum light payload longitudinal acceleration is 8.5g, which would translate as a lateral load. Max deflection under 10G load is 0.082”, which can be seen in Figure A.7-8. Much of this is dependent on SC structure, interfaces, etc., so this estimate may not be bounding or conservative. The bus distortions are much lower, on the order of 0.030”. Under 10G lateral load, the max snubber axial force is ~8.1lbf and max shear force on perpendicular members is ~8.6 lbf.

6

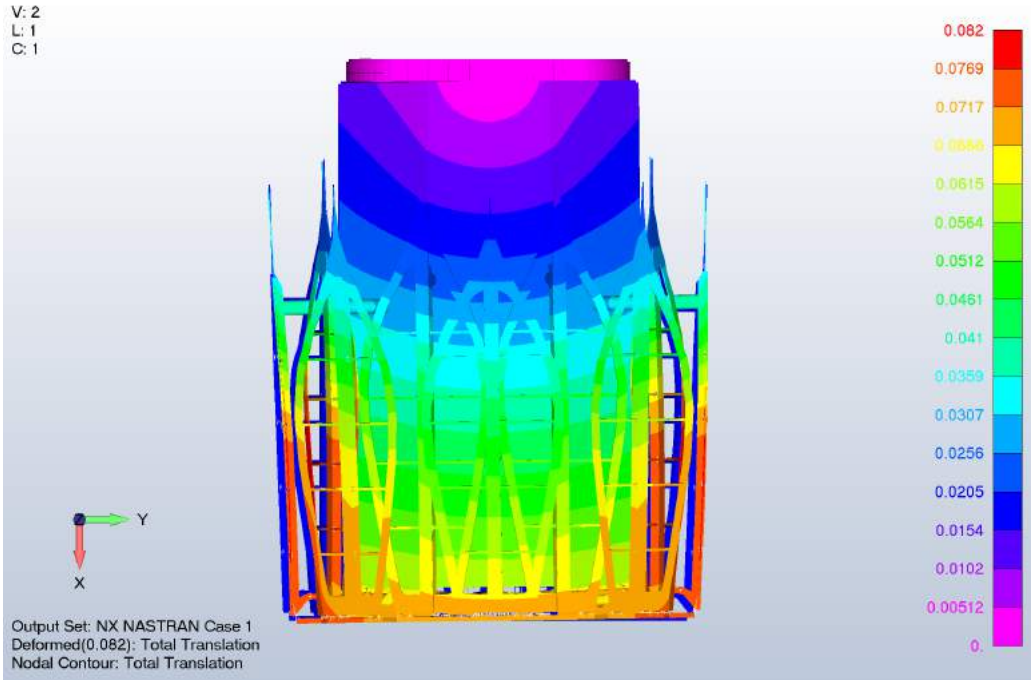

Figure A.7-8: 10G lateral load.

Deployed Results

A modal analysis of deployed Starshade was also performed in a free-free condition. The first mode is at 11.3 Hz seen in Figure A.7-9 with the petals in a crossed flapping pattern. Numerous similar modes are seen in same frequency range with variations on active petals and which are synchronous or asynchronous. The mode shapes change to the shorter petals being active at 13.1Hz. At 18.4 Hz the modes switch to various petal twisting combinations, seen in Figure A.7-10.

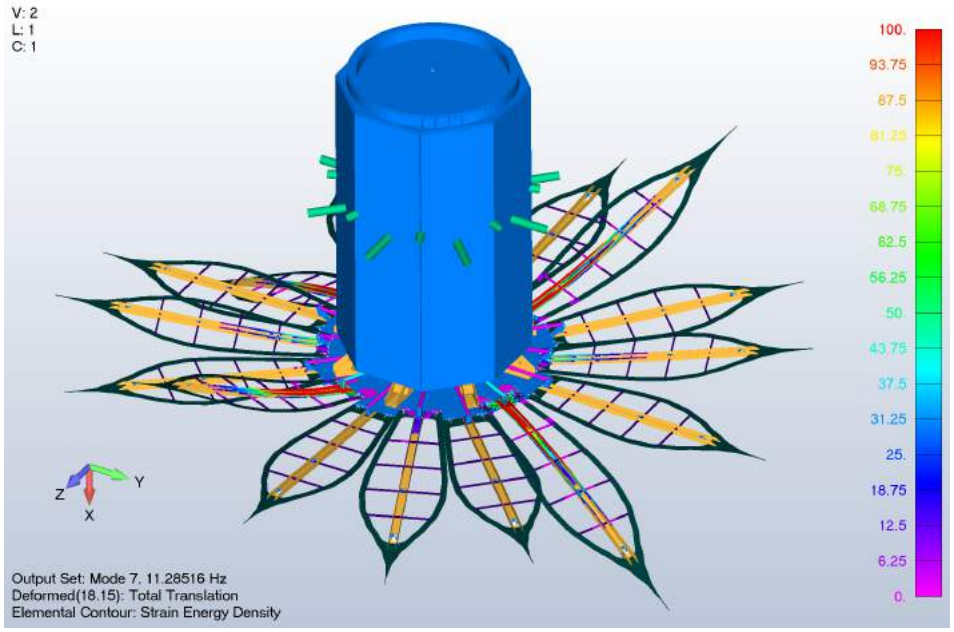

Figure A.7-9: Deployed, free-free, 1st mode, 11.3Hz.

6

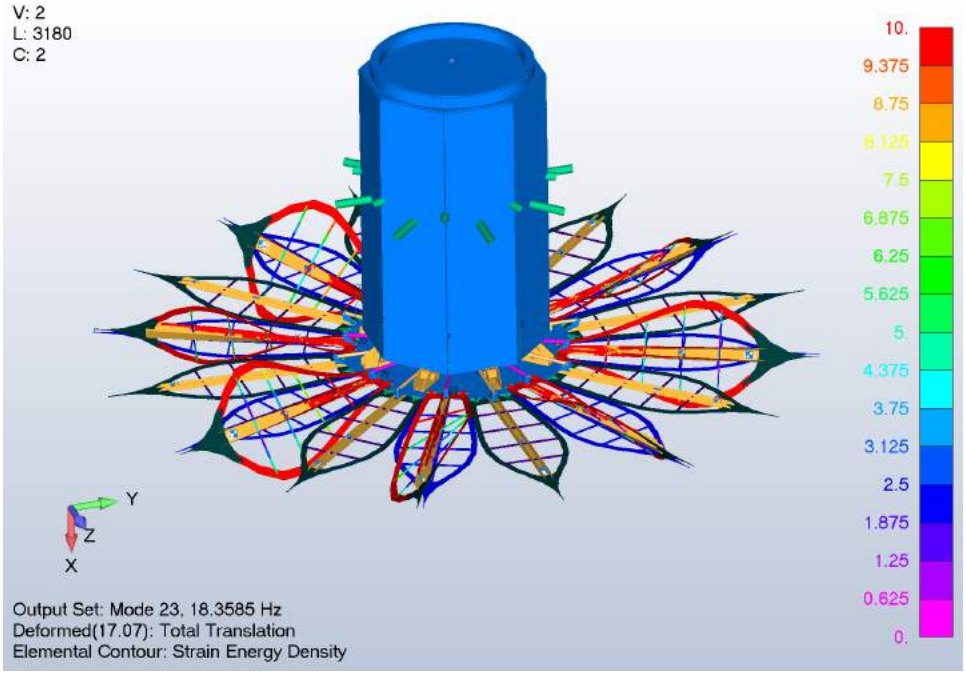

Figure A.7-10: Deployed, free-free, 18.4Hz petal twisting.

A.7.2 Thermal Analysis

A thermal analysis was performed by Jamie Abbott and the results provided to Tendeg. The thermal model was run for three conditions: normal operation, and two hot cases. The normal operation temperatures were mapped at ten timestamps to the structural FEA model. For the other cases the min/max temperatures were summarized by member.

- Normal Operations: Beta 0 orbit, +Z points to Earth
- Hot 1: Beta 90 orbit, +X points to Sun
- Hot 2: Beta 90 orbit, -X points to Sun

6

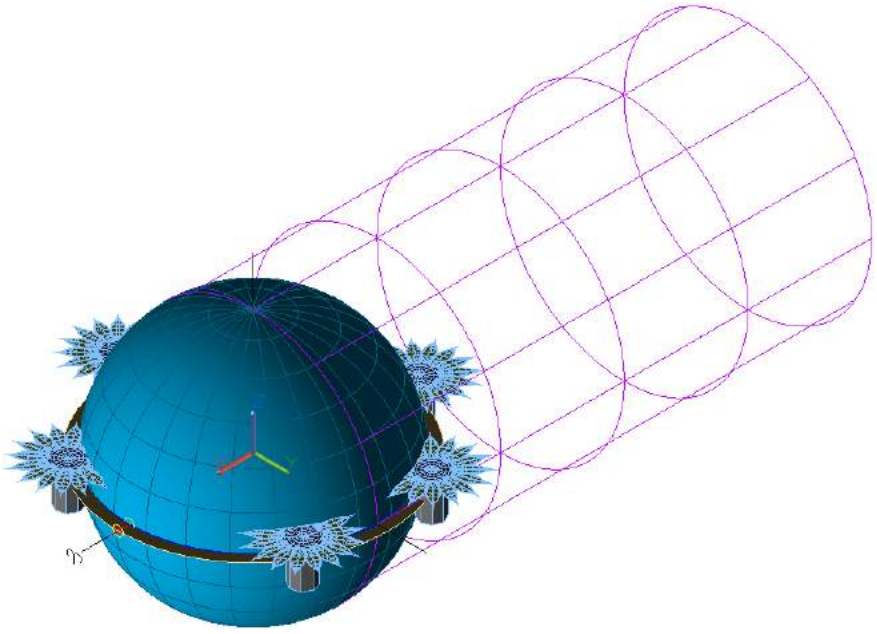

Figure A.7-11: On-orbit thermal model, beta = 0 degrees.

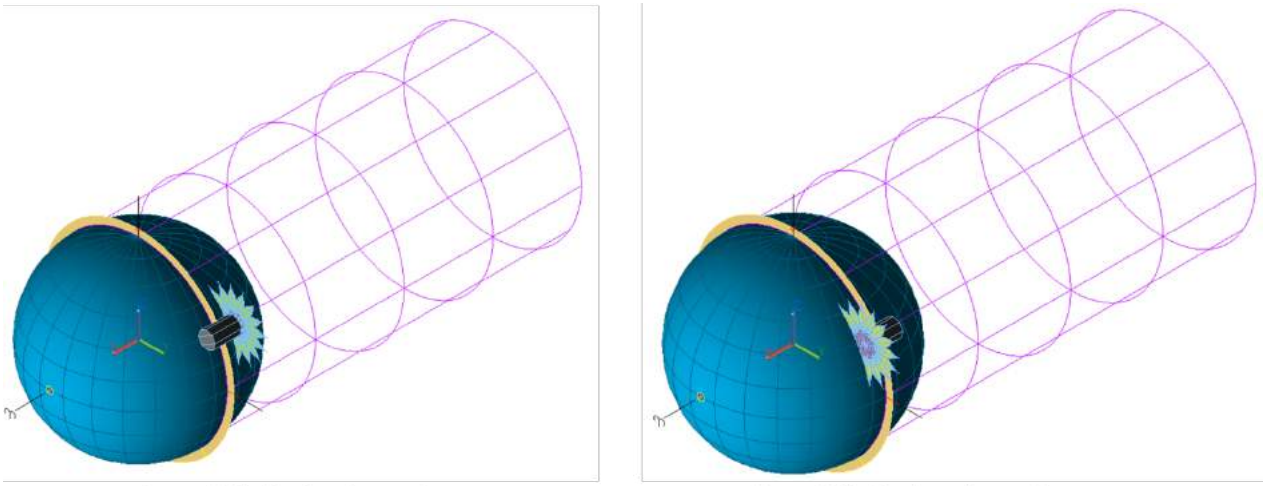

Figure A.7-12: On-orbit thermal model, beta = 90 degrees.

6

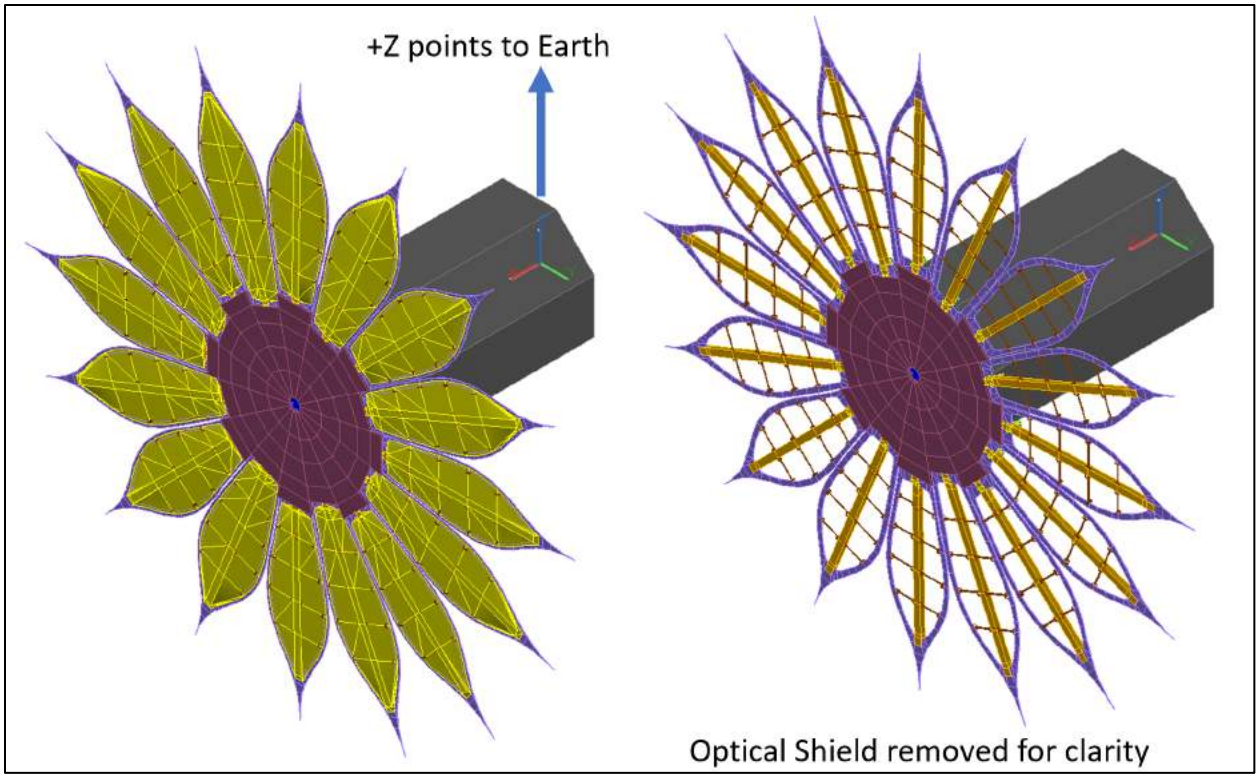

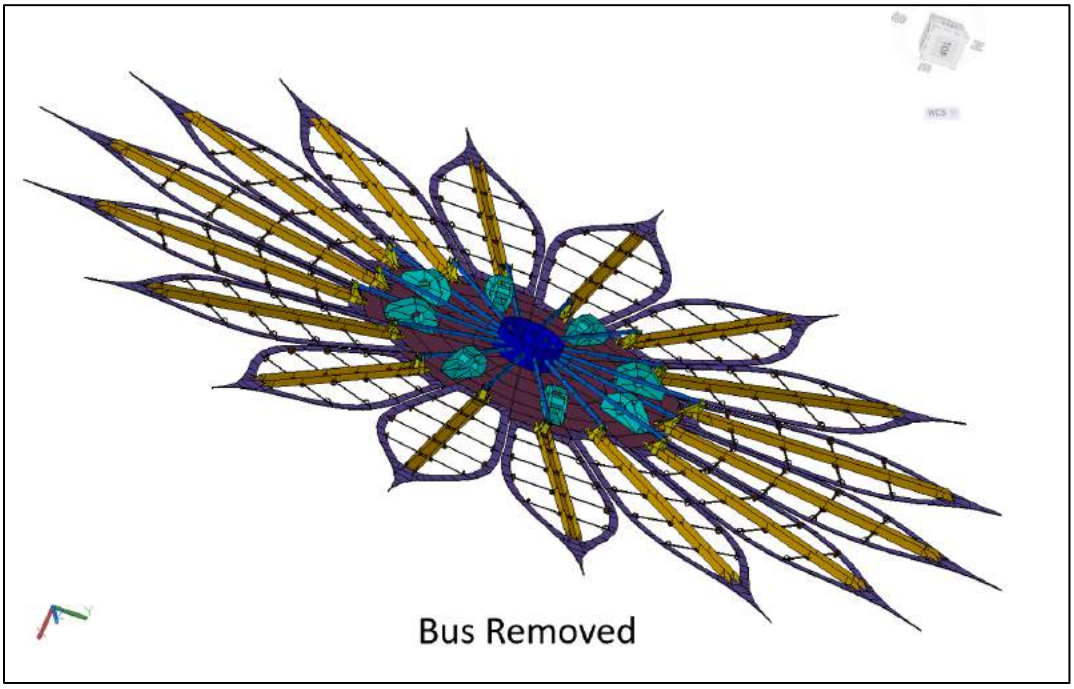

Figure A.7-13: Thermal Desktop model.

The orbital data and environmental data are summarized in Table A.7-1 and Table A.7-2.

6

Table A.7-1: Orbital stats.

Beta	0.0			
Altitude	600.0	km		
Period	5801.2	s	96.69	min
Eclipse entry	1836.1	s		
Eclipse exit	3965.2	s		
Eclipse duration	2129.1	s	35.48	min
Eclipse %	36.7%			

Table A.7-2: Environmental heating data.

	Normal Beta 0	Hot Beta 90	
Solar	1366.0	1421	W/m^2
Earth IR	237.0	261	W/m^2
Albedo	0.3	0.4	

The temperature mix and max over all cases by member are shown in Table A.7-3.

Table A.7-3: Temperatures min/max.

Name	Min Value(C)	Max Value(C)
BATTEN	-87	89
BRACKETS	-73	86
CENTERPLATE	-69	105
HUB	-8	53
PETALS	-88	90
TUBES	-58	94
U_CHANNEL_SPINE	-88	96
OPTSHLD_MX	-101	111
OPTSHLD_PX	-101	118
BUS	-50	27

For the normal case, the temperature at representative elements on two different petals is plotted over time and shown in Figure A.7-14 and Figure A.7-15. It can be seen the Starshade petals do not achieve a steady state equilibrium in eclipse.

6

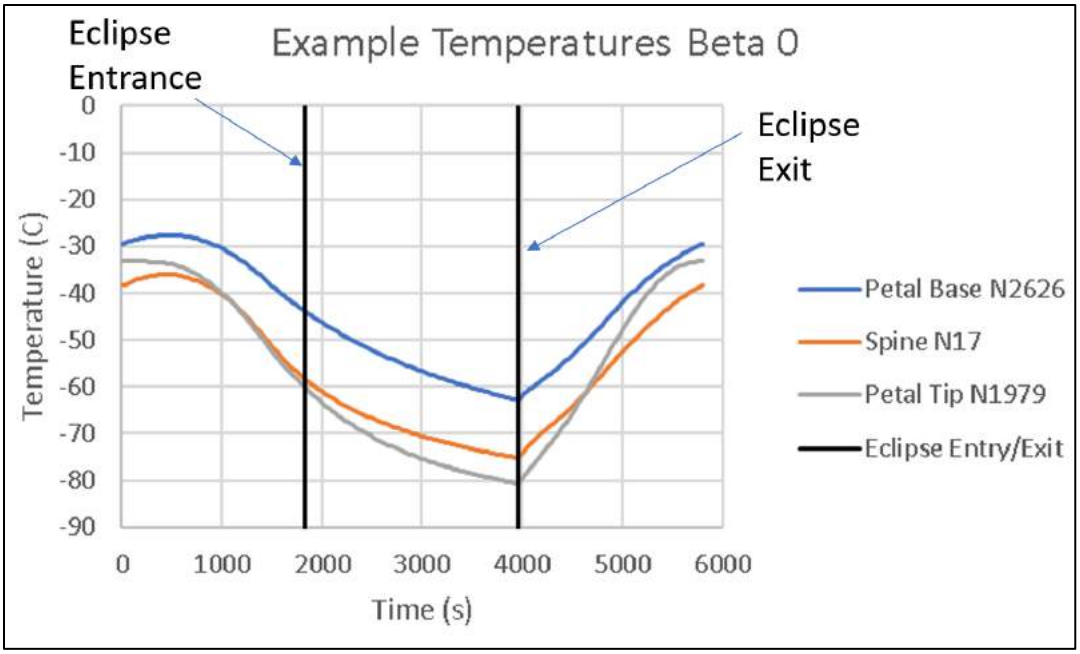

Figure A.7-14: Temperatures, petal near y-axis.

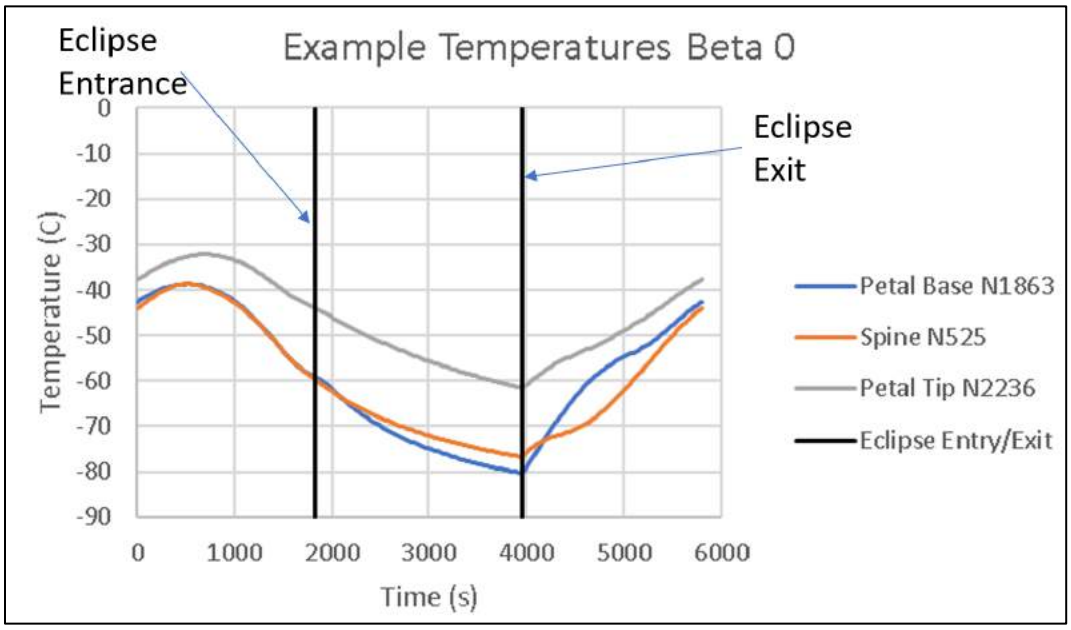

Figure A.7-15: Temperatures, petal near z-axis.

All ten normal operation temperatures were mapped nodally to the structural FEA. The times and their relative time to eclipse are shown in Table A.7-4. Some sample mapped temperatures are shown on the structural model.

6

Table A.7-4: Mapped temperature times.

Mapping Times			
Case no.	orbital time and load set number	Relative time (seconds)	Relative time (minutes)
1	1830	-6.1	-0.10
2	1980	143.9	2.40
3	2130	293.9	4.90
4	2280	443.9	7.40
5	2430	593.9	9.90
6	2580	743.9	12.40
7	2730	893.9	14.90
8	2880	1043.9	17.40
9	3030	1193.9	19.90
10	3180	1343.9	22.40

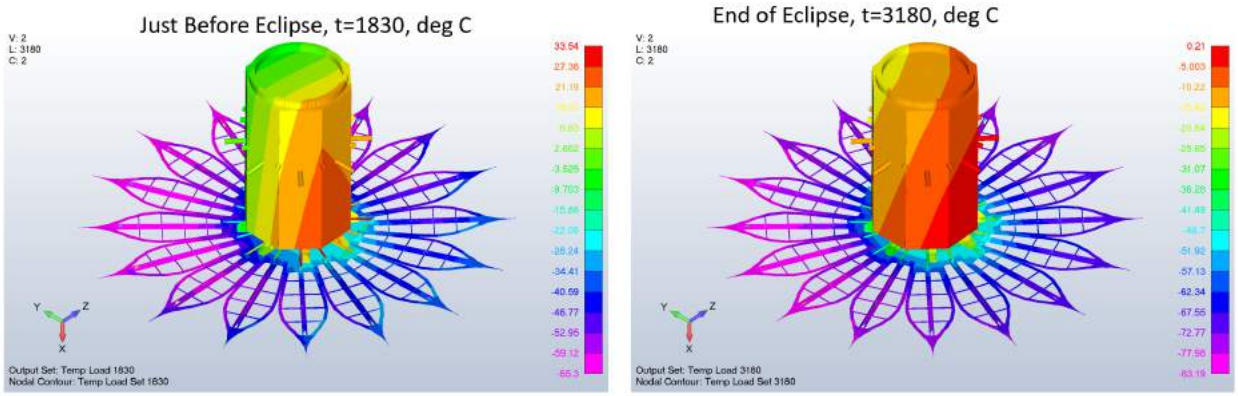

Figure A.7-16: Mapped temperatures.

Thermal Elastic Distortion

Using the mapped temperatures and deployed structural model, thermal elastic distortion analyses were performed at all ten normal operation temperature cases. For starshade optical performance, the primary metric of concern is tangential deflection. Distortions remained below 0.001”, or 25 microns, indicating this design should be thermally stable enough to perform starshade science. Sample distortions at three timestamps: just before eclipse, middle of eclipse, and end of eclipse, are shown in Figure A.7-17. Temperature dependent CTE curves were used for the analysis and are from validated data. Out of plane distortions are also shown in Figure A.7-18.

6

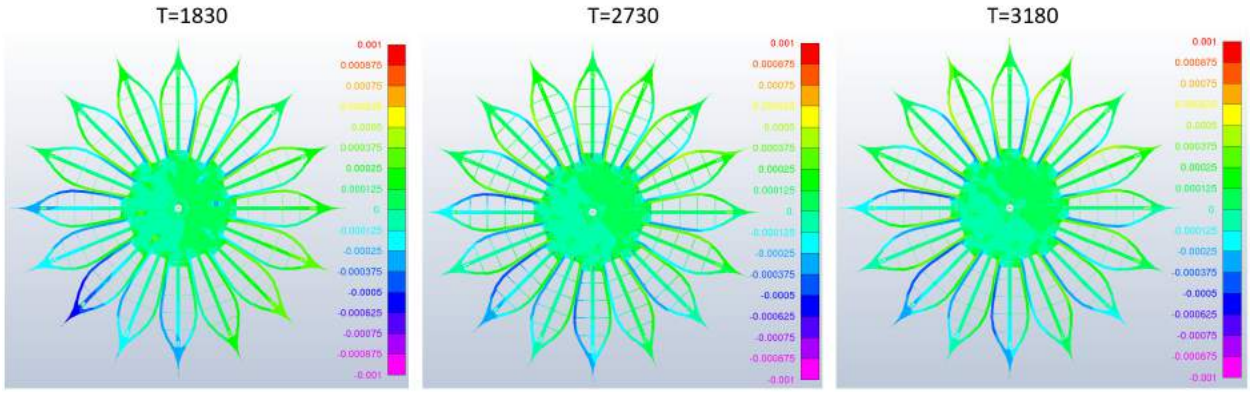

Figure A.7-17: Thermal distortions, in-plane, tangential.

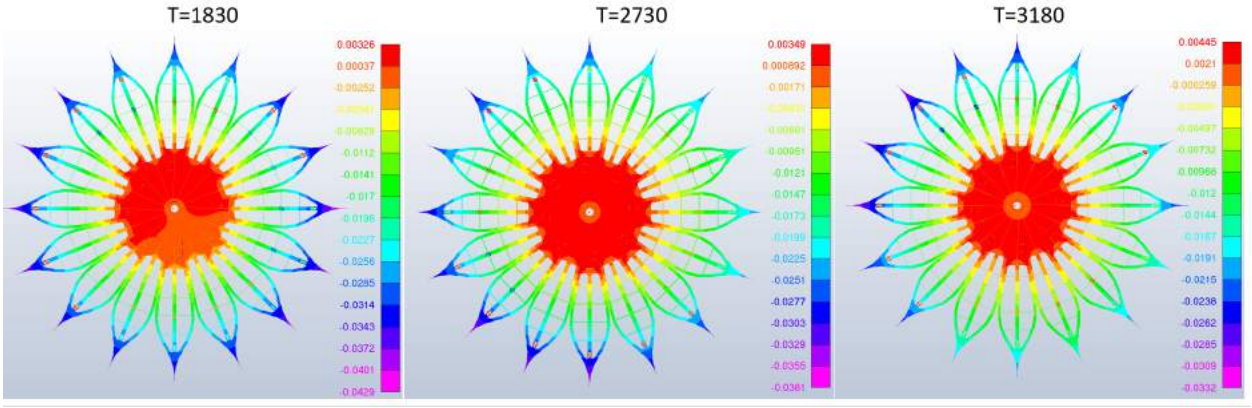

Figure A.7-18: Thermal distortion, out-of-plane.

To show the changes near the middle of the eclipse, thermal distortion results from time 2730 (minute 14.90) were subtracted from time 2880 (minute 17.40). Figure A.7-19 shows how the distortions will evolve during the critical middle period of imaging during eclipse. The changes are very low with the in-plane tangential change in the 0.0004” range, and out-of-plane changes in the 0.002” range.

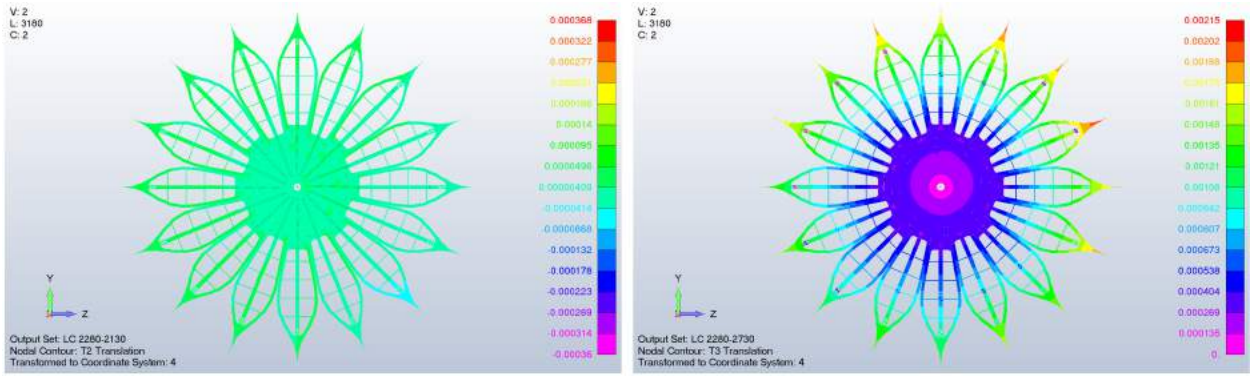

Figure A.7-19: Change in distortions minute 14.9 to 17.4.

A.7.3 Dynamic Response during Operations

The above results indicate that although the petals do not achieve equilibrium during eclipse with regards to temperature and distortion, the displacements are very small and the rate of change is very small. This initial study does not include detailed time domain thermal and structural response analysis. However, a simplified dynamic analysis was performed to show that the distortions and strain energy in the petals should not present any station keeping concerns during starshade operations. The resulting dynamic analysis very conservatively assumed that the strain energy in the petals as the starshade initiates operations is fully released as an initial condition. An exponential decay response analysis was then done to look at peak accelerations as a function of time. From the FEM, the maximum strain energy in any petal at the initiation of operations (T+15min after entering eclipse) is 0.016 in-lbs. The resonant frequency of the petal is 11.3 Hz and with a mass of 1.4 lbm yields an equivalent stiffness of 18.3 lb/in. Strain energy is equal to ½*K*d^2. This gives an equivalent displacement of 0.042". This is perhaps a bit conservative relative to Figure A.7-18 above that shows at T=2730 that the petal tip is deflecting 0.038" and near the CG is closer to 0.020". This suggests that some of the strain energy is in-plane and not out-of-plane. The in-plane frequency modes are much higher so for this analysis it will be assumed that all the strain energy is from out-of-plane distortions. For a single degree of freedom (SDOF) vibration system with a resonance at 11.3 Hz and peak displacement of .042", the peak acceleration is 0.55G. If this energy were released into the petal as an initial condition of a SDOF mass-damper system the acceleration response would decay very rapidly with expected damping as shown in Figure A.7-20. The petals with multiple layers of optical shielding and shield separators will likely have a damping ratio above 2.5% but even at 1% the accelerations are negligible within 5 seconds. Again, this is a very conservative and bounding case since the thermal analysis shows that there is not a rapid change in temperatures or distortions that could excite the petal first mode. In fact, the thermal analysis is suggesting that the petal is getting colder through eclipse and the initial condition entering eclipse was below room temperature so there is actually a gradual increase in strain energy during eclipse. Overall, with the petal modes at 11.3 Hz and with the structural and thermal mass properties of the petal, the likelihood of a thermal snap event appears minimal for the operating orbits.

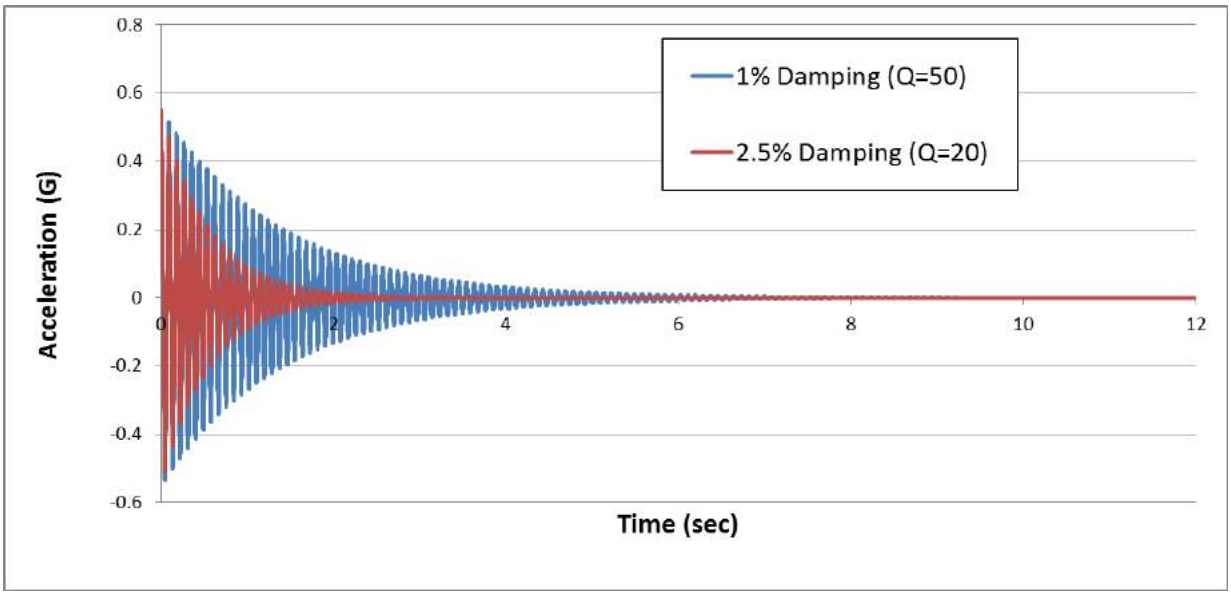

Figure A.7-20: Petal acceleration exponential decay with 1 and 2.5% damping if all the strain energy were released at 15 minutes into eclipse.

6

A.7.4 Mass Properties

FEA mass properties were calculated at coordinate system at the center of the ESPA ring, with X axis along octo-chassis length.

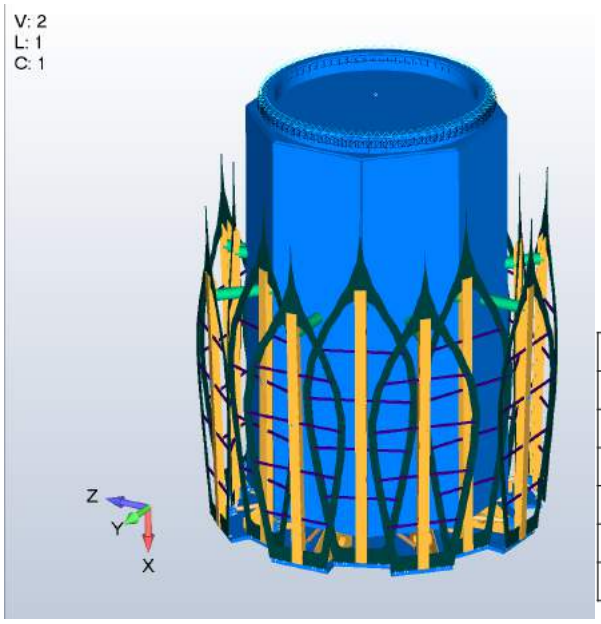

FEA Masses	
Item	**Mass (lbm)**
SC/Octo	300.23
Snubbers	0.91
Petals	22.52
Floor & HW	12.74
Total	336.40

Inertia (lbm-in^2)	Ixx	Iyy	Izz	Irt	Itz	Izr	CG (X, in)
Stowed	15,699.1	277,886.5	277,886.6	0.0	0.0	0.0	27.36
Deployed	39,961.2	332,078.8	332,078.8	0.0	0.0	0.0	28.82

Figure A.7-21: Mass properties.

FEA Masses w/out SC	
Item	**Mass (lbm)**
Snubbers	0.91
Petals	22.52
Floor & HW	12.74
Total	36.17

Inertia (lbm-in^2)	Ixx	Iyy	0	0	0	0	CG (X, in)
Stowed	9,798.4	62,176.9	62,177.0	0.0	0.1	0.6	39.1
Deployed	33,806.1	115,783.7	115,783.7	0.0	0.0	0.0	51.7

Figure A.7-22: Mass properties without SC or OctoChassis.

6

A.8 Radiation Effects on Subcomponent Level

High-energy particles affect the spacecraft by creating Single Event Effects (SEE) including Single Event Upsets (SEU), Single Event Latchups (SEL), Single Event Gate Rupture (SEGR), Single Event Burnout (SEB), Displacement Damage (DD), and Enhanced Low Dose Rate Sensitivity (ELDRS). High-energy particles such as Galactic Cosmic Rays (GCR) are modeled using Crème96 in SPENVIS. The effect on the S/C can be correlated with component-specific susceptibility in later phases.

SEL is the most critical catastrophic damage issue affecting many CMOS circuits, which are sensitive to the effects. Difficult and costly, the best alternative is to eliminate latchup-prone devices. SEGR and SEB affect power MOSFETs and pulse-width modulators. Testing and qualification methods are required to accommodate these effects. mDOT requires that components are SEB and SEL immune.

Additional effects such as Displacement Damage (DD) and ELDRS are also considered. DD is a cumulative parametric degradation that can lead to functional failure and is usually characterized as Non-ionizing Energy Loss (NIEL) in a given material resulting from a portion of energy deposition by impinging radiation. Linear integrated circuits, light emitting diodes, optical detectors, and optocouplers are known to be susceptible.

Some bipolar devices show extreme degradation at low dose rates. This Enhanced Low Dose Rate Sensitivity (ELDRS) has a wide variation among manufactures, and the topic is not completely understood. In addition, instrument bias due to the radiation environment may also occur. Devices with high maximum voltage ratings are often problematic. Low doping levels and increased oxide thickness will help to protect against damage.

Spacecraft

Spacecraft components that do not meet the 8 kRad dose design guideline, and are susceptible to radiation effects, will require additional shielding. Susceptible components may be placed interior to the spacecraft, receiving shielding from the surrounding systems, or additional aluminum shielding can be placed around susceptible components. Potentially sensitive components include radio(s), memory storage, CMOS sensors, transistors (MOS and bipolar), oscillators, and integrated circuits.

Testing

For those components where radiation susceptibilities are not yet defined, high fidelity simulations or laboratory testing will help to classify the limits for dose exposure. In future phases, Monte Carlo and ray tracing simulations on the components, subsystems, and full satellite model will determine the areas where additional shielding is needed. COTS satellite components have a relatively short shelf life (around 1-3 years) due to variability in manufacturing location and practices.

Radiation testing would adequately determine susceptibility of the spacecraft subcomponents and estimate additional shielding requirements when relevant data is not available. Tests will comply with MIL-STD-883 Standards Test Method 1019. Typical testing estimates Single Event Upset (SEU) cross-section and Single Event Latchup (SEL) characteristics, and Total Ionizing Dose (TID) tolerance. Radiation sources may involve proton beams (maximum energy: 500 MeV), Cobalt-60 testing, or heavy-ion accelerators and neutron sources if needed.

[6]

Potential test sites include: NASA Space Radiation Facility, Lawrence Berkeley National Laboratory Accelerator Space Effects Facility, University of California at Davis Crocker Nuclear Lab, and Texas A&M University Cyclotron. For radiation hardness assurance, mDOT will either buy components with radiation susceptibility data or buy components and test radiation susceptibility in-house or through an external vendor.

[6]

A.9 Methodology for Science Modeling

In order to accurately model the sensitivity of the mDOT instrument to extrasolar debris disks, a fiducial instrument model must be assumed, sources of noise contributions must be estimated, and brightness of the target debris disks must be estimated. The instrument properties and noise sources used for this purpose are summarized in Table 9-1. While the exact values of instrument parameters may not precisely match the design specifications, they are very close.

Table 9-1. Instrument Architecture and Noise Sources

Instrument Properties		Noise Sources	
Starshade Suppression	10^{-7}	Starshade light leakage	Target Magnitude - 17.5
Telescope Diameter	10 cm	Starshade backlight (from Earth)	22.2 magnitudes for 6 AM/PM LTAN
Optical Transmissivity	0.95	Starshade backlight (from Full Moon)	30 magnitudes
CCD Quantum Efficiency	0.65	Local Solar Zodi Foreground	22.7 magnitudes / arcsec^2
CCD Size (angular FOV)	1280 x 960 pixels (10.65’ x 7.98')	CCD read noise	5 electrons RMS
Filter Wavelengths	400-500 nm	CCD dark current	0.01 electrons / pixel / second

The telescope camera CCD is fairly standard, with around ~1 million 0.5” arcsec square pixels, and an overall transmissivity (optical + quantum efficiency) of ~0.6. We assume the spectral dependence throughput is a step function over the bandwidth, for simplicity, and that the CCD has fairly low but not optimal read noise and dark current.

The noise contribution from starshade backlight (much akin to the phenomenon of Earthshine on the moon), was estimated for a reasonable orbital configuration directly above the terminator, with a minimum solar point-away angle of 15 degrees, assuming an Earth and starshade albedo of 0.3 and 0.1

[6]

respectively, using isotropic phase functions for the scattering, and treating the starshade as a thin disk. It is conceivable that the starshade albedo could be engineered down an order of magnitude, with specialized absorptive black paints, but the CCD noise sources currently dominate. Observations in the baseline noon/midnight LTAN eliminate that contribution to the noise.

In order to determine a spatial map of the instrument sensitivity, we are interested in finding the PSF of the light leak from the star behind the starshade. To do this we model the starshade with an offset-hypergaussian apodization function (Cash 2011)

The electromagnetic field behind the occulting mask for an incident plane wave can be calculated numerically using the angular spectrum method of Fresnel propagation, which uses the discrete Fourier transform to convolve the aperture illumination with the free-space propagation kernel. We calculate the electric field on-axis at z = 500 km behind the starshade, and pass the electric field through a circular aperture of diameter 10 cm, corresponding to the size of the telescope. Assuming the telescope optics behave ideally, we can use the Fraunhofer approximation to obtain the electric field distribution in the image plane using the inverse Fourier transform, to obtain a PSF which is a characteristic annular ring around the edge of the starshade. This PSF is saved for later normalization to host star intensity accounting for the depth of the contrast in the shadow.

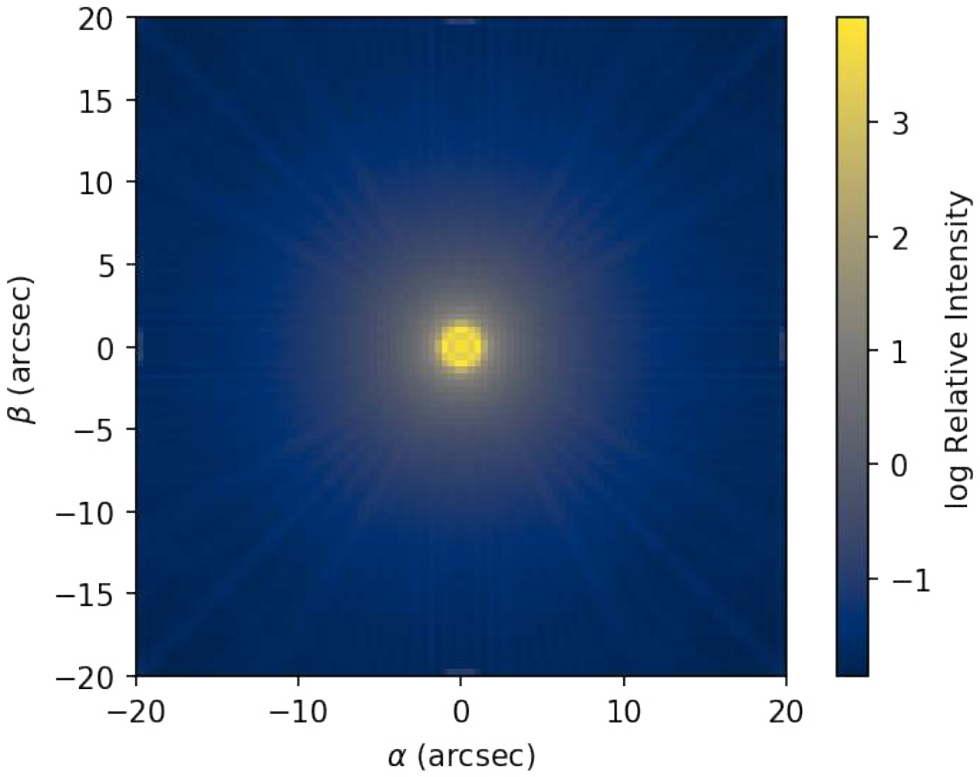

Figure A.9-1: Annular PSF formed from light leakage around 3-m starshade.

Likewise, the spatial contribution of the starshade backlight can be calculated by convolving the starshade object with the telescope PSF, and normalizing the total intensity to the estimate obtained for its brightness. The starshade backlight most strongly contributes to the central ~4 pixels, which are

[6]

inside the IWA. The spatial distribution of the local solar zodi foreground is assumed to be uniform across the image (although it varies marginally relative to the location of the ecliptic), and the dark current is assumed to be spatially uniform as well. For the spatial variation of the read noise, we use a Poisson distribution.

With all of these noise maps in hand, it is possible to calculate a the spatial distribution of the signal-to-noise ratio (SNR) for a target disk of generic surface brightness, which is measured as a ratio of photoelectron counts in the detector. However, we must first calculate the brightness of a zero magnitude reference, in units of photons per second. With this reference brightness, it is possible to convert noise sources in magnitudes or magnitudes/arcsec^2 directly to their brightnesses in photons per second in a single pixel. Once all of the source brightnesses have been converted into powers, measured in photons/sec, it is straightforward to arrive at the number of photoelectron counts produced by multiplying by the exposure time and transmissivity of the instrument (both optical and quantum efficiency.) Finally, the SNR is calculated as a ratio of these photoelectron counts, where the signal is the number of counts from the target, and the noise is the square root of the counts from the target plus all of the other contributions from the noise sources.

This SNR calculation implicitly assumes that it is possible to separate the contributions from the target and the background noise, which is equivalent to having perfect PSF subtraction, and perfect noise characterization. However, since the SNR is calculated individually for each pixel, it does not account for additional detection capabilities that can be achieved by examining multiple pixels, which is a boost to sensitivity, considering the extended nature of the sources. A truly bayesian statistical framework for the detection of exoplanetary debris disks does not exist, to our knowledge. After the SNR map is calculated, it is averaged azimuthally to obtain a radial SNR function. For a given target with a given surface brightness (estimated in the next section), we set the needed SNR value at the IWA of 0.6 arsec to be 5-sigma, and iteratively increase the number of exposures until this sensitivity is obtained. The number of necessary exposures needed for particular surface brightnesses result in the contours of ***Figure 4-5***.

In addition to knowing the instrument architecture and noise contributions, the actual brightness of the targets must be estimated, so that sufficiently bright targets can be selected. However, due to the nature of mDOT's orbital configuration, the total mission lifetime is set by the delta-v budget of onboard fuel available for reconfigurations. Since a broad survey is not possible, maximizing the potential science output requires solving a traveling-salesman type problem for targets over their locations on the sky. Since (approximately), the reconfiguration between targets scales like the difference in their declination, and the cost to maintain formation on a single target over multiple polar orbits scales as the difference in declination from the nominal declination of +/- 8 degrees, a completely optimized mission would simply choose all of the targets in a line, with increasing right ascension, along the optimal declination.

However, targets of astrophysical interest are not so nicely placed. In order, to ascertain a good mission strategy that effectively uses the delta-v budget while attempting to maximize the scientific output of the mission, it is necessary to review the literature to find known disk targets within a reasonable range of declination, that have sufficient surface brightness to be readily detectable by mDOT. For all targets, we use a range of +/- 20 degrees in declination as the cutoff as being inaccessible to the orbital configuration. The known disks which fit this criterion that we were able to find are summarized in Table 9-2A, along with our estimates for their surface brightness.

6

Table A.9-1: Known imaged Disk Targets.

Target Name	Stellar Type	B (mag)	Dist (pc)	Detection Instrument	Observing Wavelength (micron)	Disk Radius (arcsec)	Estimated Surface Brightness (mag / arcsec^2)	References
Eps Eri	K2	4.61	3.2	Spitzer SOFIA CSO	3.5 35 350	3.11	21.7	Backman 2009 Su+ 2017
49 Cet	A1	5.67	59	HST / NICMOS	1.1	2.18	21.94	Choquet+ 2017
HD 377	G2	8.22	39.1	HST / NICMOS	1.1	2.20	22.95	Choquet+ 2016
HD 15115	F2	7.15	45.2	HST / STIS	0.2-1.1	12.6	20.24	Schneider+ 2014
HD 32297	A	8.32	112.4	HST / STIS	0.2-1.1	13.88	21.55	Schneider+ 2014
HD 107146	G2	7.61	28.5	HST / ACS	0.6, 0.8	4.56	22.18	Ardila+ 2004
HD 157587	F5	8.96	107.4	HST / STIS	0.2-1.1	4.67	(22)	Padget & Stapelfeldt 2015

Estimating the surface brightness for these targets is a rather heterogeneous process, as there is no direct convention adhered to by the various authors of what values to report. Some report total integrated intensity in Jy, in which case we have to estimate the area of the disk they have integrated over. Some report integrated intensity over a specified region, which can be more directly converted into our units. However, the worst case scenario was seen for HD 157587, where no magnitude or intensity information was reported at all. For this target we simply assume its surface brightness to be 22 magnitudes/arcsec^2, which is fairly comparable with the other targets detected by HST. For Epsilon Eridani, we use the estimated magnitude produced by Backman 2009, which combines multiple observations to model the multiple component debris disk.

[6]

In addition, we examine potential targets included in the HOSTS survey (Ertel+ 2018), which uses nulling interferometry on the LBTI to search for zodiacal excess from nearby stars. The paper reports detections on a few, and upper limits on the surface brightness of many other targets. Their targets within our range of declinations are summarized in ***Table A.9-2***.

Table A.9-2: Thermally-detected or non-detected targets.

Target Name	Target Type	EEID (mas)	Stellar Flux (Jy)	Zodi Level	Sigma Zodi	Estimated Brightness (mag / arcsec^2)
Beta Eri	Upper limit	248	289.80	37.8	26.7	21.35
Eta Crv	**Detection**	125	56.77	**2649**	**210**	**18.60**
Delta Crv	Upper limit	251	297.92	-32.6	26.8	21.31
Mu Vir	Upper limit	151	84.35	93.8	56.7	22.05
1 Ori	Upper limit	205	150.70	152.5	95.3	20.75
Beta Leo	**Detection**	336	552.20	**117.4**	**12.5**	**19.15**
Alpha Aql	Upper limit	570	1730.18	56.5	50.1	18.145
Xi Peg A	Upper Limit	132	56.766	140	103	21.88
GJ 105 A	Upper Limit	73	8.06	-506	533	22.44
Xi Gem	Upper limit	196	130.045	56.4	44.6	21.75
40 Leo	Upper limit	98	34.205	-12	192	21.87
Tau Boo	Upper limit	114	43.460	-208.3	98.7	22.27
Lambda Ser	Upper limit	121	41.504	21.0	39.2	23.30
Gamma Ser	Upper limit	151	78.360	99.7	53.7	22.19

[6]

For HOSTS targets with SNR < 2, we take the measurement uncertainty as the upper limit of the brightness of the zodi, and convert in B-magnitudes/arcsec^2. If their SNR > 2 we use the mean zodi value for our surface brightness estimate. In order to convert zodi levels into surface brightnesses, we follow the conventions laid forth in Kennedy+ 2014, so that the scattered light surface brightness can be calculated with

$$S_{sca} = F_{nu,star} / (4 \pi) * (d / r)^2 * \omega / (1 - \omega) * \Sigma_m(r).$$

Here $F_{nu,star}$ is the stellar flux in Jy, r is the distance in AU to the particular location in the disk, d is the distance to the system in pc, omega is the dust albedo assumed to be ~0.1, and Σ_m is the dust surface density profile

$$\Sigma_m(r) = z * \Sigma_{m,0} * (r / r_0) ^{-\alpha}$$

which is assumed to follow a power law with exponent $-\alpha = -0.34$, the constant $\Sigma_{m,0} = 7.12 * 10^{-8}$ is the nominal dust surface density, z is in units of zodis, and the location of r_0 is referenced to the Earth Equivalent Insolation Distance (EEID), which is 1 AU for the sun, but in general will be $r_0 = \sqrt{L_{star} / L_{sun}}$ due to the inverse square law of radiation. See **Figure A.9-2** for an example.

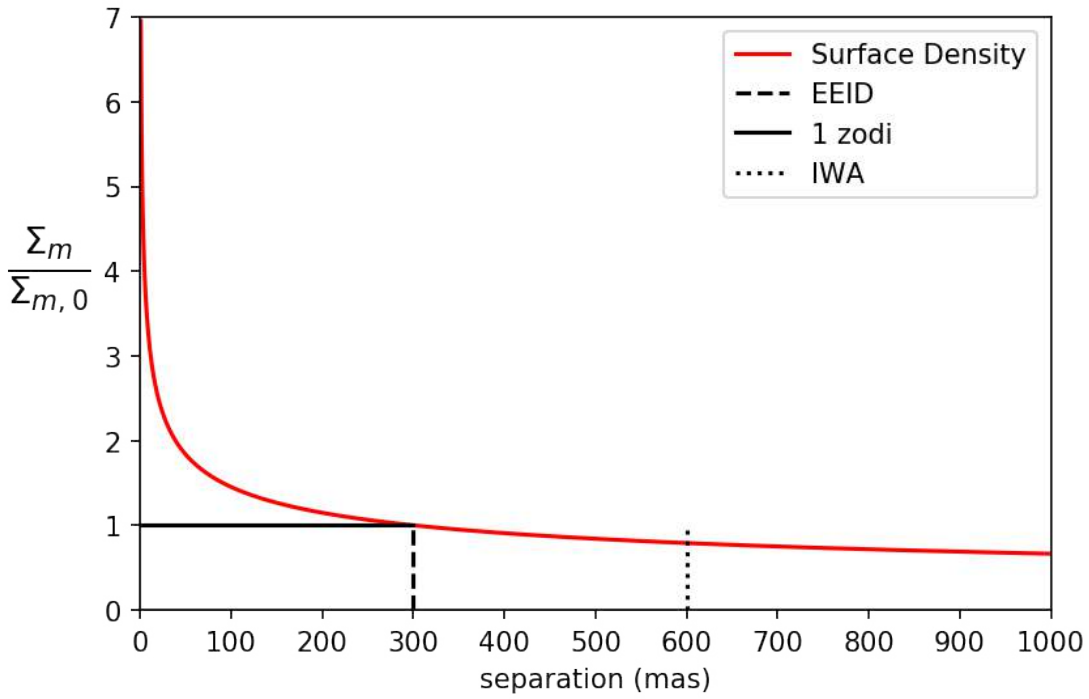

Figure A.9-2: The HOSTS zodiacal dust model for a 1 zodi disk and an EEID of 300 mas. We extrapolate the surface density profile to the location of the inner working angle when estimating the scattered light surface brightness.

Surface brightness estimates along with target star brightnesses for the known disks and the HOSTS targets within our accessible declination range are plotted in **Figure A.9-3**. In addition, a few nearby stars with B magnitude < 6 and a nominal 21 magnitudes / arcsec^2 disk (approximately 10 zodis) are included.

6

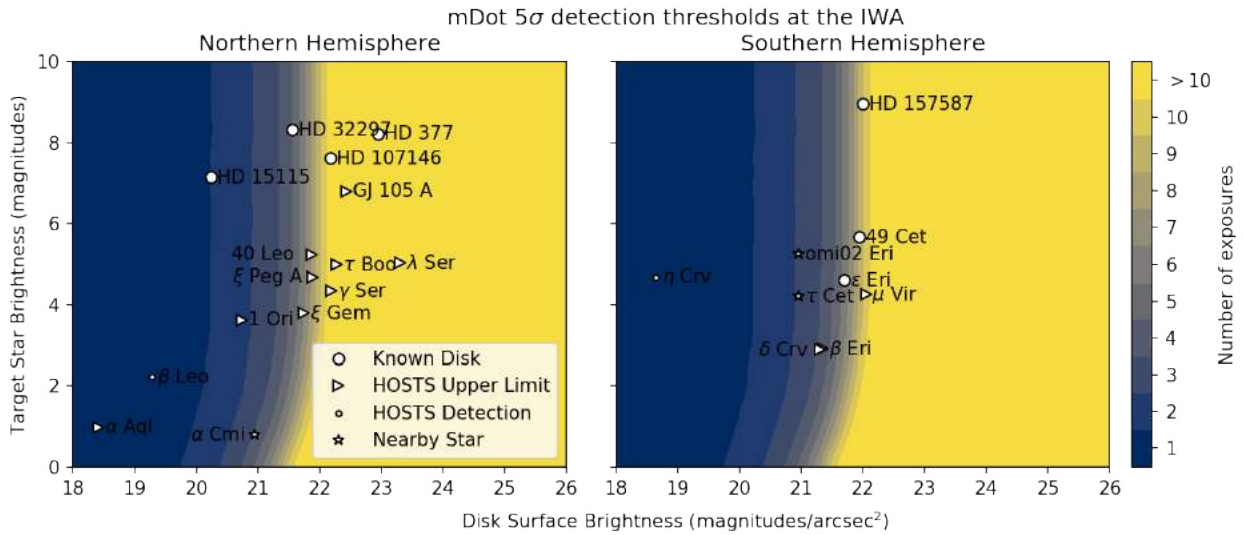

Figure A.9-3: Estimating detection possibilities for potential targets of various types. The contours indicate the number of exposures required to obtain a 5-sigma detection in each pixel where a disk with the given surface brightness would (putatively) exist, at the location of the IWA. The detection contour is defined roughly by two components, a vertical barrier, which is independent of the target host star brightness, set by parameters such as the detector read noise and dark current, along with the solar zodi foreground, and a slanted barrier, which is set by the contrast provided by the starshade, which dominates for very bright targets

A.9.1 Design reference mission target selection

Comparing the instrument SNR model to the surface brightness estimates allows one to design a mission intelligently around the delta-v budget requirements, attempting to maximize the scientific output while working around the traveling salesman problem of optimizing the orbital geometry. In addition to picking good potential targets, it is important to have reference targets for each exposure, which have no strong disk signal, for ideal PSF Subtraction around the IWA. For each target we decide to include in a mission, we attempt to find a bright reference star which is nearby, and devoid of bright companions, which may ruin the annular starshade PSF formed. To do this, we use the V/50 bright star catalog, and the Washington Double Star catalog to vet out reference targets with nearby binaries. Further reference vetting to check reference star IR excess remains to be done to ensure the reference stars are unlikely to contain a disk signal of their own. Two potential mission architectures have been selected in this manner, and are displayed in ***Table A.9-3*** and ***Table A.9-4*** for the Northern and Southern Hemisphere respectively. (Note that the delta-V costs here are from a parametric model; the detailed simulations presented in Section 4 provide more precise formulation.

Table A.9-3: Northern Hemisphere Mission.

Target Name	HD #	Target Type	RA (hrs)	DEC (deg)	B mag	N_expo	Obs Cost (m/s)	Reconfig cost (m/s)
--	15115	Known Disk	2.43	6.29	7.15	2	4.22	--
u Tau	23466	Reference	3.76	6.05	5.23	2	4.60	1.14

6

1 Ori	30652	HOSTS UL	4.83	6.96	3.63	5	13.99	4.28
--	32297	Known Disk	5.04	7.46	8.32	5	12.07	2.35
gam Ori	35468	Reference	5.41	6.34	1.42	1	1.67	5.22
alf Ori	39801	Reference	5.91	7.40	2.3	1	0.85	4.97
alf CMi	61421	Nearby Star	7.65	5.22	0.79	4	14.94	10.26
zet Hya	76294	Reference	8.92	5.94	4.11	9	46.63	3.39
tet Leo	97633	Reference	11.23	15.42	3.33	4	29.28	44.57
bet Leo	102647	HOSTS det	11.81	14.57	2.22	1	5.462	4.03
--	107146	Known Disk	12.31	16.54	7.61	9	91.63	9.29
gam Aql	186791	Reference	19.77	10.61	4.24	9	50.51	27.89
alf Aql	187642	HOSTS UL	19.84	8.86	0.98	3	5.60	8.20
							Total Cost	**407.11**

Table A.9-4: Southern Hemisphere Mission.

Target Name	HD #	Target Type	RA (hrs)	DEC (deg)	B mag	N_expo	Obs Cost (m/s)	Reconfig cost (m/s)
bet Cet	4128	Reference	0.72	-17.98	3.06	2	9.35	--
49 Cet	9672	Known Disk	1.57	-15.67	5.667	8	45.18	28.65
tau Cet	10700	Nearby Star	1.73	-15.93	4.22	3	12.69	5.86
eps Eri	22049	Known Disk	3.54	-9.45	4.61	8	38.42	35.91
del Eri	23249	Reference	3.72	-9.76	4.46	8	40.99	5.23
omi02 Eri	26965	Nearby Star	4.25	-7.65	5.25	3	5.35	9.74
ome Eri	31109	Reference	4.88	-5.45	4.64	10	60.02	11.64
del Crt	98430	Reference	11.32	-14.7	4.68	2	7.04	46.30
eta Crv	109085	HOSTS det	12.53	-16.19	4.69	2	7.65	34.46
							Total	**404.56**

The Northern Hemisphere is very lucky, since many of the targets are close the optimal declination, making reconfigurations cheaper and allowing the inclusion of more targets. The mission includes 7 potential disk targets, each with its own reference star (except for Beta Leo and HD 107146, which share a reference star.) The case for the Southern Hemisphere is more difficult, as many of the targets are far from the optimal declination, and so reconfigurations are expensive. The suggested mission architecture includes 5 potential disk targets and 4 references (49 Cet and Tau Cet share a reference), but it also includes one of the more compelling systems, Epsilon Eridani.

A.9.2 Epsilon Eridani

Epsilon Eridani is one of the nearest Sunlike stars to our solar system, and has a known RV planet (Mawet+ 2018) along with a complex dust system, observed with ALMA, Spitzer, CSO, SOFIA, LMT, Herschel, among others. (Booth+2017, Backman 2009, Su+2017, Chavez-Dagostino+2016, Greaves+2014). Careful analysis of the SED of the IR excess (Backman 2009), can be used to create a radial dust distribution model, which we use in a simulated example of mDOT performance capabilities. A more extensive analysis would attempt to use the more recent set of observations, to model the entirety of the dust distribution, but this is very complicated. The Backmann 2009 model is straightforward to implement, as they have produced a radial quantity, the perpendicular optical depth of the dust, tau_perp, which can then be directly translated into an optical surface brightness profile using the relationship

$$R = \tau_{perp} / (4 * \pi) * (d_{pc} / r_{AU})^2 * P * \phi(\gamma) / \cos(i) .$$

Here R is the ratio of dust surface brightness per square arcsec to the star's brightness, tau_perp is the perpendicular optical depth of the dust, d_pc is distance to the system in units of parsecs, r_AU is the radial location of the dust in AU, P is the geometric albedo, again assumed to be ~0.1, phi(gamma) is the phase function value for the scattering angle gamma, and cos(i) is the inclination of the disk to the plane of the sky.

In order to simulate an image formed by the instrument, an "object" brightness distribution was formed from all of the known sources in the FOV, including background stars from GAIA DR2 and deep Keck AO imaging in the vicinity of the star, along with the light leak PSF formed by the starlight diffracting around the starshade normalized to the appropriate intensity, and the contributions from the disk model. Because Backman assumes the disk is face-on, but later observations (ALMA) show the disk is slightly inclined, we mimic forward scattering in the disk using the relative values of a mie scattering phase function, calculated using BHMIE, the python implementation of scatterlib, averaged over the relevant range of viewing angles and particle sizes in the disk. The object brightness distribution is convolved with the telescope PSF, for all of the points outside the IWA, with the exception being the star behind the starshade, whose PSF was previously found. Finally, 5, 5-minute exposures are stacked with the nominal instrument parameters, to obtain the final image measurement in counts of photoelectrons, including all sources of noise. A simulated image is shown in **Figure A.9-4.**

6

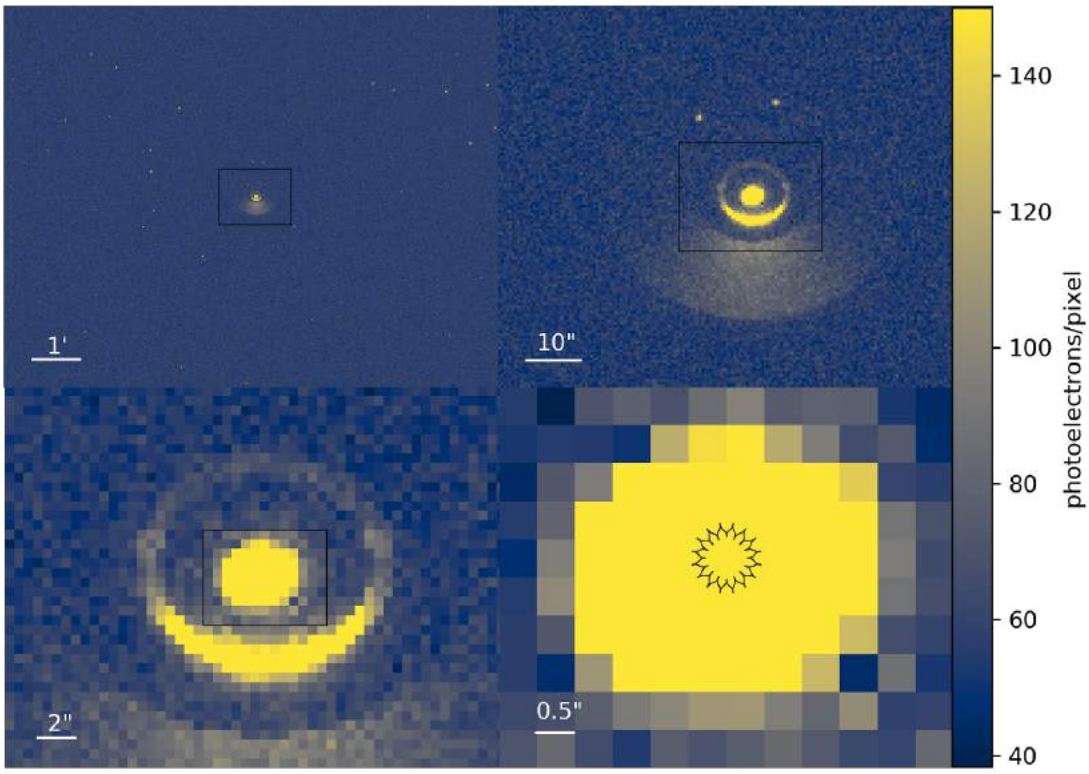

Figure A.9-4: Simulated image of the Epsilon Eridani ring system with 5 x 5 minute exposures, using the model from Backman et al. 2009. Each subsequent panel is a zoom-in on the box in the previous, with angular scales indicated in each figure. In the first panel, ~100 background stars are visible, populated using GAIA DR2 estimated B-magnitudes, as well as background stars known from Macintosh et al. 2001. The second and third panel show the ring system up close, with multiple gaps, and strong forward scattering on the near-inclined side of the disk. The last panel indicates the relative size of the starshade in the image, roughly two pixels across. The inner disk is detectable, but mixed strongly with the star leak annular PSF and starshade bac

One can see the three ring components, clearly separated by gaps, although the inner disk gets strongly mixed with the light-leak PSF and starshade backlight. The middle disk ring is visible in both forward and backward scattering, although the outer, more diffuse disk is only visible only on the forward scattering edge. While the current mission architecture is not sensitive enough to see the RV planet, a slightly upgraded version of the mission may be able to. Assuming the RV planet (with mass ~1 MJup), has a similar albedo and phase function as Jupiter, it could be as bright as 25th magnitude, with orbital separations ranging for 0.5 - 1 arcsec depending on when the observations are being made (see Brianna's & Lea's plot, addendum.) This would require the starshade to have a marginally deeper shadow around 10^-8.5 (which is designable, but more difficult to manufacture), and a slightly larger telescope, around 20cm aperture, to resolve the nearby point source. The putative second planet "eps eri c," would be even fainter, as dynamical constraints suggest its mass is <0.1 MJup, and becomes increasingly difficult to see.

Appendix 9 references

[1] D. R. Ardila et al. A Resolved Debris Disk around the G2 V Star HD 107146. The Astrophysical Journal Letters, Volume 617, Number 2.

[2] D. Backman et al. EPSILON ERIDANI'S PLANETARY DEBRIS DISK: STRUCTURE AND DYNAMICS BASED ON SPITZER AND CALTECH SUBMILLIMETER OBSERVATORY OBSERVATIONS. The Astrophysical Journal, 690:1522–1538, 2009. doi:10.1088/0004-637/690/2/1522

[3] M.S. Bessell, F. Castelli, and B. Plez. Model atmospheres broad-band colors, bolometric corrections and temperature calibrations for O-M stars. Astron. Astrophys. 333, 231–250 (1998)

[4] Booth, Mark & R. F. Dent, William & Jordán, Andrés & Lestrade, Jean-Francois & S. Hales, Antonio & C. Wyatt, Mark & Casassus, Simon & Ertel, Steve & S. Greaves, Jane & Kennedy, Grant & Matrà, Luca & Augereau, Jean-Charles & Villard, Eric. (2017). The Northern arc of ε Eridani's Debris Ring as seen by ALMA. Monthly Notices of the Royal Astronomical Society. 469. 10.1093/mnras/stx1072.

[5] Webster Cash. ANALYTIC MODELING OF STARSHADES. 2011 August 12. The Astrophysical Journal, Volume 738, Number 1.

[6] Chavez-Dagostino, M. et al. Early science with the Large Millimetre Telescope: Deep LMT/AzTEC millimetre observations of ε Eridani and its surroundings. 2016. MNRAS, 462, 2285

[7] Élodie Choquet, Marshall D. Perrin, Christine H. Chen, Rémi Soummer, Laurent Pueyo, James B. Hagan, Elena Gofas-Salas, Abhijith Rajan, David A. Golimowski, Dean C. Hines. FIRST IMAGES OF DEBRIS DISKS AROUND TWA 7, TWA 25, HD 35650, AND HD 377. The Astrophysical Journal Letters, Volume 817, Number 1.

[8] Choquet, É. et al. 2017. First Scattered-light Images of the Gas-rich Debris Disk around 49 Ceti. ApJ, 834, L12

[9] S. Ertel, D. Defrère, P. Hinz, B. Mennesson, G. M. Kennedy, W. C. Danchi, C. Gelino, J. M. Hill, W. F. Hoffmann, G. Rieke. 2018 April 17. The HOSTS Survey—Exozodiacal Dust Measurements for 30 Stars. The Astronomical Journal, Volume 155, Number 5

[10] Greaves, J. S. et al. Extreme Conditions in a Close Analog to the Young Solar System: Herschel Observations of epsilon Eridani. 2014, ApJ, 791, 5

[11] Grant M. Kennedy, Mark C. Wyatt, Vanessa Bailey, Geoffrey Bryden, William C. Danchi, Denis Defrère, Chris Haniff, Philip M. Hinz, Jérémy Lebreton, Bertrand Mennesson. EXO-ZODI MODELING FOR THE LARGE BINOCULAR TELESCOPE INTERFEROMETER. The Astrophysical Journal Supplement Series, Volume 216, Number 2.

[12] Bruce A. Macintosh, E. E. Becklin, Denise Kaisler, Quinn Konopacky, and B. Zuckerman. Deep Keck Adaptive Optics Searches for Extrasolar Planets in the Dust of ϵ Eridani and Vega. The Astrophysical Journal, Volume 594, Number 1

6

[13] Mawet, Dimitri & Hirsch, Lea & J. Lee, Eve & Ruffio, Jean-Baptiste & Bottom, Michael & Fulton, Benjamin & Absil, Olivier & Beichman, Charles & Bowler, Brendan & Bryan, Marta & Choquet, Elodie & Ciardi, David & Christiaens, Valentin & Defreère, Denis & Gomez Gonzalez, Carlos & W. Howard, Andrew & Huby, Elsa & Isaacson, Howard & Jensen-Clem, Rebecca & Ygouf, Marie. (2018). Deep exploration of ϵ Eridani with Keck Ms-band vortex coronagraphy and radial velocities: mass and orbital parameters of the giant exoplanet.

[14] Deborah Padgett and Karl Stapelfeldt. Warm Debris Disks with WISE and HST. Young Stars & Planets Near the Sun Proceedings IAU Symposium No. 314, 2015. doi:10.1017/S1743921315006456

[15] Glenn Schneider, Carol A. Grady, Dean C. Hines, Christopher C. Stark, John H. Debes, Joe Carson, Marc J. Kuchner, Marshall D. Perrin, Alycia J. Weinberger, John P. Wisniewski. PROBING FOR EXOPLANETS HIDING IN DUSTY DEBRIS DISKS: DISK IMAGING, CHARACTERIZATION, AND EXPLORATION WITH HST/STIS MULTI-ROLL CORONAGRAPHY. 2014. The Astronomical Journal, Volume 148, Number 4.

[16] Kate Y. L. Su, James M. De Buizer, George H. Rieke, Alexander V. Krivov, Torsten Löhne, Massimo Marengo, Karl R. Stapelfeldt, Nicholas P. Ballering, and William D. Vacca. The Inner 25 au Debris Distribution in the ϵ Eri System. 2017 April 25. The Astronomical Journal, Volume 153, Number 5

[6]

A.10 Cost Variances from Original Proposal

The increase of the total mDOT PI-Managed Mission Costs from $35M in the original proposal to $50M is largely due to the design changes to the SS, which has increased by $6M. The new design will be custom build instead of relying largely on a COTS/MOTS solution, and includes changes to the propulsion and communications systems (see Appendix A.4). The increased cost of the SS also yields higher PM, SE, and SM&A, MOS/GDS, and implementation and closeout costs, as these costs are derived from analogous estimates that are a function of the hardware costs.

Reserves have increased from $7M in the original proposal to $14M to account for the risks identified in Section 4.3.4, while allotting adequate unencumbered reserves of 25%, the standard for AO proposals. Note that this represents a 40% total reserve level.

In discussions with Tyvak, a smallsat vendor, they believed the parametric methodology singificantly overestimated cost and developed a first-order bottom-up cost using of off-the-shelf hardware including a 30% reserve that would reduce cost to $35M.